SCALING BEHAVIORS AND MECHANICAL PROPERTIES OF POLYMER GELS

DISSERTATION

Presented to the Graduate Council of the
University of North Texas in Partial
Fulfillment of the Requirements

For the Degree of

DOCTOR OF PHILOSOPHY

By

Chunfang Li, B.S., M.S.
Denton, Texas

May 1, 1994

SCALING BEHAVIORS AND MECHANICAL PROPERTIES OF POLYMER GELS

DISSERTATION

Presented to the Graduate Council of the
University of North Texas in Partial
Fulfillment of the Requirements

For the Degree of

DOCTOR OF PHILOSOPHY

By

Chunfang Li, B.S., M.S.
Denton, Texas

May 1, 1994

Chunfang Li, Scaling Behaviors and Mechanical Properties of Polymer Gels
Doctor of Philosophy (Physics), May, 1994, 154 pp., 3 tables, 56 illustrations, bibliography, 84 titles.

Polymer gels undergo a volume phase transition in solvent in response to an infinitesimal environmental change. This remarkable phenomenon has resulted in many potential applications of polymer gels. The understanding of its mechanical properties has both scientific and technological importance.

For this purpose, we have developed a novel method for measuring Poisson's ratio, which is one of the most important parameters determining the mechanical property of gels. Using this method, Poisson's ratio in N-isopropyacrylamide (NIPA) and polyacrylamide (PAAM) gels has been studied. We obtained that Poisson's ratio goes through a negative dip in both neutral and ionic NIPA gels, but positive in the PAAM gels. It was found that the scaling exponent δ depends on the details of chemical ingredients and polymerization process. In the salt solution, the δ depends on both the network ionization and the solvent salt concentration. The study of acoustic attenuation and velocity of NIPA gels reveals the dynamic scaling behavior of NIPA gels near the transition point.

It has been found that there are four different pattern regions on the surface of constrained gel films depending on the temperature (or acetone concentration) and ionic strength of the sample, these patterns are associated with the mechanical instability of gel surface.

The work presented in this dissertation will help ones both in the theoretical understanding and practical application of the gel system.

ACKNOWLEDGEMENT

I wish to thank my professor Zhibing Hu for his enthusiastic guidance, encouragement and warm friendship during this research.

I wish to thank all the committee members for their reading my thesis.

Special thank is made to Drs. West, Deering, and Kowalski for their kindly supporting this work. Special thank is also made to Dr. Littler for his sharing the lab with us.

I also wish to thank Dr. Yong Li in Kimberly-Clark Co., for his fruitful discussions during this work.

This research is support by the Donors of the Petroleum Research Fund, administered by the American Chemical Society, and by the U.S. Army Research Office under Grant No. DAAH04-93-G-0215.

TABLE OF CONTENTS

LIST OF TABLES

LIST OF ILLUSTRATIONS

CHAPTER 1

INTRODUCTION

A gel is a form of matter intermediate between a liquid and a solid. It consists of a cross-linked polymer network, and a solvent which fills up the pores of the network. Gels exist widely in biological systems and food products (often as thickening agents like starch and gelatin). The capacity of the gels to absorb water or solvent is enormous and can be as much as 1000 times the weight of the dry gel. This makes the gel an ideal absorption material, such as baby diaper.

In recent years, the volume phase transition and critical phenomena in polymer gels have attracted much attention because of their scientific interest and technological importance. The studies of the gel volume phase transition have led to many discoveries and applications. The phase transition of gels has been found to be universal [1] and the phase transition can be induced by many factors, such as temperature, solvent composition, pH, electric field, external osmotic pressure [1], light, and biochemical reaction [1]. The high swelling ability and molecular size pores ($\leq$ 100 Å) make gels useful in the industrial consolute separation technology, biological slurry dewatering technology [2], etc.

The application of polymer gel systems for drug delivery devices has been of increasing interest. Changes in swelling states of gels can influence the diffusion of solutes from within the gels to the outside aqueous media [2] and make polymer gel a good material for controlled drug release. Using hydrogel

membranes, it is possible to design human implantable self-regulating insulin delivery systems sensitive to glucose concentration [2]. Furthermore, polyelectrolyte gels that expand and contract under electrical control can be used as switches, artificial muscle [1], and serve as general-purpose chemical valves.

In this work, two kinds of polymer gels were used, which are polyacrylamide (PAAM) gel and N-isopropylacrylamide (NIPA) gel. In some experiments sodium acrylate (NaAc) was also copolymerized with any one of the above two gels. These copolymerized gels are called polyelectrolyte gels or ionic gels because of the extra ionic charges in the polymer chains. PAAM gel is a hydrophilic, solvent sensitive but temperature insensitive, gel. Because of its hydrophobic properties, NIPA gel is temperature sensitive.

For the application of polymer gels, the understanding of their mechanical properties is very important. With a large fraction of mass being solvent, polymer gels are very soft and sometimes even sticky. This makes it very difficult to measure gel mechanical properties such as Poisson's ratio, bulk and shear moduli, and scaling components. It is much more difficult to perform the mea-surement near the gel's critical point, at which the fluctuation of density in gels is very high. The main purpose of this work is to study the mechanical proper-ties, the scaling exponents of polymer gels, and particularly, near the phase transition point.

Poisson's ratio σ, which is a combination of the (static) shear and bulk moduli, is one of the most important quantities of a gel network system [3]. It characterizes the response of a material under anisotropic external pressure.The fact that σ is a function of the ratio of material moduli makes it ideal for studying scaling behavior of mechanical properties of gels [1]. Poisson's ratio

plays a vital role in many phenomena, for example, the bending of polyelectrolyte gels in electric fields [4], gel surface pattern formation [6], network swelling kinetics [1], and gel volume phase transition [6]. Some of these phenomena have potential applications in the areas of artificial muscle, actuators, switches, controlled release, and membrane separations. In the semi-dilute regime, the quality of a gel solvent (good, theta (Θ), or poor) can be defined by the Poisson's ratio of the gel [7].

Poisson's ratio can be obtained by measuring the shear (G) and bulk (K) modulus [8]. The measurement of the shear modulus G of gels is often straightforward. Most of the methods involve measuring the instantaneous elongation/compression of a gel sample under known pressure [3]. With these methods, it is critical to complete the measurement quickly, before the sample changes volume. Another problem often encountered is friction between the sample and instrument causing the sample to have non-uniform strain (e.g., a cylindrical sample could become drum shaped under pressure). The bulk modulus of gels can be directly measured by the osmotic pressure method, which involves the measurement of gel volume change under known osmotic pressure from the surrounding polymer solution [9]. Light scattering techniques have also been used to indirectly measure the longitudinal modulus [4,9]. However, due to the inevitable inhomogeneity of the system, an average over many scattering volumes is often required to have a meaningful result. Other methods used in measuring gel mechanical properties include shear wave and ultrasound propagation and small angle neutron and X-ray scatterings.

Poisson's ratio in gels can be also obtained by measuring the swelling kinetics of gels [6], and directly by measuring the equilibrium deformation of the

gel under uniform elongation or compression [6]. In the elongation experiment, the sample is usually dried first in order to be fixed onto the stretching instrument. However, it is conceivable that the drying process may change the sample's mechanical properties and therefore influence the measured results (A significant swelling ratio reduction with ionic gel samples has been observed after going through a room temperature drying process). In the equilibrium compression experiment, non-uniform deformation often occurs, making data analysis difficult.

Thermal dynamic stability conditions require that the value of Poisson's ratio be between -1 and 0.5 ($0 < K/G < \infty$) for three dimensional materials [8]. For most common materials, the Poisson's ratio is positive, i.e., the sample undergoes a transverse contraction under axial stretching or a transverse expansion under axial compression. However, a few cases of negative Poisson's ratio have been reported, including highly anisotropic crystals [10] and polymer foams with reentrance cells [11]. The Monte-Carlo simulation also predicts possible negative Poisson's ratio in the two dimensional cyclic hexamers lattice [12]. Recently, Hirotsu measured the temperature dependence of the neutral N-isopropyacrylamide (NIPA) gel deformations under constant pressure and obtained negative Poisson's ratio in a neutral NIPA gel near the phase transition [13]. In Hirotsu's experiments, the sample was first dried so that it could be mounted to the instrument. Using a simple method [14], Poisson's ratio of both ionic and neutral NIPA gels were measured and the negative Poisson's ratio near the critical temperature was found in all samples investigated [15].

The application of scaling methods to polymers in solution has led to some dramatic successes in both theoretical understanding and experimental

The application of scaling methods to polymers in solution has led to some dramatic successes in both theoretical understanding and experimental applications [16]. It has been shown that many properties of gel networks exhibit scaling behavior [16], and that the origin of the gel scaling behavior can often be traced back to the scaling behavior of polymers in solution [16].

Water in general is assumed to be a good solvent for polyacrylamide (PAAM) gel. Some recent studies have shown that the scaling behavior of dilute PAAM gel is quite universal [9] but less so at higher concentrations [17]. The systematical studies of the scaling exponent δ as a function of monomer and crosslinker concentration have been investigated [18]. It was found that the exponent δ depends on the details of chemical ingredients and process. It increases as the crosslinker or monomer concentration increases [18].

From application point of view, polyelectrolyte gels offer some unique opportunities. They have much higher swelling capability for given stiffness. Typically, these gels are sensitive to pH, solvent ionic strength (salt concentration) [19], and external electric field [1]. The large, discontinues volume phase transition of these materials make them promising "intelligent materials" in various fields [20]. Many researchers have attempted to derive theories to describe the swelling behavior of these gels. Recent progress was reported by Prud'homme and Yin [21]. They have developed a comprehensive polyelectrolyte gel swelling theory with ion condensation and finite chain extension effects included [21]. Most of these works, however, are verified by swelling data and do not deal with the network mechanical properties directly. More detailed study of mechanical properties of polyelectrolyte gels is thus needed to meet the challenges of both theoretical understanding and practical applications [22].

The static behavior of phase transition in NIPA gels have been extensively investigated for the past few years. The recent efforts have been directed toward to understand the dynamic behavior of phase transition in gels. It was shown that the kinetics of gel swelling processes are related to the relaxation of the gel elasticity and the friction between the network and the solvent [1]. The dynamics of density fluctuations of gels was observed by the dynamic light scattering spectroscopy. It was shown that the collective diffusion coefficient diminishes at the critical point and the kinetics of the transition becomes infinitely slow [1]. The NMR study of polyacrylamide gel in acetone/water mixture found that the proton-lattice relaxation time diverges and the effective diffusion constant approaches zero near the critical acetone concentration [23]. The phase transition having large volume change is accompanied by formation and evolution of transient patterns which appear on the surface of a gel [24]. A recent theoretical model predicts that the apparent collective diffusion constant D_e and the relaxation time τ is gel geometry dependent [25]. Measurements of ultrasonic velocity and the attenuation provide important information about the dynamical aspects of relaxation processes near a critical point [26]. Specifically, critical fluctuations can interact strongly with the acoustic sound waves and result in soft modes and strong wave attenuation [26].

Pattern formation on the surface of polymer gels has recently attracted considerable attention [24,27]. The study of these patterns not only leads to better understanding of gel mechanical properties and gel kinetic process near the volume phase transition [24], but also helps to explain the formation and evolution of patterns found in biological systems.

The acrylamide/sodium acrylate (PAAM/SA) gels are widely used for

studying patterns of gels during the swelling process [5]. Based on elasticity theory [5,28], the swelling pattern can be understood in terms of frustration of the free gel surface that is constrained by an unswollen bottom surface.

In contrast to the swelling pattern, the patterns produced by the gel shrinking process is much more complex and less understood. When the lengths of cylindrical acrylamide gels were fixed in an acetone/water mixture, patterns including irregularly arranged bubbles, regularly arranged (necklace-like) bubbles, bamboos, and tubes were observed [27]. When the temperature of N-isopropylacrylamide (NIPA) gel beads was increased, irregularly arranged bubbles were observed as well [24].

Both the swelling and the shrinking patterns are sensitive to the initial and the final states of the transition [24,27]. These patterns are the result of large equilibrium gel volume change. This change corresponds to the relaxation of a gel osmotic pressure jump. The osmotic pressure jump, either positive (causing swelling) or negative (causing shrinking), can be achieved by changing temperature, solvent, electric field, light, ph of the solvent, or other parameters. Therefore, the study of gel patterns will help us to understand the volume phase transition mechanism.

This thesis is organized as follows. In Chapter 2, a new method for measuring Poisson's ratio of polymer gels has been proposed and has been experimentally demonstrated. The method is based on different swelling behaviors of free and constrained gels. Using this method, the anomaly of Poisson's ratio near volume phase transition point was studied for both N-isopropylacrylamide (NIPA) and acrylamide gels (Chapter 3). It was found that Poisson's ratio exhibits a negative dip near the transition temperature for both neutral and ionic

NIPA gels. The dip becomes deeper and shifts to a higher temperature as the ionic strength increases. The negative Poisson's ratio of NIPA gels suggests that the bulk modulus is much smaller than the shear modulus as gels undergo the phase transition. Poisson's ratio of acrylamide gel, however, was found to be positive throughout the measured region.

The ratio of bulk modulus to shear modulus, K_e/G_e, of PAAM gels was studied in Chapter 4. This ratio is directly related to a scaling exponent, δ. It was found that δ depends on the details of chemical ingredients and polymerization process. It increases as the crosslinker or monomer concentration increases. The behavior of acrylamide/sodium acrylate gel was found to be dramatically different from the non-ionic gels. As sodium acrylate (SA) concentration increases from zero to 2 mol%, δ decreases from 2.09 to 1.08. Further increase of SA results in the formation of surface pattern and the value of δ increases slightly, eventually reaching a plateau around 1.25. In the salt solution, the value of δ depends on the network ionization and solvent salt concentration. When excess amount of NaCl is added, δ value recovers to about 1.8. The experimental results are in good agreement with theoretical predictions.

In Chapter 5, the ultrasonic attenuation and velocity in NIPA gels have been measured as a function of temperature over the frequency range 5-30 MHz. The velocity drops to a minimum but the attenuation exhibits the maximum near the transition temperature. The maximum of the attenuation increases as the frequency increase and shifts to a higher temperature. Critical behavior in the swelled phase near the phase transition was analyzed in terms of a dynamic-scaling theory. The data collapses reasonably onto a scaling function as the theory predicted.

In Chapter 6, the pattern formation and evolution in constrained acrylamide/sodium acrylate (PAAM/SA) gels have been investigated in acetone/water mixture. The constraint is achieved by crosslinking the gel slabs onto a rigid substrate. All samples are initially kept in water with the hexagonal pattern develop on the surface before being immersed in the acetone/water mixture. Depending on the solvent composition and ionic strength of the sample, different patterns, i.e., hexagonal, grains, and bubbles, have been observed. These patterns are formed at acetone concentration, below, near and above the concentration at which the gel volume phase transition occurs. The wavelengths of hexagonal and bubble patterns are found to be the same while that of the grain pattern is four times smaller. It is suggested that the shrinking patterns are formed due to the dense gel surface produced during the shrinking process.

In Chapter 7, Surface patterns in ionic NIPA gels have been investigated under external constraint. Hexagonal, grain and bubble patterns have been observed at temperatures below, near, and above the phase transition temperature T_c. It is found that the behavior of these patterns depends not only on temperature, time and external constraint, but also on the thermal path. The time dependence of the gel thickness has revealed that there is a plateau period and that the end of the plateau period corresponds to the onset of the bubble pattern. The experiments show that each hexagonal cell evolves into a bubble for NIPA gels, while a bubble can be present in the middle of a hexagonal cell for acrylamide gels. The mechanism for the shrinking patterns will be also discussed.

This work is summarized in Chapter 8.

CHAPTER 1 REFERENCES

1. T. Tanaka, Scientific American **244**, 124(1981); Y. Li and T. Tanaka, Ann. Rev. Mat. Sci. **22**, 243(1992).
2. H. G. Schild, Prog. Polym. Sci. **17**, 163(1992).
3. E. Geissler and A. M. Hecht, Macromolecules, **13**, 1276(1980).
4. T. Shiga, Y. Hirose, A. Okada, and T. Kurauchi, J. Appli. Polym. Sci. **44**, 249(1992).
5. (a) T. Tanaka, S-T. Sun, Y. Hirokawa, S. Katayama, J. Kucera, Y. Hirose, and T. Amiya, Nature, **325**, 796(1987).(b) T. Tanaka, S-T. Sun, Y. Hirokawa, S. Katayama, J. Kucera, Y. Hirose, and T. Amiya, Molecular Conformation and Dynamics of Macromolecules in Condensed Systems, Ed. M. Nagasawa, Elsevier, Amsterdam 1988.
6. Y. Li, Ph.D thesis, Structure and Critical Behavior of Polymer Gels, Massachusetts Institute of Technology, 1989.
7. M. Daoud and P. G. de Gennes, J. Phys. (Paris), **38**, 85(1977).
8. L.D. Landau and E.M. Liftschitz, Theory of Elasticity (Pergamon Press, New York, 1959).
9. E. Geissler, A. M. Hecht, F. Horkay, and M. Zrinyi, Macromolecules, **21**, 2594(1988).
10. Y. Li, Phys. Status Solidi **38**, 171 (1976).
11. R. Lakes, Science **235**, 1038 (1987).
12. K.W. Wojciechowski and A.C. Branka, Phys. Rev. A **40**, 7222(1989).
13. S. Hirotsu, Macromolecule **23**, 905(1990); J. Chem. Phys. **94**, 3949

(1991).

14. Y. Li, Z. Hu and C. Li, J. Appl. Polym. Sci. **50**, 1107(1993).

15. C. Li, Z. Hu, and Y. Li, Phys. Rev. E **40**, 603(1993).

16. P. G. de Gennes, Scaling Concepts in Polymer Physics, Cornell University Press, 1979.

17. Y. Cohen, O. Ramon, I. J. Kopelman, and S. Mizrahi, J. Polym. Sci. (Phys.) **30**, 1055(1992).

18. Z. Hu, C. Li, and Y. Li, J. Chem. Phys. **99**, 7108(1993).

19. L. Brannon-Peppas and N. A. Peppas, Int. J. Pharm. **70**, 53(1991).

20. Y. Osada and S. B. Ross-Murphy, Scientific American, May, 82(1993).

21. R. K. Prud'homme and Y. Yin, ACS Polym. Mat. Sci. Eng. **69**, 527(1993).

22. Y. Li, C. Li, and Z. Hu, in ACS Symposium Series xx, Edited by N.A. Peppas and F.L. Buchholz, May 1994.

23. F. Tabak, M. Corti, L. Pavesi, A. Rigamonti, J. Phys. C: Condensed Matt. Phys.**20**, 5691(1987).

24. E. Sato Matsuo and T. Tanaka, J. Chem. Phys. **89**, 1695, 1988.

25. Y. Li and T. Tanaka, J. Chem. Phys. **92**, 15 (1990).

26. C. Li, Z. Hu, and Y. Li, submitted to Phys. Rev.

27. E. Sato-Matsuo and T. Tanaka, Nature **358**, 482 (1992).

28. T. Hwa and M. Kardar, Phys. Rev. Lett. **61**, 106(1988).

CHAPTER 2

NEW METHOD FOR MEASURING POISSON'S RATIO IN POLYMER GELS

2.1 Introduction

Poisson's ratio σ, which is a combination of the (static) shear and bulk moduli, is one of the most important quantities of a gel network system [1,2]. The fact that σ is a function of the ratio of material moduli makes it ideal for studying scaling behavior of mechanical properties of gels [3,4,5]. Poisson's ratio plays a vital role in many phenomena, for example, the bending of polyelectrolyte gels in electric field [6], gel surface pattern formation [7], network swelling kinetics [8,9], and gel volume phase transition [10,11]. Some of these phenomena have potential applications in the areas of artificial muscle, actuators, switches, controlled release, and membrane separations. In the semi-dilute regime, the quality of a gel solvent (good, theta (Θ), or poor) can be reflected by the Poisson's ratio of the gel [2,12,13].

Poisson's ratio σ is related to the shear (G) and bulk (K) modulus of the material by [14]

$$\sigma = \frac{1}{2}\frac{3K-2G}{3K+G} \tag{2.1}$$

Therefore, σ is a function of (K/G) only. Note that Poisson's ratio can be expressed in terms of any two of the following moduli: Lame's constant, Young's modulus, bulk modulus, and shear modulus. Here we choose to express Poisson's ratio in terms of the bulk and shear moduli.

The measurement of the shear modulus, G, of gels is often straight forward. Most of the methods involve measuring the instantaneous elongation/ compression of a gel sample under known pressure [1]. With these methods, it is critical to complete the measurement quickly, before the sample changes volume. Another problem often encountered is friction between the sample and instrument, causing the sample to have non-uniform strain (e.g., a cylindrical sample could become drum shaped under pressure). The bulk modulus of gels can be directly measured by the osmotic pressure method, which involves the measurement of gel volume change under known osmotic pressure from the surrounding polymer solution [4,5]. Light scattering techniques have also been used to measure indirectly the longitudinal modulus [1,5]. However, due to the inevitable inhomogeneity of the system, an average over many scattering volumes is often required to have a meaningful result. Other methods, used in measuring gel mechanical properties, include shear wave, ultrasound propagation, small angle neutron and X-ray scatterings.

Poisson's ratio in gels can be obtained by measuring G and K separately [1,2,4,5], or by measuring the swelling kinetics of gels [8,9]. It can also be obtained directly by measuring the equilibrium deformation of the gel under uniform elongation or compression [10,11]. In the elongation experiment, the sample is usually dried first in order to be fixed onto the stretching instrument. However, it is conceivable that the drying process may change the sample mechanical properties and therefore influence the measured results (we have observed a significant swelling ratio reduction with ionic gel samples after going through a room temperature drying process). In the equilibrium compression experiment, nonuniform deformation often occurs, making data analysis difficult.

In this chapter, a simple and yet non-ambiguous way of measuring Poisson's ratio of gels is reported. This method involves the measurement of gel equilibrium dimensions under uniform constraint. The uniform constraint is achieved by covalently fixing the gel film onto a polyester sheet. The gel sample does not have to be dried before the measurement. Using this method, Poisson's ratio of polyacrylamide (PAAM) gel has been measured as a function of crosslinker concentration.

2.2 Basic theory of elasticity

The mechanics of solid bodies, usually as continuous media, forms the theory of elasticity. Under the applied forces, the solid bodies exhibit deformation in shape and volume. Define the position of any point before deformation as vector **r** and after deformation as vector **r'**, then the vector

$$\boldsymbol{u}=\boldsymbol{r}-\boldsymbol{r}' \tag{2.2}$$

is called the displacement vector.

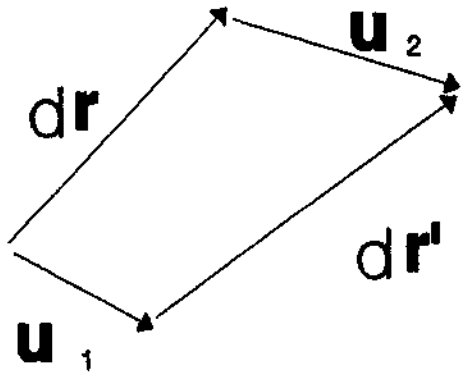

Figure 2.1 A vector before and after deformation.

When a body is deformed, the distances between its points change. Let a distance vector be dr, after deformation, the distance vector becomes dr'(Fig. 2.1), in Figure 2.1, dr' is

$$dr'=dr+du \tag{2.3}$$

Using the Einstein summation rule, the square of the distance change can be written as

$$dr'^2=(dr+du)^2=dr^2+2u_{ik}dx_idx_k \tag{2.4}$$

where u_{ik} is the strain tensor and is defined as

$$u_{ik}=\frac{1}{2}\left(\frac{\partial u_i}{\partial x_k}+\frac{\partial u_k}{\partial x_i}+\frac{\partial u_n}{\partial x_i}\frac{\partial u_n}{\partial x_k}\right) \tag{2.5}$$

Under the small deformation, u_{ik} is small, therefore we can neglect the second order term in the u_{ik} expression. Then the strain tensor is

$$u_{ik}=\frac{1}{2}\left(\frac{\partial u_i}{\partial x_k}+\frac{\partial u_k}{\partial x_i}\right) \tag{2.6}$$

From its definition we can see the strain tensor is symmetrical, that is

$$u_{ik}=u_{ki} \tag{2.7}$$

Because of its symmetricity, the strain tensor can be diagonalised at any point. If the strain tensor is diagonalised at a given point, the volume change after the deformation dV' can be written as

$$dV'=dV(1+u_{ii}) \tag{2.8}$$

and

$$u_{ii}=\frac{dV'-dV}{dV} \tag{2.9}$$

is the local fractional volume change and this deformation is called hydrostatic compression.

The internal energy change of a deformed body $d\epsilon$ is

$$d\varepsilon = TdS+\sigma_{ik}du_{ik} \tag{2.10}$$

where $\sigma_{ik}du_{ik}$ is the work done by the internal stress.

In thermodynamics, the free energy of the body is $F = \epsilon - TS$, therefore,

$$dF=-SdT+\sigma_{ik}du_{ik} \tag{2.11}$$

From the above equation the stress tensor σ_{ik} can be defined as

$$\sigma_{ik}=(\frac{\partial F}{\partial u_{ik}})_T \tag{2.12}$$

The strain tensor can be separated into two parts, a pure shear and a hydrostatic compression,

$$u_{ik}=(u_{ik}-\frac{1}{3}\delta_{ik}u_{nn})+\frac{1}{3}\delta_{ik}u_{nn} \tag{2.13}$$

In the same way, the free energy of the deformation can be written as

$$F=G(u_{ik}-\frac{1}{3}\delta_{ik}u_{nn})^2+\frac{1}{2}Ku_{nn}^2 \tag{2.14}$$

where K and G are the bulk modulus and the shear modulus respectively. The first term comes from the pure shear deformation and the second term is from

the hydrostatic compression. Using the relation $\delta_{ik}(u_{ik} -1/3\delta_{ik}u_{nn}) = 0$ and $du_{nn} = \delta_{ik}du_{ik}$, we have the relations:

$$\sigma_{ik}=Ku_{nn}\delta_{ik}+2G(u_{ik}-\frac{1}{3}\delta_{ik}u_{nn}) \tag{2.15}$$

and

$$u_{ik}=\frac{1}{9K}\delta_{ik}\sigma_{nn}+\frac{1}{2G}(\sigma_{ik}-\frac{1}{3}\delta_{ik}\sigma_{nn}) \tag{2.16}$$

Eqs. (2.15) and (2.16) represent the relations between the experimental quantities σ_{ik} and u_{ik} and the material mechanical properties K and G.

For a homogeneously elongated rod, with uniform elongational force applied to its ends (in the z-axis), the strain tensor u_{ik} and the stress tensor σ_{ik} are both constant through the body. Then from the boundary conditions, we conclude that $\sigma_{ik} = 0$ except the $\sigma_{zz} = p$ on the end surface where p is the force on the unit area.

Using $\sigma_{zz} = p$ and Eq. (2.16), we find

$$u_{ik}=0,(i\neq k)$$

$$u_{xx}=u_{yy}=-\frac{p}{3}(\frac{1}{2G}-\frac{1}{3K}),u_{zz}=\frac{p}{3}(\frac{1}{3K}+\frac{1}{G}) \tag{2.17}$$

The components u_{xx} and u_{yy} give the relative compression of the rod in the transverse direction. The component u_{zz} gives the relative lengthening of the rod. The ratio of the transverse compression to the longitudinal extension is called Poisson's ratio, σ:

$$\sigma = -\frac{u_{xx}}{u_{zz}} \qquad (2.18)$$

2.3 Experimental methods

2.3.1 Sample preparation and measurement

The PAAM gel samples were made by free radical polymerization. A mixture of 5 g of acrylamide (Bio-rad Co.) and various amounts of methylene-bisacrylamide (BIS) (45 to 500 mg) as crosslinker and tetramethylethylenediamine (240 μl) as accelerator were dissolved in 100 ml of deionized and distilled water. Nitrogen gas was bubbled through the solution to remove dissolved oxygen. The polymerization initiator, ammonium persulfate (AP), was added to the solution. The solution was then transferred into a narrow gap (0.457mm $\times$ 25mm $\times$ 75mm) between a GelBond® sheet (FMC Co.) and a microslide. The microslide was coated with a water repelling chemical (Sigmacoat®, Sigma Chemical Co.) for easy separation from the gel film. The gel started to form in about 15 minutes. To observe the effect of initiator concentration, samples were prepared at two levels of AP (40mg and 400mg). Since the surface of the GelBond sheet contained polymerization active chemical groups, it became covalently attached to the gel film. The back of the GelBond was pre-glued onto a glass slide to keep it from bending. For each gel film fixed on GelBond, a companion free gel film of the same chemical ingredient and the same dimension was made as well. The samples were left untouched for more than 12 hours before being transferred to a water bath to swell to equilibrium at room temperature.

The samples were immersed in water for several days before being

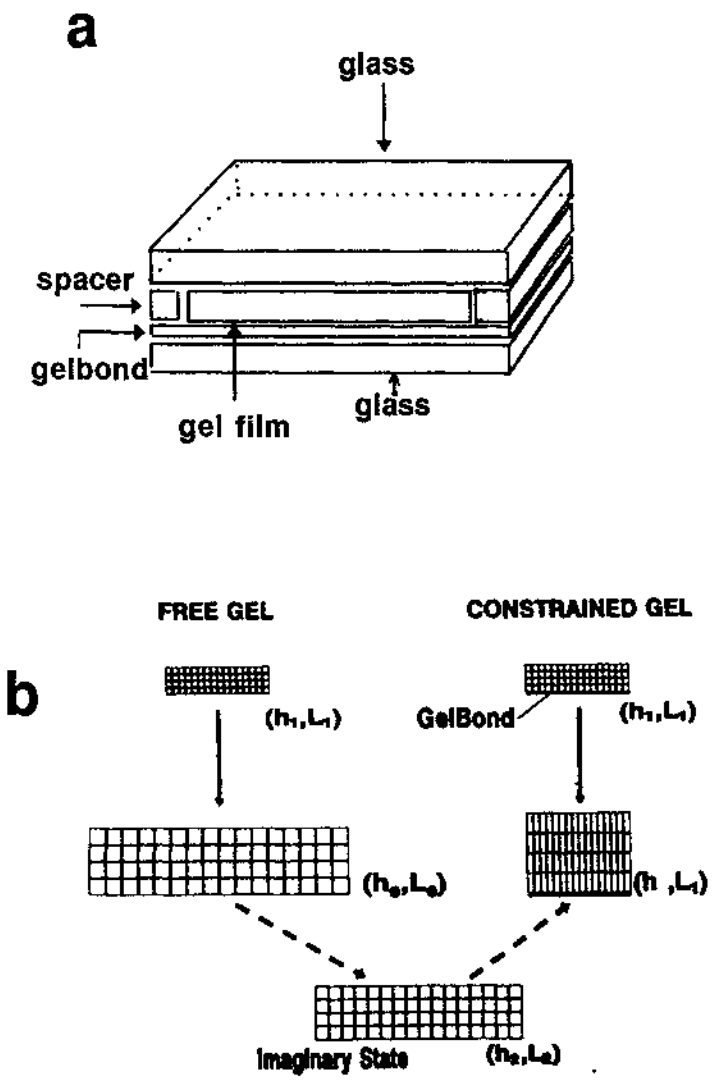

FIG. 2.2 (a) The diagram shows the gel film sample when made.

(b) The schematic description of the cross section of samples at various stages. Free and constrained gel films of the same initial dimensions (h_1, L_1) were allowed to swell in water. An imaginary intermediate state (h_2, L_2) of the constrained gel is shown. The volume of the imaginary state is the same as that of the final state. The swollen state of the free gel film (h_0, L_0) was used as the reference state for the deformation of the constrained gel.

measured. The ones constrained by attachment to the GelBond can swell only in one direction. The free gels swelled isotropically in all directions. Sketches of the swelling processes of constrained and free gel films are shown in Fig. 2.2. After the samples had reached equilibrium, their thicknesses were measured using a spherometer. The accuracy of the measurement was within 0.005 mm. For each sample, thickness measurements were made at three different locations and the average used in calculating Poisson's ratio.

2.3.2 Theoretical consideration

We will use Landau's elasticity theory introduced in section 2.2 for data analysis. The samples are assumed to be isotropic at preparation. We choose the direction perpendicular to the gel film as the z-direction. Since the samples are all thin gel films, the edge effect of constrained samples can be neglected and the deformation of the sample is therefore homogeneous, i.e., the strain tensor u_{ik} is a constant throughout the sample. Furthermore, the only non-zero elements are $u_{xx} = u_{yy}$ and u_{zz}, as a result of the symmetry of the system. Using the u_{ik} and σ_{ik} relation of Eq.(2.15), we find that all off diagonal stress tensor elements are zero. In fact, we will show that σ_{zz} is zero as well, leaving $\sigma_{xx} = \sigma_{yy}$ the only non-zero elements.

Since σ_{zz} is a constant, it can be determined by the boundary condition $\sigma_{ik}n_k = P_i$, where n_k is the normal vector to the boundary and P_i the external stress (force per unit area) applied to the boundary. Since there is no external force on the top and bottom of the gel film along z-direction ($P_z = 0$), we have $\sigma_{zk}n_k = 0$. Use $n_x = n_y = 0$ and $n_z = 1$, we have $\sigma_{zz} = 0$. Therefore we conclude that $\sigma_{xx} = \sigma_{yy} = P$ are the only non-zero stress tensor elements. This indicates that the constraint of the samples from GelBond can be viewed as a

radially applied external pressure P.

Substituting $\sigma_{xx} = P$ and $\sigma_{zz} = 0$ in Eq.(2.15), we have

$$u_{xx} = \frac{P}{3}\frac{3K+4G}{6KG} \tag{2.19}$$

$$u_{zz} = -\frac{P}{3}\frac{3K-2G}{3KG} \tag{2.20}$$

Combining these results with Eq.(2.1), one can easily verify that

$$\sigma = \frac{u_{zz}}{u_{zz}-2u_{xx}} \tag{2.21}$$

For a gel under small deformation,

$$u_{zz} = \frac{h-h_0}{h_0} \tag{2.22}$$

$$u_{xx} = \frac{L_1-L_0}{L_0} = \frac{h_1}{h_0} - 1 \tag{2.23}$$

Where h and h_0 are the thickness of the fixed and free samples, respectively, and h_1 is the thickness of the samples at preparation (h_1 =0.457mm).

The measured h_0 and h of the samples with 40mg/100ml ammonium persulfate as a function of BIS concentration are shown in Fig. 2.3. The swelling ratios of these samples are all lower than their corresponding samples initiated with 400mg/100ml ammonium persulfate which is shown in Fig. 2.3. This indicates that the samples with 40mg/100ml AP are better crosslinked. In both cases, h_0 and h decrease as BIS concentration increases.

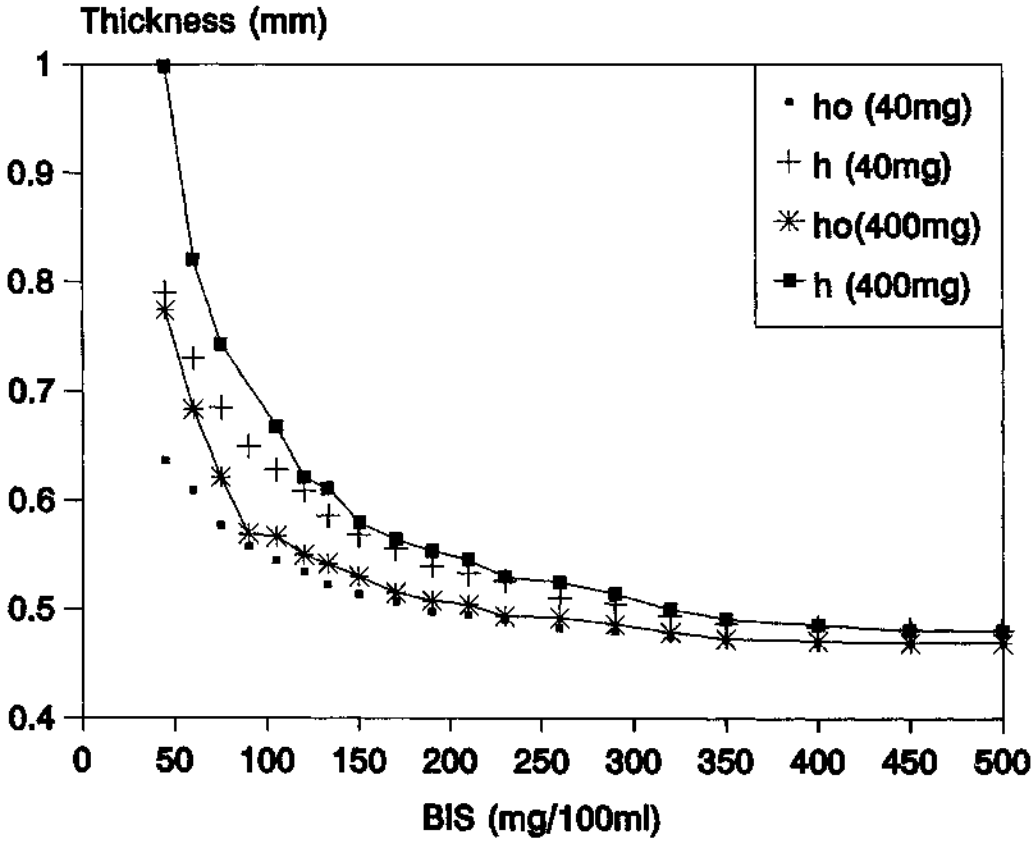

FIG. 2.3 The thickness of free swollen polyacrylamide gel films (h_0) and of constrained swollen polyacrylamide gel films (h) as a function of initial crosslinker (BIS) concentration. The samples were prepared with the ammonium persulfate (AP) initiator concentration equal to 40mg/100ml. The initial thicknesses (h_1) of all samples were equal 0.457mm. The error of the measurement is within 0.01 mm.

2.4 Discussion

The change of the sample from the reference state (the free gel state) to the final state (the constrained gel state) can be achieved by two imaginary steps, as shown in Fig. 2.2. First, the reference state is isotropically shrunken by a factor of $(V/V_0)^{1/3}$, that is, h_0 shrank to $h_2 = h_0(V/V_0)^{1/3}$, and L_0 shrank to $L_2 = L_0(V/V_0)^{1/3}$. The volume of this shrunken state is obviously the same as the final constrained gel state. The second step is to elongate the scaled state (h_2,L_2) to the final state (h,L_1). In this step the change of volume is zero, therefore it is a pure shear deformation. The degree of bulk (volume) and shear deformation of the system can, therefore, be represented by (V_0/V) and $h/h_2 = (V_0/V)^{1/3}(h/h_0)$. As shown in Fig. 2.4, other than the samples with very low BIS concentration, the bulk and shear deformations of the samples are both fairly small (less than 30%) compared with the deformation range used in other methods [5]. We expect that in the small deformation regime, the linear analysis we have outlined earlier should be valid. For the samples under large deformation, the non-linear terms should be considered if more accurate analysis is desired.

Using the measured values for h_0 and h and Eq.(2.22), Poisson's ratios of samples of both series are obtained and shown in Fig. 2.5. The σ values of the first series (AP = 40mg/100ml) are consistently higher than the second series (AP = 400mg/100ml). Upon increasing BIS concentration, Poisson's ratio of both series initially increases. Since K/G is monotonically related to σ and the gel network concentration (inverse of volume swelling ratio) is monotonically related to BIS concentration, this indicates that as the network concentration increases, K increases more than G. This agrees with the fact

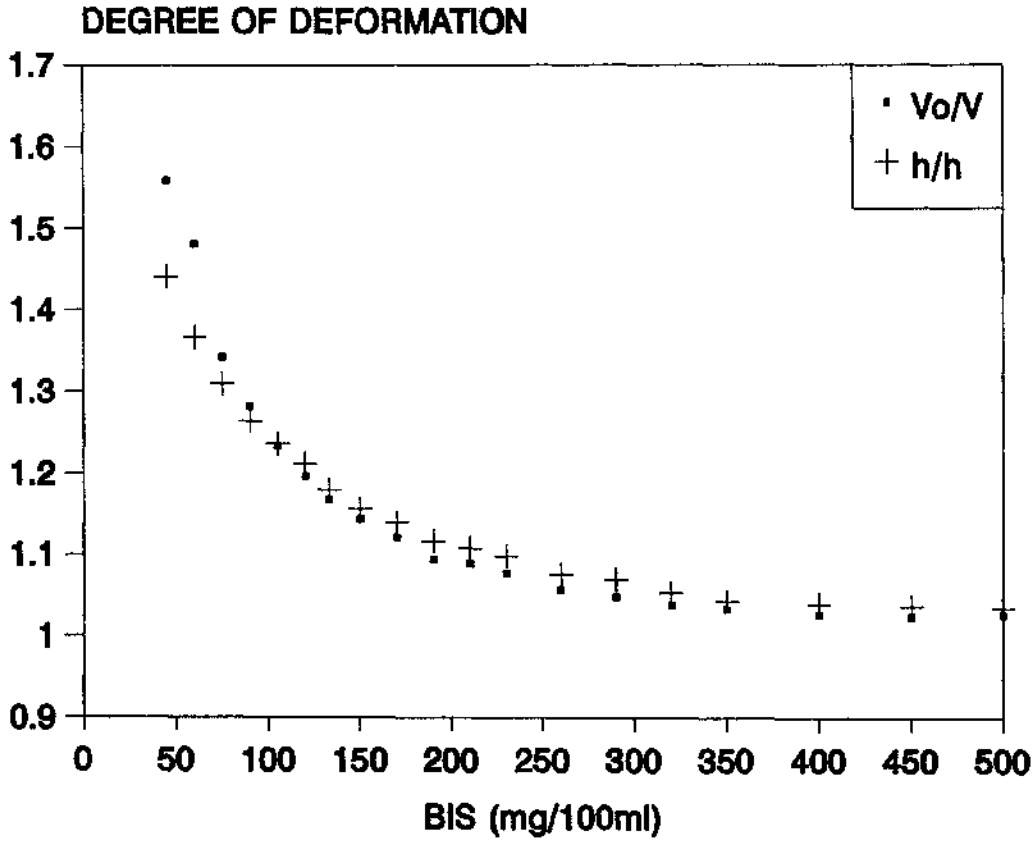

FIG. 2.4 The degree of bulk (V_0/V) and shear (h/h_2) deformation of constrained polyacrylamide gel films of different crosslinker (BIS) concentration. The samples were the same as the ones used in Fig. 2.3. Except for the first three samples with low BIS concentration, all relative deformations are smaller than 30%.

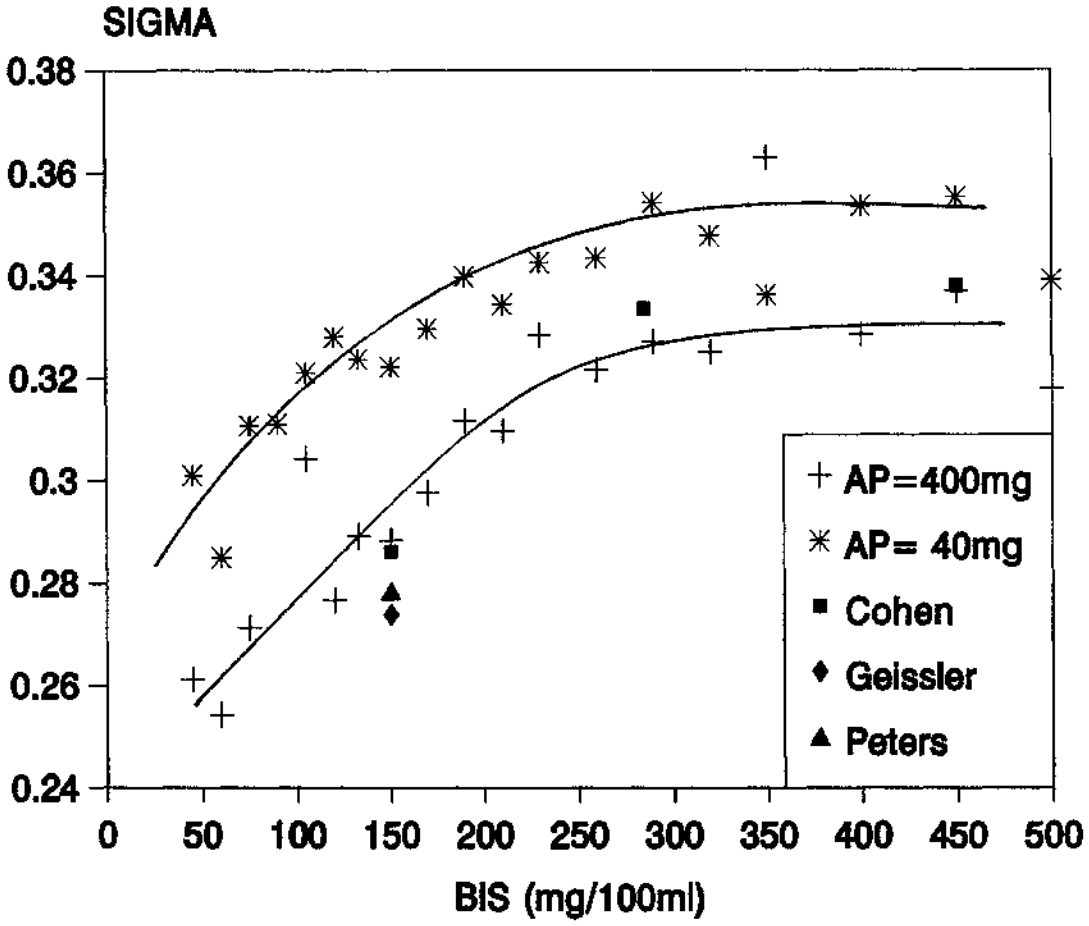

FIG. 2.5 Poisson's ratio σ of polyacrylamide gels of different crosslinker (BIS) concentration. The samples made with lower ammonium persulfate concentration (40mg/100ml) have higher σ values than the corresponding samples made with higher ammonium persulfate concentration (400mg/100ml).

that, in general, the bulk modulus K has a much stronger polymer concentration dependence than the shear modulus G. As the BIS concentration further increases, its crosslinking efficiency decreases, causing the σ value to reach a plateau. For semi-dilute gels in good solvent, σ is expected to be around 0.278 [13]. This corresponds to BIS $\sim$ 110mg/100ml region for AP = 400mg/100ml series, or BIS $\sim$ 50mg/100ml region for AP = 40mg/ml series. The results obtained by Cohen et al. using the osmotic de-swelling technique are also plotted in Fig. 2.5 for comparison. The result from the swelling kinetics technique by Peters and Candau [8], and that from the combination of shear modulus and scattered light intensity by Geissler et al. [5] are also presented in the Fig. 2.5. The agreement between these results and our AP = 400mg/100ml series is excellent.

We would like to point out that this method, although simple, is limited by the fact that not all gels can be easily attached to a rigid substrate. Also, for any given system, the degree of deformation may not be controlled easily. When large deformation occurs, a non-linear elasticity theory would be required when accurate quantitative information is desired.

2.5 Conclusion

In this chapter, a new method to directly measure Poisson's ratio of gels based on different swelling behavior of constrained and free gel slabs have been demonstrated. This method is precise and easy to use. The results from PAAM gels indicate that the mechanical properties of gels are sensitive to the polymerization parameters. Our results, at the higher level of ammonium persulfate (400mg/100ml), are in excellent agreement with previously reported values of σ.

CHAPTER 2 REFERENCES

1. E. Geissler and A. M. Hecht, Macromolecules, **13**, 1276(1980).
2. E. Geissler and A. M. Hecht, Macromolecules, **14**, 185(1981).
3. S. Candau, J. Bastide, and M. Delsanti, Adv. Polym. Sci., **44**, 27(1982).
4. F. Horkay, E. Geissler, A. M. Hecht, and M. Zrinyi, Macromolecules, **21**, 2589(1988).
5. E. Geissler, A. M. Hecht, F. Horkay, and M. Zrinyi, Macromolecules, **21**, 2594(1988).
6. T. Shiga, Y. Hirose, A. Okada, and T. Kurauchi, J. Appli. Polym. Sci. **44**, 249(1992).
7. (a) T. Tanaka, S-T. Sun, Y. Hirokawa, S. Katayama, J. Kucera, Y. Hirose, and T. Amiya, Nature, **325**, 796(1987).(b) T. Tanaka, S-T. Sun, Y. Hirokawa, S. Katayama, J. Kucera, Y. Hirose, and T. Amiya, Molecular Conformation and Dynamics of Macromolecules in Condensed Systems, Ed. M. Nagasawa, Elsevier, Amsterdam 1988.
8. A. Peters and S. J. Candau, Macromolecules, **19**, 1952(1986).
9. Y. Li and T. Tanaka, J. Chem. Phys., **90**, 5161(1989).
10. S. Hirotsu, Macromolecules, **23**, 905(1990).
11. Y. Li, Ph.D thesis, Structure and Critical Behavior of Polymer Gels, Massachusetts Institute of Technology, 1989.
12. M. Daoud and P. G. de Gennes, J. Phys. (Paris), **38**, 85(1977).
13. F. Horkay and M. Zrinyi, Macromolecules, **15**, 1306(1982).
14. L. D. Landau and E. M. Liftschitz, Theory of Elasticity (Pergamon Press,

New York, 1959).

15. The active chemical groups are firmly attached to the GelBond film. They only affect the structure of the portion of the gel that is microscopically close to the GelBond sheet. This has been confirmed by our private communication with FMC, the manufacturer of the GelBond sheets.

16. Y. Li and T. Tanaka, J. Chem. Phys., **92**, 1365(1990).

17. Y. Cohen, O. Ramon, I. J. Kopelman, and S. Mizrahi, J. Polym. Sci. (Phys.), **30**, 1055(1992).

CHAPTER 3

POISSON'S RATIO IN POLYMER GELS NEAR THE PHASE TRANSITION POINT

3.1 Introduction

In this chapter, a direct measurement on Poisson's ratio of neutral and ionic N-isopropylacrylamide (NIPA) gels and neutral polyacrylamide (PAAM) gels is discussed using the method proposed by the previous chapter. The method has been tested for polyacrylamide (PAAM) gel in water [1]. The results are in excellent agreement with ones obtained by other method.

Under an external stimulus such as temperature and acetone concentration, polymer gels undergo a volume phase transition [2]. Since this transition involves a large deformation of the volume, the elastic quantities of gels must play a vital role at the critical point. Poisson's ratio (σ), one such quantity, characterizes the transverse deformation of materials under uniaxial pressure. The quantity σ is related to the shear (G) and bulk (K) modulus of the material by,

$$\sigma = \frac{1}{2}\frac{3K-2G}{3K+G} \tag{3.1}$$

Therefore, σ depends on (K/G) only. Thermal dynamic stability conditions require that $-1 < \sigma < 0.5$ ($0 < K/G < \infty$)for three dimensional materials [3]. For most common materials, Poisson's ratio is positive, i.e., the sample undergoes a transverse contraction under axial stretching or a transverse expansion under

expansion under axial compression. However, a few cases of negative Poisson's ratio have been reported, including highly anisotropic crystals [4] and polymer foams with reentrance cells [5]. The Monte-Carlo simulation also predicts possible negative Poisson's ratio in the two dimensional cyclic hexamers lattice [6].

Recently, Hirotsu measured the temperature dependence of the neutral N-isopropyacrylamide (NIPA) gel deformations (both axial and radial) under constant pressure [7]. By combining the bulk and shear elastic moduli, Hirotsu obtained negative Poisson's ratio in a neutral NIPA gel near the phase transition. In Hirotsu's experiments, the sample was first dried so that it can be mounted to the instrument. Although the drying process does not affect the apparent swelling properties of the neutral NIPA gel, we have observed dramatic change in degree of swelling from ionic gels that were first dried and then swelled. Fig. 3.1 shows the drying effect of an ionic (20 mM NaAc) NIPA gel. In our experiment, the gel sample does not have to be dried before the measurement.

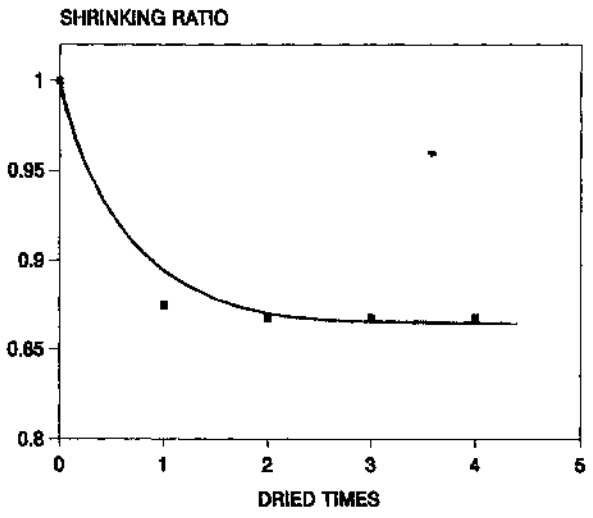

FIG. 3.1 The swelling ratio of ionic gel after each drying.

3.2 Sample preparation

The NIPA gel samples were made by free radical polymerization [2]. A mixture of 7.8 g of N-isopropyacrylamide (Kodak Co.), 133 mg of methylene-

bis-acrylamide as crosslinker, tetra-methyl-ethylene-diamine (240 μl) as accelerator, and sodium acrylate (SA), ionic group, were dissolved in 100 ml of deionized and distilled water. The concentration of SA (0-8mM) was varied. Nitrogen gas was bubbled through the solution to remove dissolved oxygen. Then ammonium persulfate (40 mg) as an initiator was added to the solution. A thin film of the solution was cast between a GelBond film (FMC Co) and a microslide with a fixed separation (0.996mm). Since the GelBond film contained polymerization-active chemical groups, the bottom surface of the gel slab was thus covalently cross-linked to the GelBond film. For each gel slab fixed to GelBond, a companion free slab of the same chemical ingredient and same dimensions was made as well. The samples were left untouched for about 12 hours before been transferred into a water bath to swell. After the samples had reached equilibrium, their thicknesses were measured by averaging over the thicknesses at three locations of the sample using a spherometer. The measurement accuracy was within 0.005 mm [8]. The details of the method was given in the previous chapter. The temperature of samples was controlled by a circulation water bath (Brinkmam Lauda Super RM-6). A platinum resistor thermometer was used to monitor the temperature near the sample within 0.05 ^{0}C. The data were taken in the warm-up run with a rate of 0.1^{0}C/day near the phase transition region.

The PAAM gel was made using the NIPA recipe with the 7.8 g of N-isopropylacrylamide monomers replaced by 5 g of acrylamide monomers. The phase transition of PAAM gels was triggered by change of acetone concentration in acetone/water mixture.

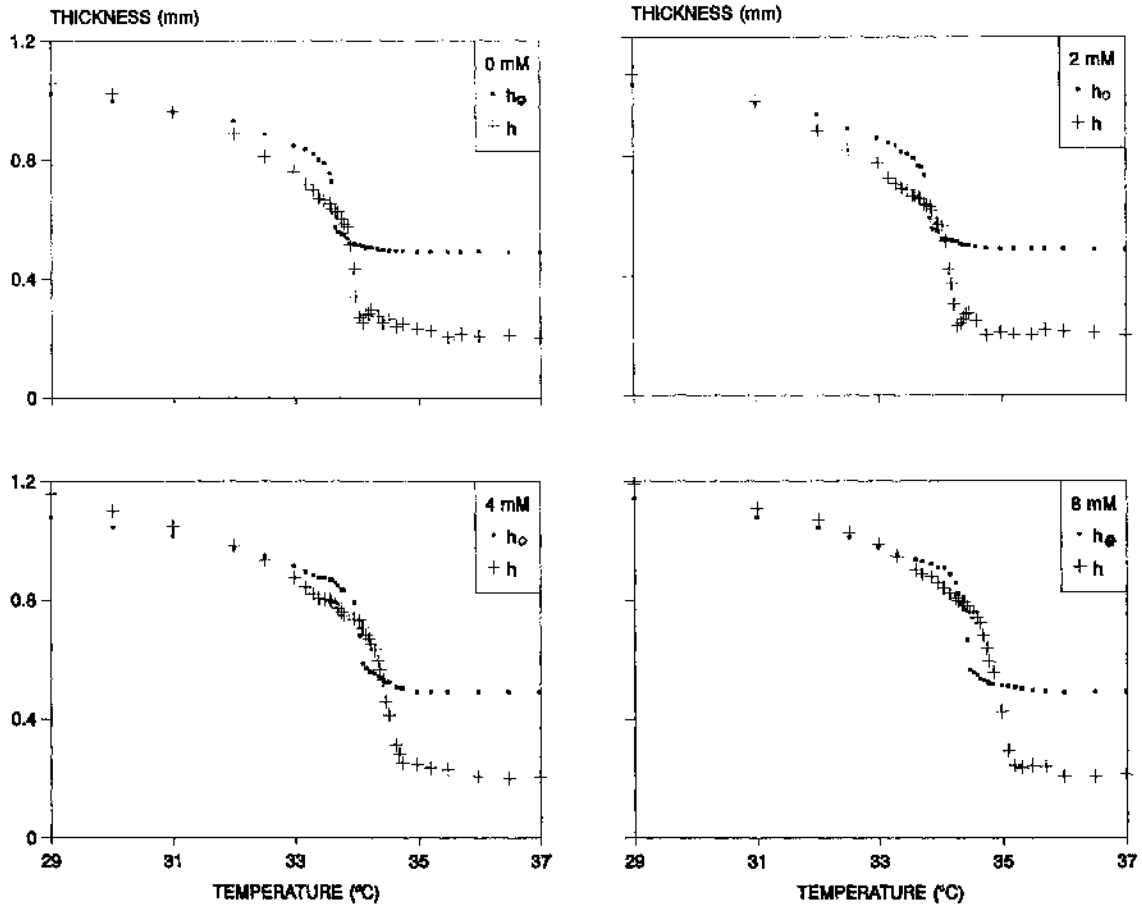

FIG. 3.2 The thickness of free (h_0) and of constrained (h) NIPA gel films as a function of temperature. The initial thickness (h_1) of all samples is 0.996 mm. The concentration of sodium acrylate varies: 0 mM, 2 mM, 4 mM, 8mM. There are three intersections between h and h_0 for all samples.

3.3 Experimetal Results and discussion

3.3.1 Experimental results

The thickness of free (h_0) and constrained NIPA gels (h) are shown in Fig. 3.2 as a function of temperature at various ionic concentrations. The thicknesses of the samples decrease as temperature increases. Following convention, we take the point at which the size of the sample shows the largest change as the transition temperature, T_c. The fixed gels have higher transition temperature than their companions, the free gels, have. The increase of T_c is apparently caused by the radial stretching pressure generated by the constraint. This effect is similar to the change of phase transition temperature of gels under uniaxial pressure [9]. The difference of transition temperatures between free and constrained samples, becomes larger as the ionic concentration increases. Fig. 3.3 shows the transition temperature T_c against

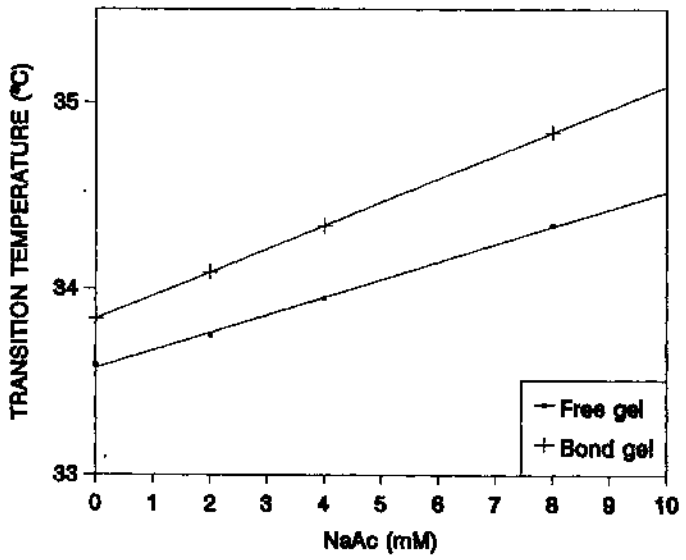

FIG. 3.3 Transition temperature against ionic concentration in free and constrained gels.

the ionic concentration. The value of T_c for both free and constrained gels linearly increase with the ionic group. There are three intersections between h_0 and h for all NIPA samples studied. At the first crossover point, both fixed and free samples reach the same thickness, which is the same as the thickness of samples when been made. This shows that the constraint from Gelbond is zero at this point. For temperatures lower than the first crossover point, the constraint corresponds to a compressional pressure; above this point, the constraint corresponds to a stretching pressure. The other two crossover points are located on either side of the phase transition temperature. These two points indicate the beginning and the end of the negative Poisson's ratio region, respectively.

Since the gel is mechanically fixed at a lower surface, it is forced to swell in the direction perpendicular to the surface. The constraint can be viewed as a radial external pressure applied to the samples [8]. Using boundary conditions and the general stress(σ_{ik})-strain(u_{ik}) relation [3] with Einstein summation convention,

$$u_{ik}=\frac{1}{9K}\delta_{ik}\sigma_{ll}+\frac{1}{2G}\left(\sigma_{ik}-\frac{1}{3}\delta_{ik}\sigma_{ll}\right) \tag{3.2}$$

Poisson's ratio (σ) can be derived as [1]

$$\sigma=\frac{u_{zz}}{u_{zz}-2u_{xx}} \tag{3.3}$$

The physical meaning of Poisson's ratio is illustrated in Fig. 3.4. In this figure, u_{zz}/u_{xx} (dashed line) and σ (solid line) are plotted as a function of K/G using Eqs. (3.1) and (3.3). For most materials, radial compression ($u_{xx}<0$) results in an axial expansion ($u_{zz}>0$), i.e., $u_{zz}/u_{xx}<0$. This corresponds to $\sigma>0$,

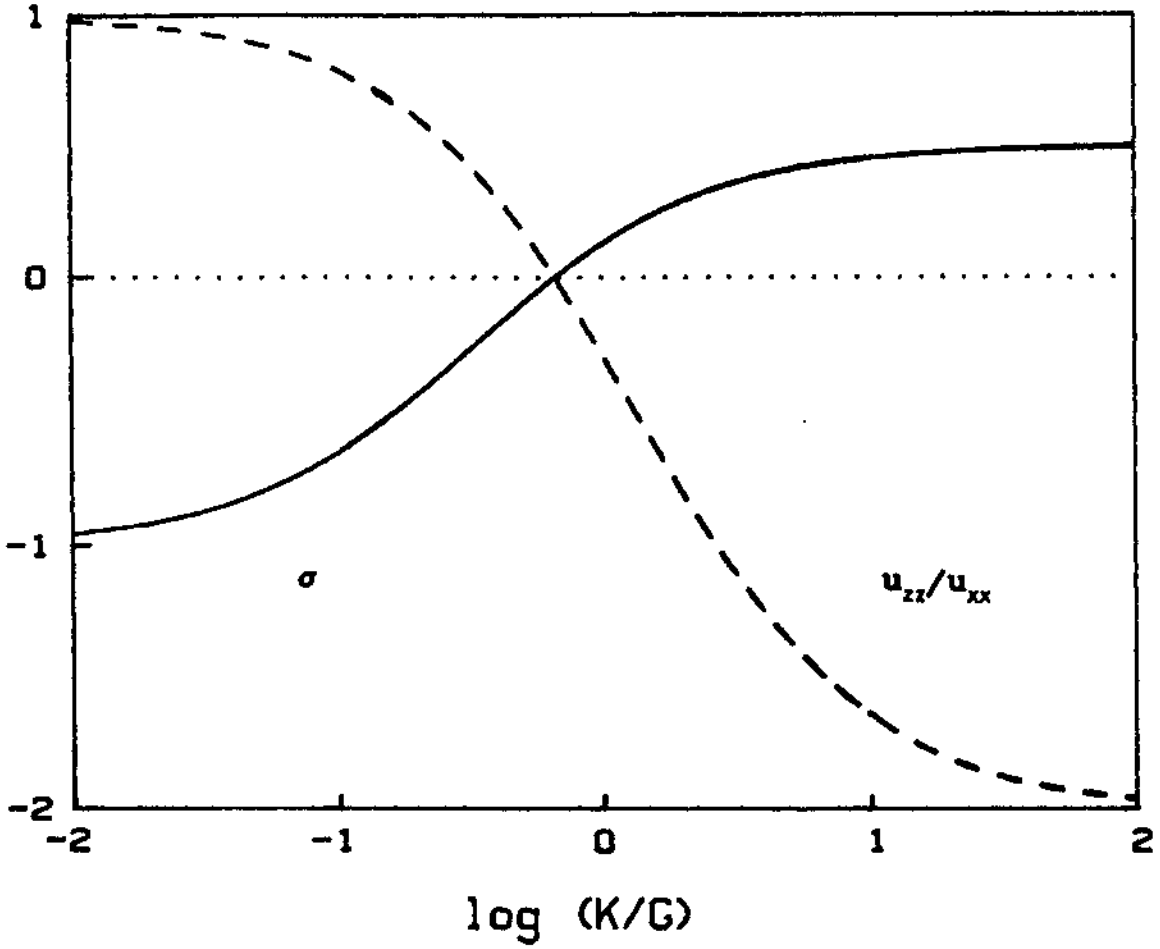

FIG. 3.4 Poisson's ratio (solid line) and u_{zz}/u_{xx} (dashed line) is plotted as a function of K/G. Zero is indicated by a dotted line.

or K/G > 2/3. Rarely, a radial compression yields axial compression, i.e., $u_{zz}/u_{xx} > 0$. This corresponds to $\sigma < 0$, or K/G < 2/3.

For small deformation, we have

$$u_{zz} = \frac{h - h_0}{h_0} \tag{3.4}$$

$$u_{xx} = \frac{L_1 - L_0}{L_0} = \frac{h_1 - h_0}{h_0} \tag{3.5}$$

Where h_1 is the thickness of the samples at preparation, h_0 and h are the thickness of the free and fixed samples, respectively. Using h_0 and h measured and Eqs. (3.3)-(3.5), Poisson's ratio of NIPA gels is obtained and is shown in Fig. 3.5 as a function of temperature for four different ionic concentrations. Poisson's ratio shows negative values for all NIPA samples studied near the critical point.

After the first intersection, the sample is under stretching ($u_{xx} > 0$). As temperature is far from the transition, $u_{zz} < 0$, the sample stretches in x-y plane while its equilibrium dimension along z-direction shrinks, corresponding to a positive Poisson's ratio. As the temperature nears the phase transition, $u_{zz} > 0$, the sample expands in both x-y plane and z-direction. This yields the negative Poisson's values. It has been pointed out that near the volume phase transition point of a gel, its bulk modulus approaches zero while the shear modulus remains finite [10,7,9]. Therefore, near the critical point, K/G → 0, and $\sigma \rightarrow -1$. In fact, near the critical point, $\sigma = -1$ is directly responsible for the slowing down of volume change kinetics [11].

As shown in Fig. 3.5, Poisson's ratio shows a dip near T_c. This dip approaches to a larger negative number and shifts to a higher temperature as

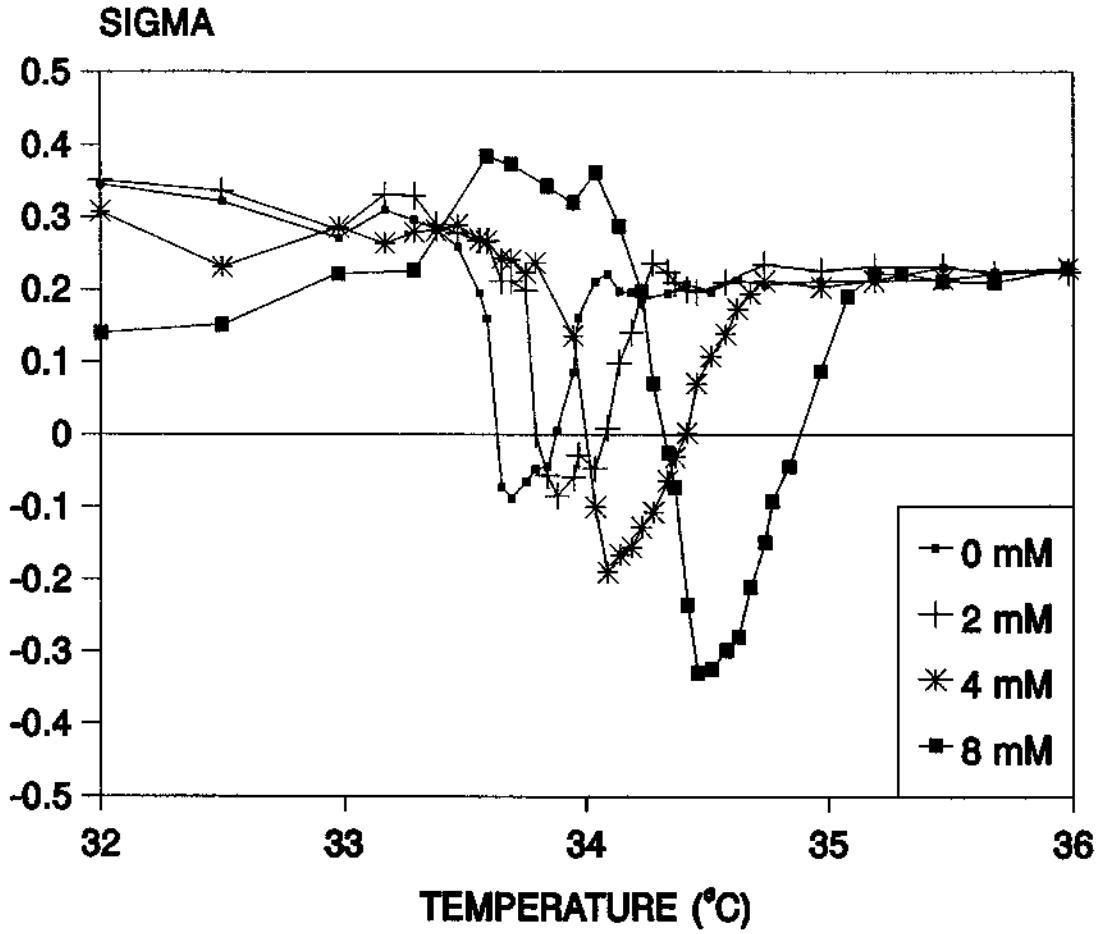

FIG. 3.5 Poisson's ratio of NIPA gels as a function of temperature for various sodium acrylate (NaAc) concentration: 0 mM, 2 mM, 4 mM, and 8 mM.

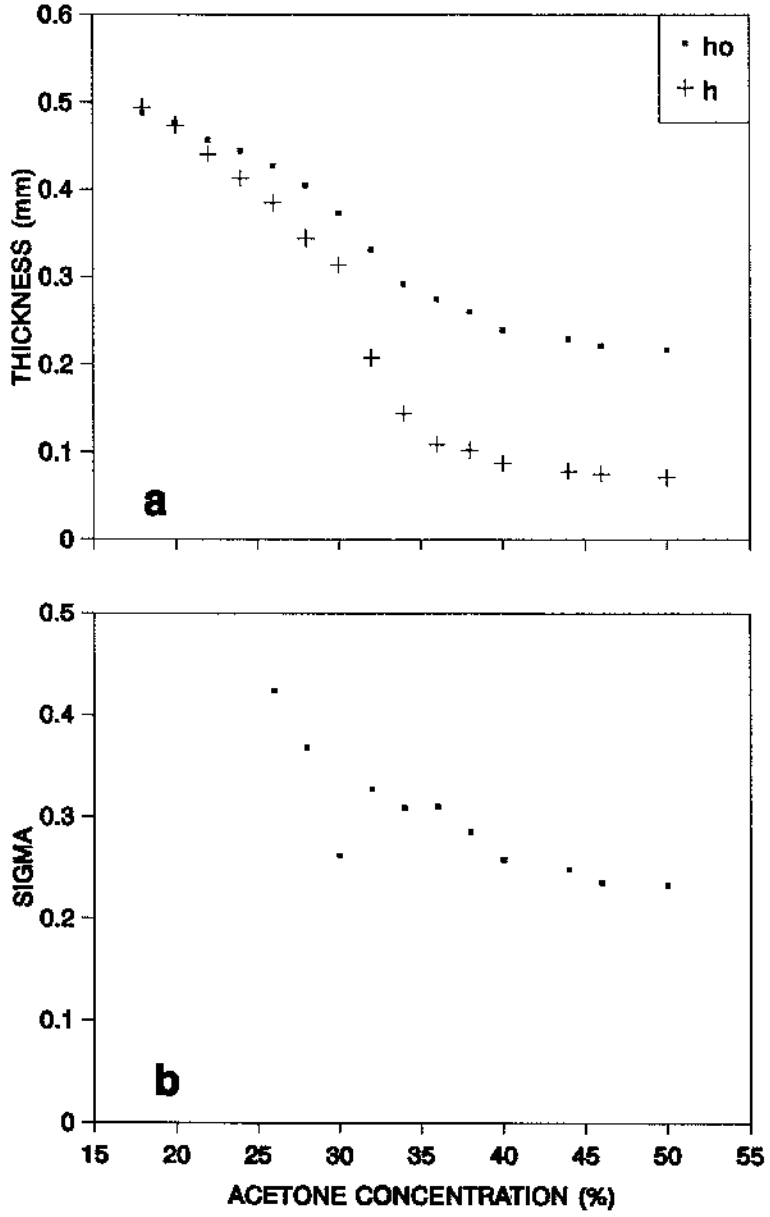

FIG. 3.6 (a) The thickness of free (h_0) and of constrained (h) PAAM gel films as a function of acetone concentration (%wt) in water/acetone mixture. The samples had a thickness (h_1) of 0.457 mm when been made. (b) The Poisson's ratio of the PAAM gel is plotted as a function of acetone concentration. No negative Poisson's ratio was observed near the transition concentration.

the ionic strength increases. The behavior of σ suggests that adding a small amount of ionic groups into NIPA gels moves the weakly discontinuous transition toward to continuous one. Furthermore, the ionization may also modify the polymer network, producing modulated structures [12]. This modification may also make the gel system closer to the critical point.

The thicknesses of free and constrained neutral PAAM gels were also measured as a function of acetone concentration in acetone/water mixture as shown in Fig. 3.6(a). The corresponding Poisson's ratio is plotted in Fig. 3.6(b). In contrast to NIPA gels, PAAM gels have only one intersection between h and h_0. Poisson's ratio is positive over the entire range measured as shown in Fig. 3.6(b). Poisson's ratio has no anomaly near the transition point, which is around 30% acetone concentration. This appears to indicate that the phase transition in PAAM and in NIPA may be quite different.

3.4 Theoretical calculation

3.4.1 Osmotic pressure of gels

According to Flory's theory of gels [8], with the proper modifications, the Helmholtz free energy F of an ionic gel can be separated into three parts: the mixing free energy F_m, the elastic free energy of the network F_e, and the electrostatic interaction free energy, F_i, i.e.,

$$F = F_m(\phi) + F_e(\alpha) + F_i(f) \tag{3.6}$$

and

$$F_m(\phi) = nTk[\ln(1-\phi) + \chi\phi) \tag{3.7}$$

$$F_e(\alpha) = (3/2)kTN[\alpha^2 - 1 - \ln\alpha] \tag{3.8}$$

$$F_{\chi}(f) = fkTMn\left(\frac{V_0\alpha^3}{nv_1}\right) \tag{3.9}$$

where χ is the polymer-solvent interaction parameter, k is the Boltzmann constant, T the absolute temperature, N the number of polymer chains, n the number of the solvent molecules, v_1 the molar volume of the solvent, f the number of counter ions per polymer chain, ϕ the polymer concentration (volume fraction), and α the equilibrium swelling ratio. The swelling ratio α is defined as

$$\alpha = \left(\frac{V}{V_0}\right)^{\frac{1}{3}} = \left(\frac{\phi_0}{\phi}\right)^{\frac{1}{3}} \tag{3.10}$$

with V as the volume of gel, V_0 as the gel volume and ϕ_0 the network volume fraction after the gelation takes place.

The equilibrium volume fraction of polymers can be obtained from the free energy by imposing an equilibrium condition. That is, the osmotic pressure on the gel network should be zero:

$$\Pi = -\frac{N_A}{v_1}\left(\frac{\partial F}{\partial n}\right)_{P,T} = 0. \tag{3.11}$$

where N_A is the Avogadro's number. Combining Eqs. (3.6)-(3.11), we obtain

$$\Pi = -\frac{N_A kT}{v_1}[\ln(1-\phi) + \phi + \chi\phi^2] + \frac{NkT}{V_0}\left[\left(f + \frac{1}{2}\right)\frac{\phi}{\phi_0} - \left(\frac{\phi}{\phi_0}\right)^{\frac{1}{3}}\right] \tag{3.12}$$

The first three terms of osmotic pressure correspond to the mixing energy, and the last two terms are the elastic contribution.

For polymer gel networks, the parameter χ is defined as [7]

$$\chi=\chi_1(T)+\chi_2\phi \tag{3.13}$$

and

$$\chi_1(T)=\frac{\delta h-T\delta s}{kT} \tag{3.14}$$

Where δh and δs are the changes of the enthalpy and entropy, respectively. It is impossible to calculate δh and δs theoretically. Therefore χ is an empirical parameter to be estimated from the swelling data.

3.4.2 Elastic moduli

The moduli of gels were measured in the equilibrium state. This means the osmotic pressure (π) of the gel network is zero (constant). The bulk (static) modulus K is defined as

$$K=[\phi(\frac{\partial\pi}{\partial\phi})_T]_{\pi=0} \tag{3.15}$$

From Eqs. (3.12) and (3.15) we obtain

$$K=\frac{RT}{v_1}[\frac{\phi^2}{1-\phi}-2\chi_1\phi^2-3\chi_2\phi^3]+\frac{NkT}{V_0}[(f+\frac{1}{2})\frac{\phi}{\phi_0}-\frac{1}{3}(\frac{\phi}{\phi_0})^{\frac{1}{3}}] \tag{3.16}$$

The shear modulus is given [8] by

$$G=(\frac{NkT}{2V_0})(\frac{\phi}{\phi_0})^{\frac{1}{3}} \tag{3.17}$$

From the Eq. (3.1) and the Eqs. (3.16) and (3.17), Poisson's ratio can be calculated.

3.4.3 Poisson's ratio calculation

TABLE 3.1 Parameters used in calculation

NaAc	f	$N/V_0(10^{19})$	ϕ_0	$\delta h(\times 10^{-14})$
0 mM	0.0	0.912	0.0725	12.463
2 mM	0.14	0.914	0.0727	12.463
4 mM	0.28	0.916	0.0728	12.470
8 mM	0.56	0.920	0.0731	12.474

In order to calculate Poisson's ratio using above theory, we need to set all the parameters. N and ϕ_0 can be estimated from the preparation of gels. The parameter ϕ is calculated from the swelling curves of free gels. And δh, δs, and χ_2 are derived from Hirotsu's paper [7], the parameters used in the calculation are shown in Table 3.1. The theoretical results of Poisson's ratio are shown in Fig. 3.7.

3.4.4 Comparison of calculated and experimental results

Comparing the experimental data and the calculated results of Poisson's ratio, we find that the theoretical calculation agrees qualitatively with the experimental observation. Both theory and experiment results show that Poisson's ratio exhibits negative value near the phase transition temperature. However, there is a disagreement about the absolute value of σ at $T > T_c$. From the experimental data, the value of σ is about 0.33 for $T < T_c$ and about 0.23 for $T > T_c$. This may be explained considering the flexibility of the polymer chains [13]. At high temperatures, the polymer chains of the shrunken gel are

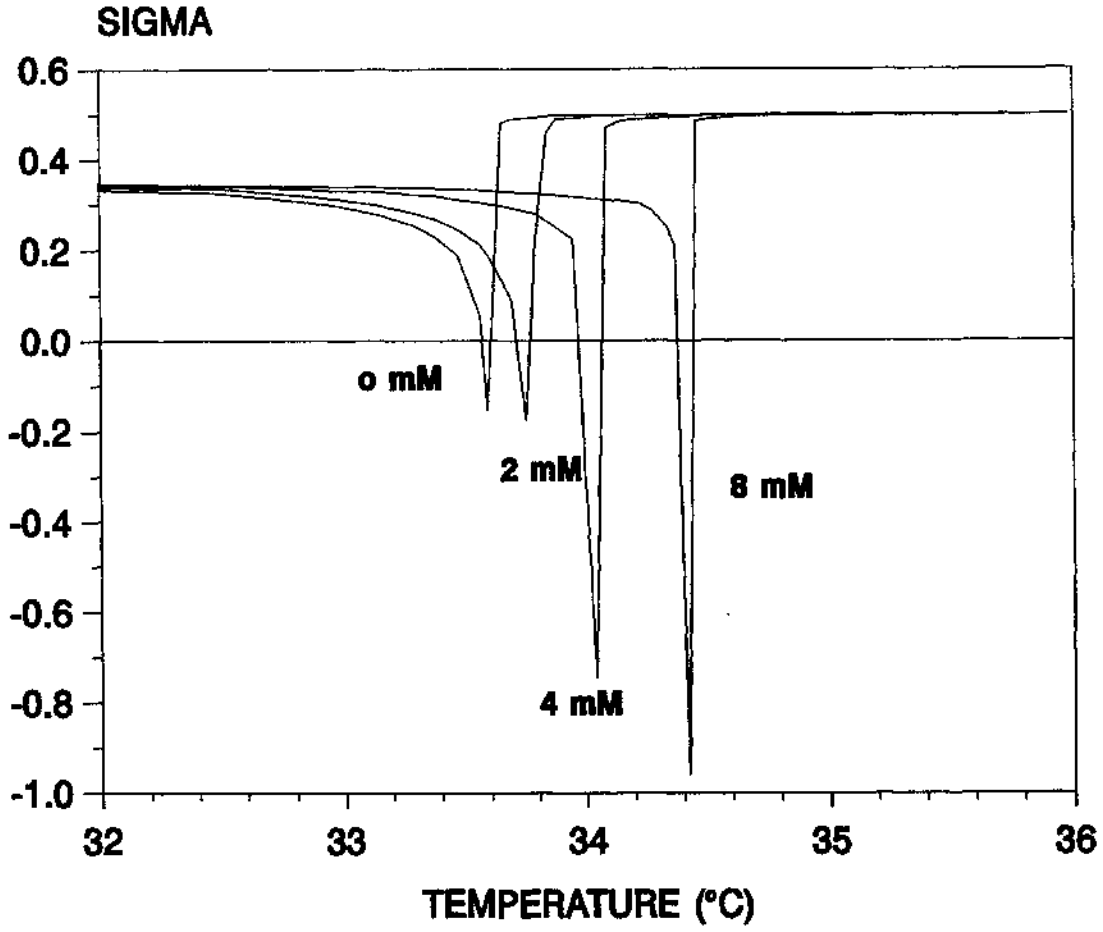

FIG. 3.7 Poisson's ratio (NIPA gel in various NaAc) calculated with the parameters in Table 3.1.

restricted near the crosslinking domains. Such restriction lowers the flexibility of the polymer chains, resulting in a decrease of σ. From the theoretical calculation, σ reaches about 0.5 for $T > T_c$, and disagrees with the experimental observation. The theory may need to be modified to include microscopic details of the polymer chains.

3.5 Summery

In conclusion, Poisson's ratio was obtained from the measurement of the swelling curves of free and constrained polymer gels. Poisson's ratio of NIPA gels exhibits a negative dip near the phase transition and position of the dip shifts to a higher temperature as ionic concentration increases. The theoretical simulations of Poisson's ratio is in a good agreement with the experimental results. In contrast to NIPA gels, Poisson's ratio of neutral PAAM gel shows no negative values throughout the measured transition region.

CHAPTER 3 REFERENCES

1. Y. Li, Z. Hu and C. Li, J. Appl. Polym. Sci., **50**, 1107(1993).
2. Y. Li and T. Tanaka, Ann. Rev. Mat. Sci. **22**, 243(1992).
3. L.D. Landau and E.M. Liftschitz, Theory of Elasticity (Pergamon, New York, 1986), Chapter 1.
4. Y. Li, Phys. Status Solidi **38**, 171(1976).
5. R. Lakes, Science **235**, 1038(1987).
6. K.W. Wojciechowski and A.C. Branka, Phys. Rev. A **40**, 7222(1989).
7. S. Hirotsu, Macromolecule **23**, 905(1990); J. Chem. Phys. **94**, 3949(1991).
8. P.J. Flory, Principles of Polymer Chemistry, Cornell University, Ithaca, New York, 1953.
9. S. Hirotsu and A. Onuki, J. Phys. Soc. Jpn. **58**, 1508(1989).
10. A. Onuki, Phys. Rev. A **38**, 2192(1988).
11. Y. Li and T. Tanaka, J. Chem. Phys. **92**, 15(1990).
12. S.J. Candau, F. Ilman, F. Schosseler, and J. Bastide, Mat. Res. Soc. Symp. Proc. **173**, 3(1990).
13. K. Urayama, T. Takigawa, and T. Masuda, Macromolecules **26**, 3092 (1992).

CHAPTER 4

THE SCALING EXPONENTS OF ACRYLAMIDE GELS

4.1 Introduction

The application of scaling methods to polymers in solution has led to some dramatic successes in both theoretical understanding and experimental applications [1,2]. It has been shown that many properties of gel networks exhibit scaling behavior [1,3], and that the origin of the gel scaling behavior can often be traced back to the scaling behavior of polymers in solution [1].

Topographically, a gel network system can be viewed as a summation of a polymer solution with crosslinking points. Assuming the osmotic pressure of the polymer solution is Π, then with the crosslinking points the swelling osmotic pressure, ω, of the gel can be written as [4]

$$\omega = \Pi - G \tag{4.1}$$

where G is the shear modulus of the network. The shear modulus is a direct consequence of crosslinking. It is well known [4] that for a non-ionic gel near equilibrium,

$$\Pi = G_e\left(\frac{\Phi}{\Phi_e}\right)^n, \tag{4.2}$$

$$G = G_e\left(\frac{\Phi}{\Phi_e}\right)^m, \tag{4.3}$$

where ϕ is the network concentration, and ϕ_e is its equilibrium value. The

proportionality constants for both Π and G are the same (G_e) since at equilibrium ($\phi = \phi_e$), $\omega = 0$. If we denote δ = n-m, then

$$\omega = G[(\frac{\Phi}{\Phi_e})^{\delta} - 1], \tag{4.4}$$

$$K = \Phi \frac{\partial \omega}{\partial \Phi} = G[n(\frac{\Phi}{\Phi_e})^{\delta} - m], \tag{4.5}$$

where K is the bulk modulus. At equilibrium, the above results yield $K_e = G_e(n-m)$, or,

$$\delta = \frac{K_e}{G_e} \tag{4.6}$$

Therefore, the ratio of (K_e/G_e) is directly related to the scaling exponent δ. Using the scaling behavior of Π of a semidilute polymer solution [2] and assuming m = 1/3, the scaling behavior of a gel system with different solvents can be proposed as follows:

	n	δ
Good	9/4	1.92
Marginal	2	1.67
Theta	3	2.67
Poor	∞	∞

The above results have been observed in various gel systems. It had been shown that the poly(vinyl acetate) (PVAc) gels in toluene and in acetone are good solvent systems with n $\sim$ 2.0-2.4 and m $\sim$ 0.34 [4]. Similar results were also obtained from poly(vinyl alcohol)/water [5] and polystyrene/benzene [6] systems. The theta condition can be achieved by varying the temperature of

PVAc/Iospropanol [7] or polystyrene/cyclohexane [8]. At theta temperature, n $\sim$3.0 and m $\sim$0.34 were obtained [7,8]. As the solvent condition becomes poorer, the value of n will increase. In the case of PVAc/Isopropanol at 25 ^{0}C, n = 13.3 [7].

Water in general is assumed to be a good solvent for polyacrylamide (PAAM) gel. Some recent studies have shown that the scaling behavior of dilute PAAM gel is quite universal [9] but less so at higher concentrations [10]. By using a simple linear elasticity theory, we have showed in Chapter 2 that the mechanical properties of gels can be probed by comparing the swelling behavior of constrained and free gels [11]. In this chapter, we investigate the scaling behavior of polyacrylamide and acrylamide-sodium acrylate copolymer gels in water using the same experimental technique.

4.2 Experimental

The gels used in this study were made by free radical polymerization. The details of the procedure were described in section 2.3.1. This chapter contains two parts. In first part, pure water is used as solvent. Three series of samples were made to study the concentration effects of repeating monomer unit (AAM), of crosslinkers (BIS), and the effect of degree of ionization (see Table 1). The first series (AAM-series) were made with varying amount of AAM (2.4% to 16.7%) and fixed amount of BIS (0.133g/100ml). The second series (BIS-series) were made with fixed amount of AAM (4.8%) but varying amount of BIS (0.045g/100ml to 0.5g/100ml, or 0.415 to 4.61 mol%, mol% is the number of BIS molecules per one hundred AAM molecules). The third series (NaAc-series), the sodium acrylate/acrylamide gels, were made with the amount of acrylamide fixed at 4.77%. The sodium acrylate (SA) varied from zero to

TABLE 4.1 The measured thicknesses of gel samples and the calculated exponent δ using Eq. (4.14). The sample thickness at preparation was 0.457 mm. In the first series of samples, the BIS concentration was fixed at 0.133g/100ml and the AAM concentration was varied. In the second series of samples, AAM = 5g/100ml and the BIS concentration was varied. In the last series, BIS = 0.133g/ml and AAM = 5g/100ml, the NaAc concentration was varied.

AAM	h_0	h		BIS	h_0	h		NaAc	h_0	h	
(%)	(mm)	(mm)	δ	(mol%)	(mm)	(mm)	δ	(mol%)	(mm)	(mm)	δ
2.4	0.593	0.725	1.97	0 415	0.636	0.79	1.68	0	0.529	0.597	2.09
2.9	0.576	0.678	1 77	0.553	0.609	0.73	1.62	0.125	0.536	0.606	1.94
3.4	0.548	0.624	1.79	0.691	0.577	0.685	1.86	0.252	0.543	0.613	1.77
3.8	0.525	0.587	2.02	0.876	0.558	0.649	1.91	0.503	0.556	0.624	1.51
4 3	0.521	0.578	1.99	0.968	0.545	0.628	2.04	0.630	0.578	0.642	1.25
4.8	0.534	0.608	2.10	1.11	0.534	0.609	2.15	1.01	0.599	0.668	1.19
5.7	0.538	0.623	2.31	1.23	0.523	0.586	2.14	1.51	0.646	0.730	1.11
6.5	0.540	0.630	2.40	1.38	0.514	0.568	2.16	2.01	0.709	0.818	1.08
7.8	0.553	0.661	2.44	1.57	0.507	0.556	2.29	2.52	0.765	0.933	1.18
9.1	0.562	0.680	2.39	1.75	0.498	0.549	2.47	3.28	0.817	1.014	1.16
10.7	0.570	0.714	2.77	1.94	0.495	0.533	2.41	4.04	0.899	1.169	1.20
12.3	0.589	0.746	2.48	2.12	0.491	0.526	2.54	4.79	0.965	1.30	1.23
14.5	0.599	0.775	2.55	2.40	0.483	0.510	2.63	5.79	1.042	1.475	1.28
16.7	0.615	0.836	2.89	2.67	0.480	0.505	2.85	6.80	1.117	1.558	1.20
				2.95	0.475	0.494	2.78	7.82	1.156	1.642	1.21
				3.23	0.472	0.487	2.60	9.33	1.199	1.755	1.24
				3.69	0.470	0.484	2.94	10.84	1.255	1.869	1.25
				4.15	0.469	0.482	2.98	12.35	1.303	1.971	1.25
				4 61	0.469	0.481	2.63				

12.35 mol% relative to AAM concentration. The second part of this chapter investigated the salt solution effect of polyelectrolyte (ionic acrylamide) gels.

4.3 Results and discussion

As defined in Chapter 2, the final thickness of the free and constrained gels are h_e and h, respectively. Using $L_1/L_e = h_1/h_e$, we have

$$\frac{\phi}{\phi_e} = \frac{h_e L_e^2}{h L_1^2} = \frac{h_e^3}{h h_1^2}, \tag{4.7}$$

where L is the length of the gel side. The gel deformation from the reference state to the constrained state can be achieved by two imaginary steps (see Fig 2.1). First, the reference state is isotropically shrunk by a factor of $(V/V_e)^{1/3} = (\phi_e/\phi)^{1/3}$, i.e., L_e shrinks to $L_2 = L_e(\phi_e/\phi)^{1/3}$ and h_e shrinks to $h_2 = h_e(\phi_e/\phi)^{1/3} = (hh_1^2)^{1/3}$. The subscript "2" denotes the imaginary state. The change from the intermediate state to the final state is a pure shear deformation and can be characterized by

$$\lambda \equiv \frac{L_1}{L_2} = \left(\frac{h_1}{h}\right)^{\frac{1}{3}} \tag{4.8}$$

Notice that since the constraint is equivalent to an x-y plane compression, λ, which is the deformation in the x-y plane, is the conjugate variable of the compression.

Using elasticity theory, it can be shown [11] that the strain components u_{xx} and u_{zz} of the fixed gels relative to their free states are equal to

$$u_{xx} = \frac{P}{3}\frac{3K+4G}{6KG} \tag{4.9}$$

$$u_{zz} = -\frac{P}{3}\frac{3K-2G}{3KG} \tag{4.10}$$

The relative change of volume is equal to

$$\frac{\Delta V}{V} = 2u_{xx} + u_{zz} = \frac{2P}{3}\frac{1}{K} \tag{4.11}$$

Therefore, as far as volume change is concerned, the two dimensional compression pressure P is equivalent to an isotropic pressure of 2P/3. The gel volume change is a result of this pressure. By equating the gel swelling pressure ω (Eq. 4.4) to 2P/3, we have

$$\frac{2P}{3} = G[(\frac{\phi}{\phi_e})^{\delta} - 1]. \tag{4.12}$$

The pure shear deformation after the volume change is characterized by the shear modulus. Using Mooney-Rivlin's definition [12], the shear modulus of an elastomer under two dimensional compression is

$$G = \frac{P}{\lambda^{-5} - \lambda} \tag{4.13}$$

(Mooney-Rivlin's equation normally quoted is the case of uniaxial elongation where $G = P/(\lambda - \lambda^{-2})$, with λ the ratio of elongation.) Combining Eqs.(4.12) and (4.13), we have

$$\delta = \ln[\frac{2}{3}(\lambda^{-5} - \lambda) + 1]/\ln(\frac{\phi}{\phi_e}) \tag{4.14}$$

4.3.1. Effect of monomer concentration

In this experiment, the concentration of AAM (C_{AAM}), was varied from 1.98% to 16.7% while the crosslink (BIS) concentration was fixed at

0.133g/100ml of water. No sodium acrylate was added and therefore these are non-ionic gels. The pre-gel solution with 1.98% AAM did not form a gel due to the low concentration of AAM.

The swelling ratio of these gels as a function of AAM concentration is shown in Fig. 4.1(a). As AAM concentration is increased, the volume of the gel decreases first, reaching a minimum at 4.3%, then starts to increase linearly. This behavior has been checked several times in our lab and was found to be reproducible. This phenomenon can be explained using the sol-gel transition concept. The fact that the 1.98% AAM pre-gel solution did not form a gel but the 2.44% one did indicates that the sol-gel transition point is between $C_{AAM} = 1.98\%$ and 2.44%. In other words, the 2.44% sample is very close to the sol-gel transition point. As we know, at this point, the network is barely connected and can swell to a very large extent. As the AAM concentration is increased, the connectivity of the network improves rapidly, causing the degree of swelling to decrease. At certain AAM concentration, the network will be well connected and any further increase in AAM will contribute mostly to the length of the chains between crosslinking molecules. This will cause the equilibrium volume to increase. For $C_{AAM} > 4.3\%$, the swelling ratio can be fitted to

$$\frac{V_e}{V_1} = 1.17 + 7.7 C_{AAM} \tag{4.15}$$

The network concentration at equilibrium is

$$\phi_e = \phi_1 \frac{V_1}{V_e} \approx \frac{C_{AAM}}{1.17 + 7.7 C_{AAM}}, \tag{4.16}$$

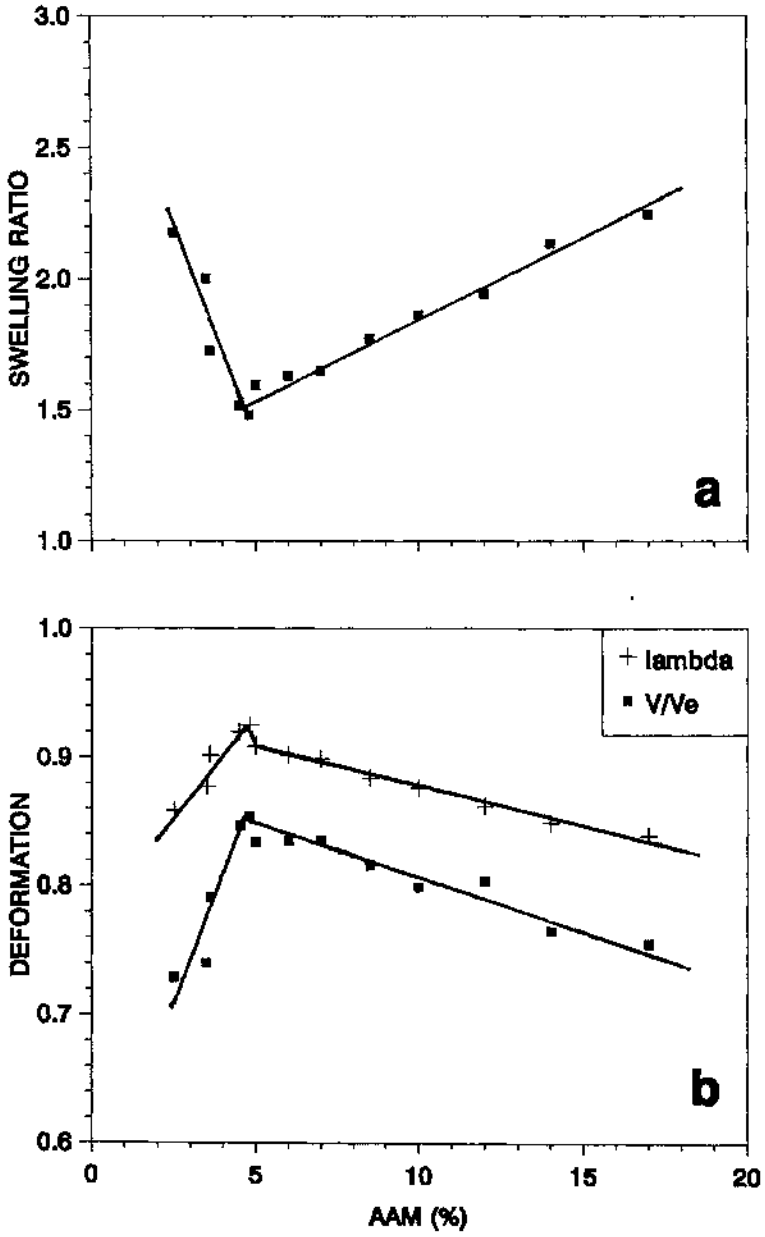

FIG. 4.1 (a) The acrylamide concentration dependence of the swelling ratio of free gels. The data can be fitted by two straight lines. (b) The shear (plus) and bulk (solid squares) deformations of constrained gels as a function of acrylamide concentration.

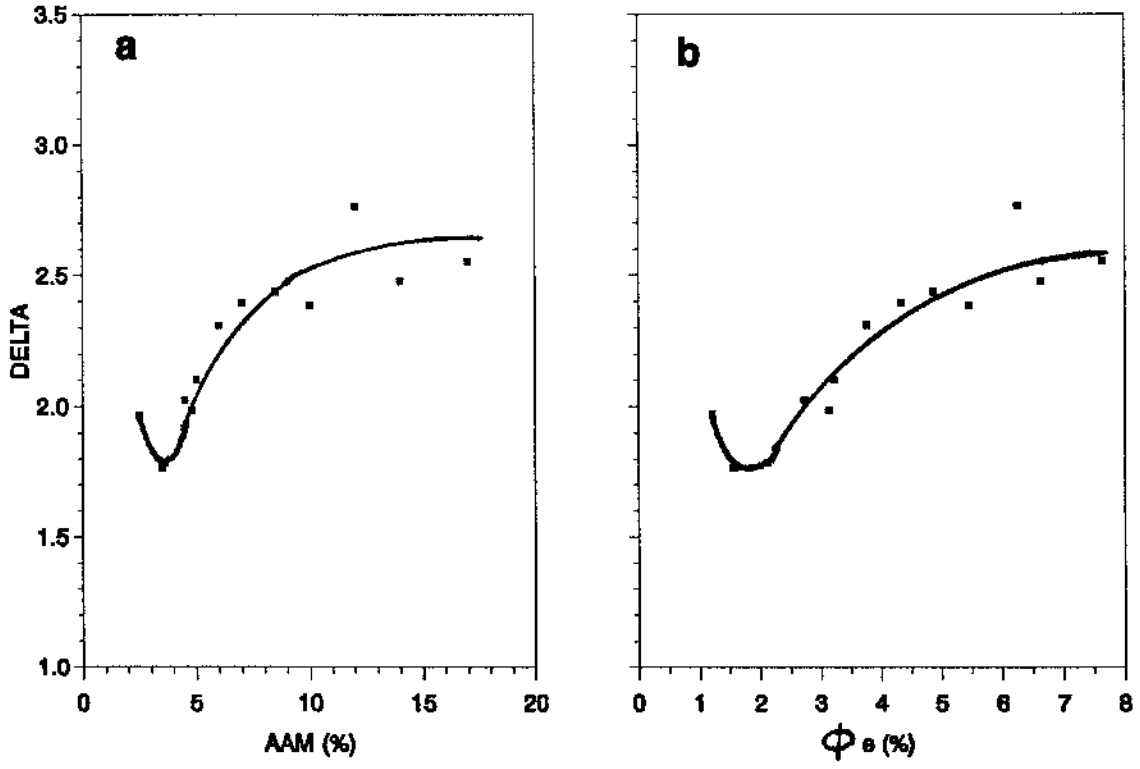

FIG. 4.2 The scaling exponent δ as a function of AAM concentration (a) and equilibrium network concentration (b).

where ϕ_1 is the network concentration at preparation. This result indicates that as C_{AAM} increases, ϕ_e increases as well. Relative to their corresponding free gels, the constrained gels are deformed both in volume and in shape. The degree of these deformations can be characterized by (V/V_e) (Eq. 4.7) and λ (Eq. 4.8), respectively, as shown in Fig. 4.1(b). The maxima of these curves at 4.3% are related directly to the swelling minimum in Fig. 4.1(a). The degrees of shear deformation λ and bulk deformation V/V_e are in the range of $0.86 < \lambda < 1$ and $0.72 < (V/V_e) < 1$, respectively. These ranges are quite small compared with the ranges PVAc and PAAM experienced in the mechanical measurements by others, [4,9] which typically have the range of $0.7 < \lambda < 1$ and $0.3 < (V/V_e) < 1$.

Using Eq. (4.14) and measured thicknesses of gel samples (compiled in Table 4.1), the exponent δ was calculated. The acrylamide monomer concentration dependence of δ is presented in Fig. 4.2(a). As the monomer concentration C_{AAM} is increased, the exponent increases and approaches 2.7, which corresponds to the theta point value. Figure 4.2(b) shows the network concentration dependence of δ. Clearly, the higher the network concentration, the higher the exponent δ, or, K_e/G_e. This can be explained based on the scaling behavior of semidilute polymer solution. As the concentration increases, the inter-chain interaction increases. This increase reduces the excluded volume effect, pushes the system toward the theta point [1,2]. This is consistent with the correlation length measurement from polystyrene/cyclohexane gel system [13].

4.3.2 Effect of crosslink concentration

In this experiment, the acrylamide monomer concentration was fixed at 4.77%, with no sodium acrylate added (non-ionic gels). The range of BIS is

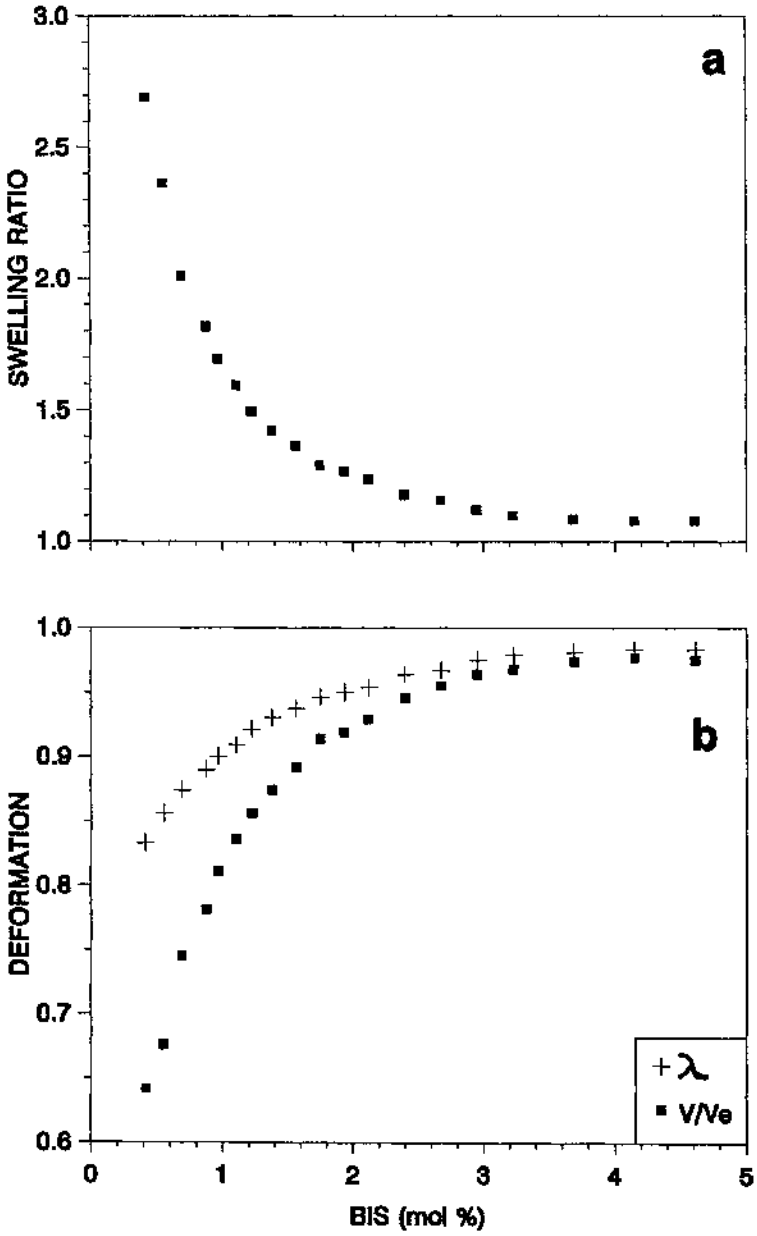

FIG. 4.3 (a) The crosslink concentration dependence of the swelling ratio of free gels. (b) The shear (plus) and bulk (solid squares) deformations of constrained gels as a function of BIS concentration.

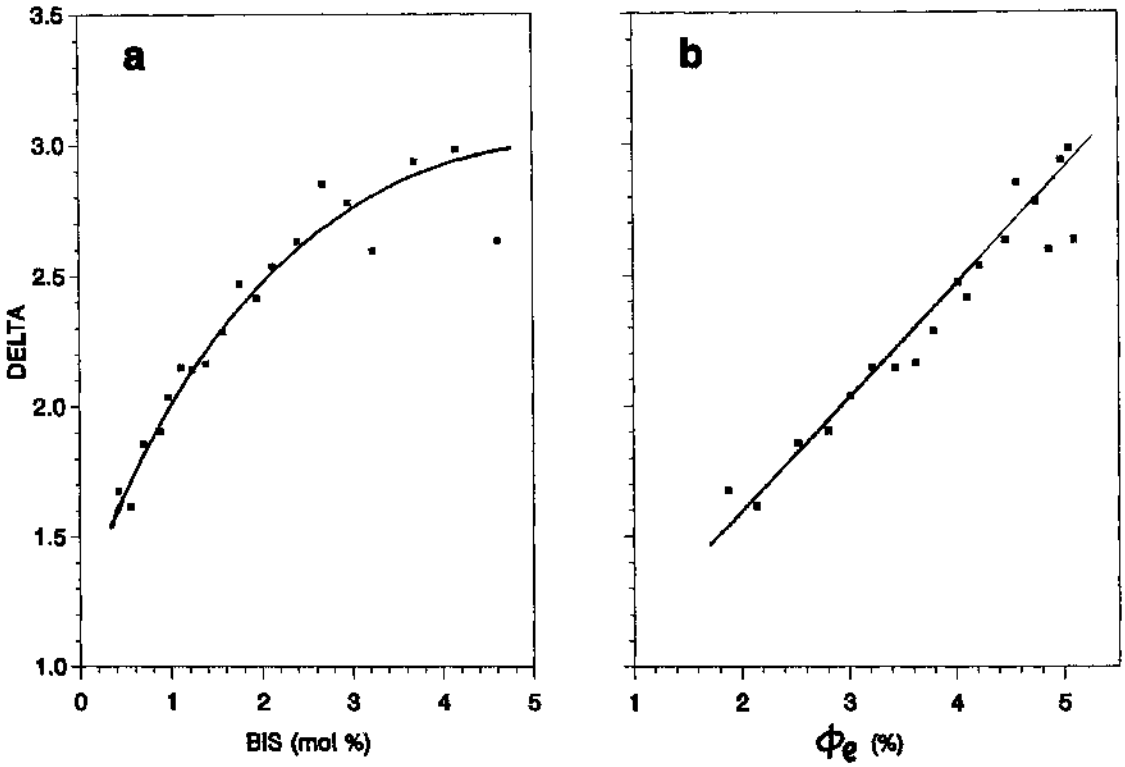

FIG. 4.4 The scaling exponent δ as a function of BIS concentration (a) and equilibrium network concentration (b). Away from the sol-gel point, the δ appears to be linearly related to the network concentration ϕ_e.

from 0.42mol% to 4.62mol%. As expected, the swelling ratio (V_e/V_1) of free gel films decreases as the concentration of crosslinking molecules is increased (Fig. 4.3(a)). Except the two samples with the lowest BIS concentrations, the range of the deformations (Fig. 4.3(b)) is similar to the range in AAM series measurement.

Fig. 4.4(a) shows that the exponent δ increases as the crosslinking (BIS) concentration increases. The range of δ indicates that the system continuously varies from a good solvent condition into a theta solvent condition and then into a slightly poor solvent condition. This can be understood based on the fact that the crosslinking molecule (BIS) is highly hydrophobic. As BIS is increased, the hydrophobicity of the network increases, resulting in decrease of the solvent quality.

In the case of AAM-series measurement, the dependence of δ on the network equilibrium concentration is non-linear (Fig. 4.2(b)). However, in the BIS series, Fig. 4.4(b) shows a linear dependence of δ on gel equilibrium network concentration,

$$\delta = 0.71 + 46\phi_e. \qquad (4.17)$$

4.3.3 Weakly ionized gels

The ionic gels were made by fixing the AAM and BIS concentration at 4.8% and 1.23 mol%, respectively. For gels with low concentration of ionic groups (less than 0.5 mol%, or less than one ionic group per two hundred repeating monomer units), the system is primarily a non-ionic gel perturbed by the small amount of ionic groups present in the network. Figure 4.5(a) shows

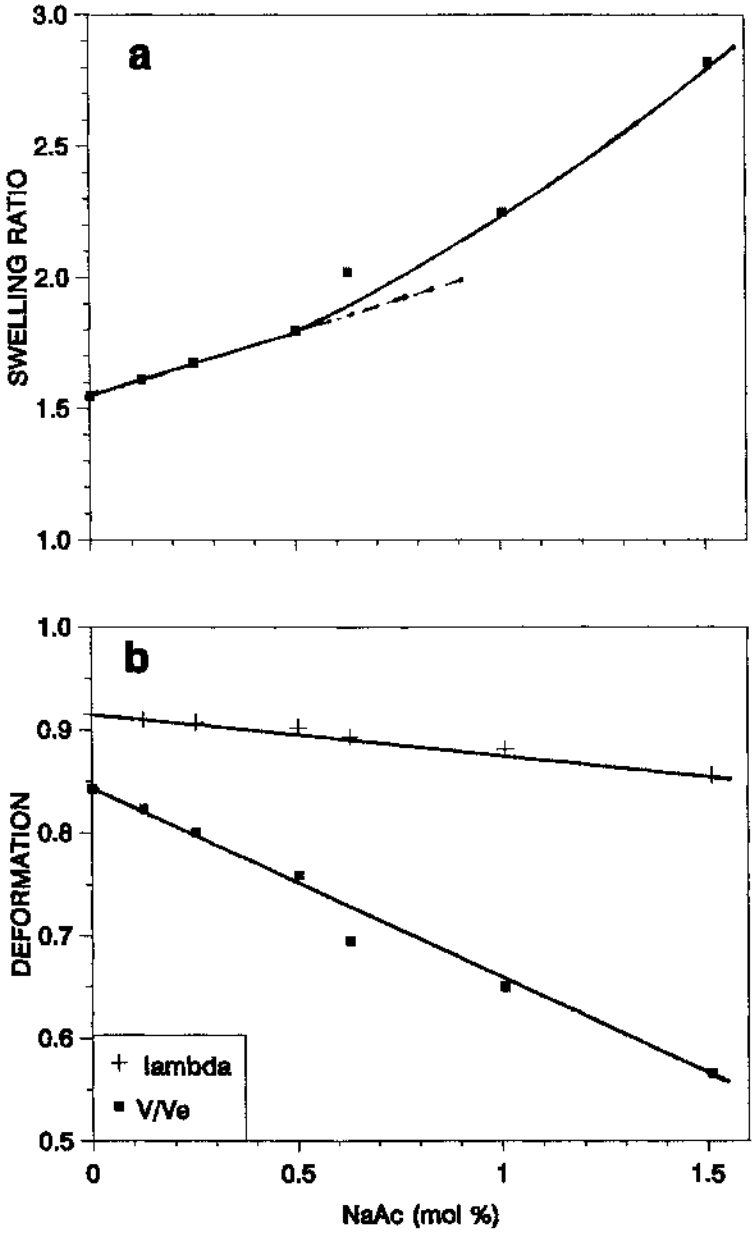

FIG. 4.5 The effect of low concentration of ionic groups on swelling ratio of free gels (a) and deformations of constrained gels (b).

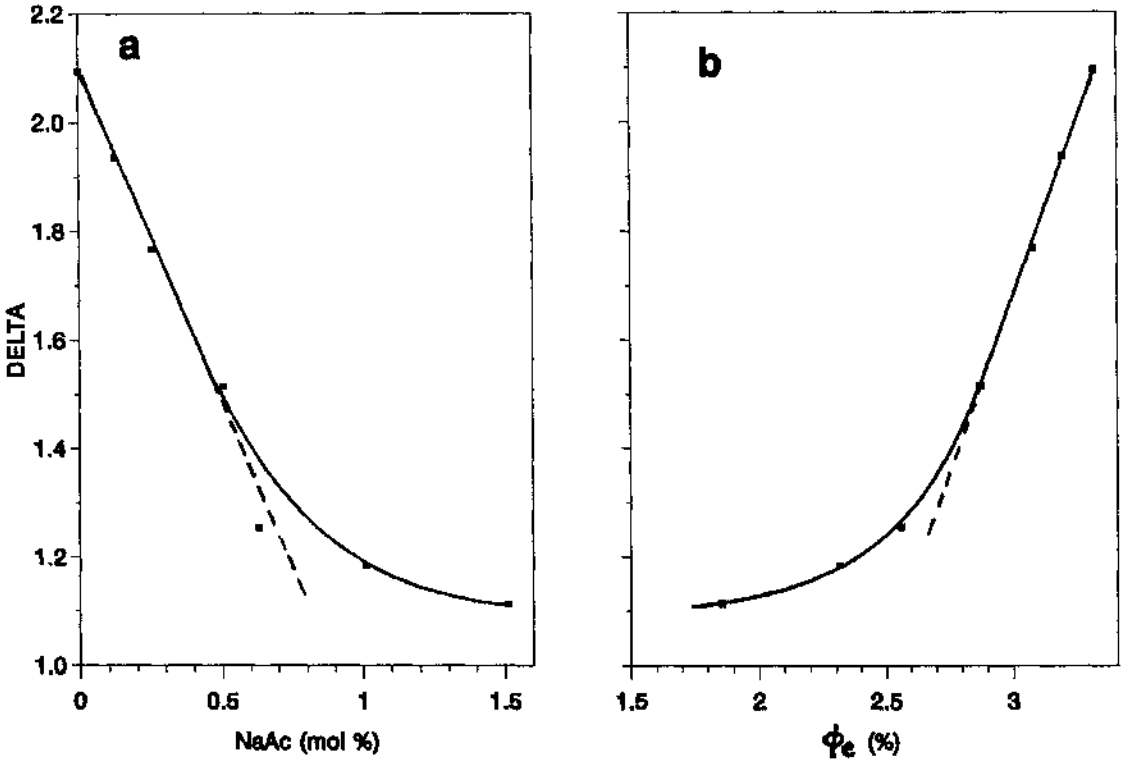

FIG. 4.6 The scaling exponent δ as a function of NaAc concentration (at low level) (a) and network concentration (b). With even a small amount of NaAc, the δ decreases dramatically.

the degree of swelling as a function of sodium acrylate concentration. In the low sodium acrylate concentration region (C_{SA} < 0.5 mol%), we have

$$\frac{V_e}{V_1} = 1.55 + 70 C_{SA}. \tag{4.18}$$

If we use the zero ionic concentration gel ($V_e(C_{SA}=0) = 1.55V_1$) as reference, then

$$\frac{\phi_e}{\phi_{e,0}} = \frac{1}{1+45 C_{SA}} \tag{4.19}$$

where $\phi_{e,0} = \phi_e(C_{SA}=0)$ is the equilibrium concentration of the non-ionic gel. Assuming that in the low ionic concentration region, the gel network structure is approximately the same as the zero ionic concentration gel, the only effect of the ionic groups is to apply an extra osmotic pressure, Π_{ion}, to the network. Using Eq. (4.1), we obtain

$$-\frac{\Pi_{ion}}{G_{e,0}} = \left(\frac{\phi_e}{\phi_{e,0}}\right)^n - \left(\frac{\phi_e}{\phi_{e,0}}\right)^m, \tag{4.20}$$

where $G_{e,0}$ is the shear modulus of the non-ionic gel. Substituting Eq. 4.19 in the above equation, we have

$$\frac{\Pi_{ion}}{G_{e,0}} \approx 45\delta C_{SA}. \tag{4.21}$$

Therefore, the contribution of one mol% of ionic groups to gel swelling osmotic pressure is comparable to the shear modulus of the gel in magnitude. This result suggests that in order to treat the effects of ionic groups as small perturbations, the concentration of the ionic groups has to be much lower than 1 mol%.

As indicated in Fig. 4.5(b), the deformations of weakly ionized gels are fairly small. Using Eq. (4.14), the exponent δ is calculated and shown in Fig. 4.6(a) and 4.6(b) as functions of NaAc concentration and free gel equilibrium network concentration, respectively. Dramatic reduction in δ value was observed as ionic groups are introduced into the network,

$$\delta = 2.09 - 133 C_{SA}. \tag{4.22}$$

The concentration dependence of δ is

$$\delta = 2.09 - 138(0.0315 - \phi_e). \tag{4.23}$$

The slope (1.38) of the ϕ_e dependence of weakly ionized gels is much bigger than that (0.46) of that of BIS controlled non-ionic gels.

4.3.4 Highly ionized gels

The degree of swelling and deformations for highly ionized gels are shown in Fig. 4.7. The AAM and BIS concentration of these samples were 4.77% and 1.23 mol%, respectively. The dominant swelling osmotic pressure is no longer the mixing term but a term arising from electrostatic interactions of the system. The swelling osmotic pressure is a combination of this term and the term from the crosslink effect. Assuming near equilibrium, the concentration dependence of these terms are characterized by exponents x and y, respectively, then

$$\omega = G_e[(\frac{\phi}{\phi_e})^x + (\frac{\phi}{\phi_e})^y]. \tag{4.24}$$

Notice here that G_e may be quite different from that of the non-ionic gels. As we have done earlier, define $\delta = x - y$, then $\delta = K_e/G_e$.

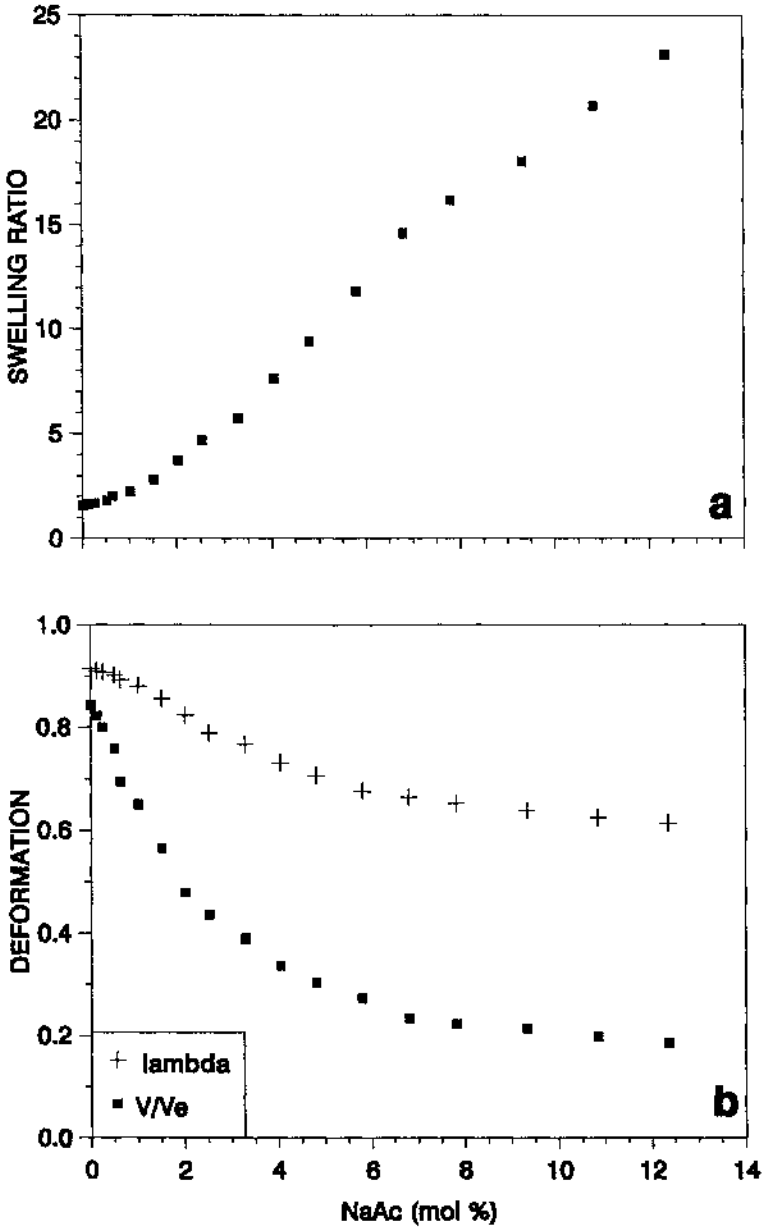

FIG. 4.7 The effect of ionic groups on swelling ratio of free gels (a) and deformations of constrained gels (b).

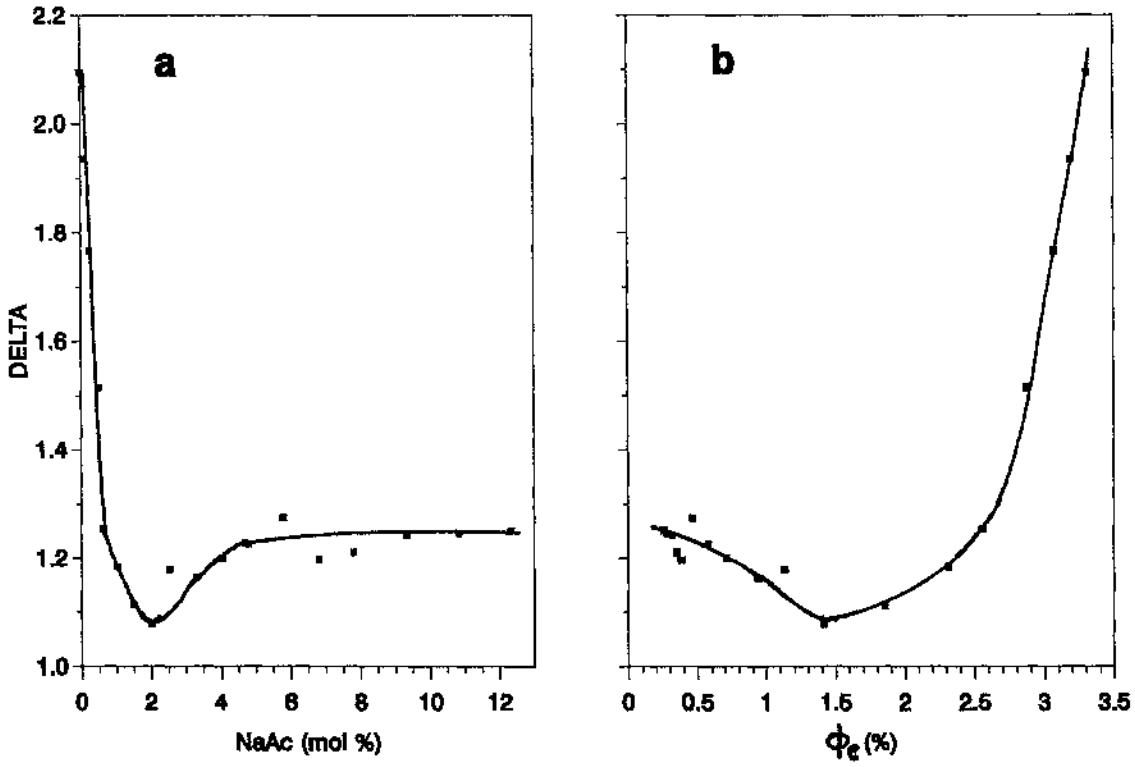

FIG. 4.8 The scaling exponent δ as a function of NaAc concentration (a) and network concentration (b). A plateau ($\delta_{plateau} \approx 1.25$) exists for samples with high NaAc concentration.

As shown in Fig. 4.8(a), the exponent δ decreases dramatically and then reaches a plateau ($\delta \approx 1.25$) when the amount of ionic groups is increased. Since the exponent y is a crosslink effect, it is conceivable that it is not affected by the ionic groups, i.e., $y \approx 1/3$. With this assumption, we have $x \approx 1.6$. That is, for a given ionic gel, the network concentration dependence of the ionic osmotic pressure Π is

$$\Pi \sim \phi^{1.6}. \tag{4.25}$$

Recall that in Flory's ideal-gas approximation, the ionic osmotic pressure is proportional to the concentration of the ionic groups, or, $\Pi \sim \phi$.

There appears to be a minimum near NaAc $\approx$ 2 mol%. Using similar argument, $\Pi \sim \phi^{1.4}$ at the minimum. As the NaAc concentration was further increased from this concentration,

swelling patterns started to appear on the surface of the fixed gels. It is not clear at this moment how the surface patterns affect the data analysis.

Fig. 4.8(b) shows the concentration dependence of δ. For $\phi_e > 1.5\%$, the slope is positive, which is similar to the observations we have made from the non-ionic gels. However, for $\phi_e < 1.5\%$, the slope appears to be negative.

4.3.5 Discussion

Figure 4.9 presents the equilibrium network concentration dependence of δ for all three series of gels. Depending upon the way the concentration is varied, the exponent δ has different behavior. As a general trend, the higher the network equilibrium concentration, the higher the exponent δ. The δ of BIS samples has a steeper slope than the AAm samples. The addition of ionic groups, even at very low dosage, reduces δ dramatically.

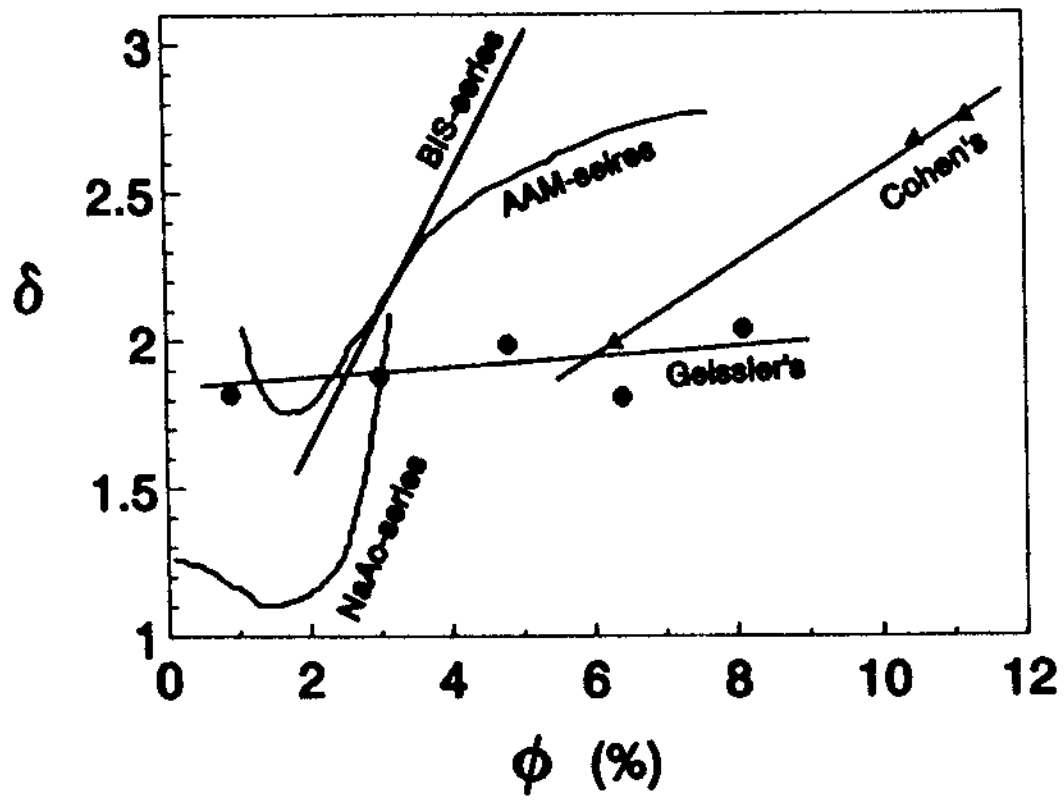

FIG. 4.9 The scaling exponent δ as a function of network concentration of free gels at equilibrium, together with results from Geissler, et al. [9] and Cohen, et al. [10]. For the sake of clarity, the fitting curves of our data are plotted. The exponent δ has different final equilibrium concentration dependence, depending upon the chemical ingredient. In general, the higher the network concentration, the higher the δ.

The results obtained by Geissler, et al. [9] and Cohen, et al. [10] are also included in Figure 4.9 for comparison. The slope of the result of Cohen, et al appears to be between the ones of BIS-series and AAM-series. The samples Cohen et al. used were made with the ratio of AAM/BIS fixed whereas in our case the AAM and BIS were fixed separately. Taking this into consideration, the slope of our result appears in agreement with the slope of Cohen's, et al. The samples Geissler et al. used were made similar to the ones Cohen et al. used. However, the results are quite different from Cohen's et al. All results are qualitatively in agreement in the sense that δ increases as the network concentration increases.

The weakly ionized gels appear to have the strongest network equilibrium concentration dependence. The value of δ falls far below non-ionic gels even for very low concentration of ionic groups.

4.4 Effect of Salt Concentration on Ionic Gels

4.4.1 Theoretical Prediction

In this section, we are going to discuss the scaling properties of ionic acrylamide (polyelectrolyte) gels in salt solvent. Although there is a lack of direct study of the mechanical properties of polyelectrolyte gels, the osmotic pressure of polyelectrolyte solutions is well understood. There are several length scales that are important to the behavior of a polyelectrolyte solution. They are the ionic group spacing A of the polymers, Debye-Huckle screening length κ^{-1} (solvent ionic strength), and Bejumme length Q. Odijk [14] proposed to consider polyelectrolytes as worm-like chains with total persistence length L_t, which equals to the summation of polymer intrinsic persistence length L_p and the electrostatic contribution L_e, i.e.,

$$L_t = L_p + L_e = L_p + \frac{Q}{4\kappa^2 A^2 f^2} \tag{4.26}$$

where f is ion condensation factor. The osmotic pressure of the solution is

$$\Pi \sim (L_t/\kappa)^{3/4}(AC)^{9/4}, \tag{4.27}$$

where C is the monomolar concentration of the polymer in solution. In pure water (without added salt), $\kappa^2 = 4\pi AC$ and $L_t \sim L_e$,

$$\Pi \sim C^{9/8}. \tag{4.28}$$

With excess salt, $\kappa^2 (= 8\pi QA)$ is independent of C and

$$\Pi \sim C^{9/4} \tag{4.29}$$

Recently, Wang and Bloomfield have successfully applied the renormalization group theory to study semidilute polyelectrolyte solutions, such as poly(styrene sofonate) [15]. They found that the existing experimental results agree well with theoretical predictions (Eqs 4.28 and 4.29) over a wide range of salt concentration, polymer molecular weight, and polymer concentration.

Given these polyelectrolyte solution results, it is interesting to see how the corresponding polyelectrolyte gels behave. Assuming the exponent m of polyelectrolyte gel is 1/3, then from Eqs (4.28), (4.29) and the relation $\delta = n\text{-}m$, we can obtain the theoretically predicted exponent δ. In Table 2, these results are tabulated for polyelectrolyte gels together with non-polyelectrolyte gels for comparison.

As shown in the following table, for polyelectrolyte in pure water, δ = 0.8. Once excess amount of salt is added, the δ value is expected to be equal

to 1.92. There is no theory at this moment that predicts the transition between no salt and excess amount of salt.

Table 4.2 The δ value of non-ionic and ionic gels in water with and without salt.

	Non-ionic Gel			Ionic Gel		
	n	m	δ	n	m	δ
Without salt	9/4	1/3	1.92	9/8	1/3	0.8
With excess salt	9/4	1/3	1.92	9/4	1/3	1.92

4.4.2 Results and discussion

The behavior of exponent δ in ionic acrylamide gels in pure water is discussed in section 4.3. At NaAc concentration of 2 mol%, the exponent δ reaches its lowest value of 1.08, this means that the n is equal to 1.4 (assuming m = 1/3). This result apparently is approaching the theoretical result of n = 1.12 [15,16].

As simple salt is added to the solvent, the screening effect reduces the electrostatic interaction dramatically. As has been argued by Odijk [14], with sufficiently high salt concentration, the osmotic pressure of polyelectrolyte solutions should behave like non-polyelectrolyte [15]. Fig. 4.10 compares the δ as a function of NaAc concentration with and without salt added. With 0.01 molar salt added to the solvent, the δ values are raised to 1.75.

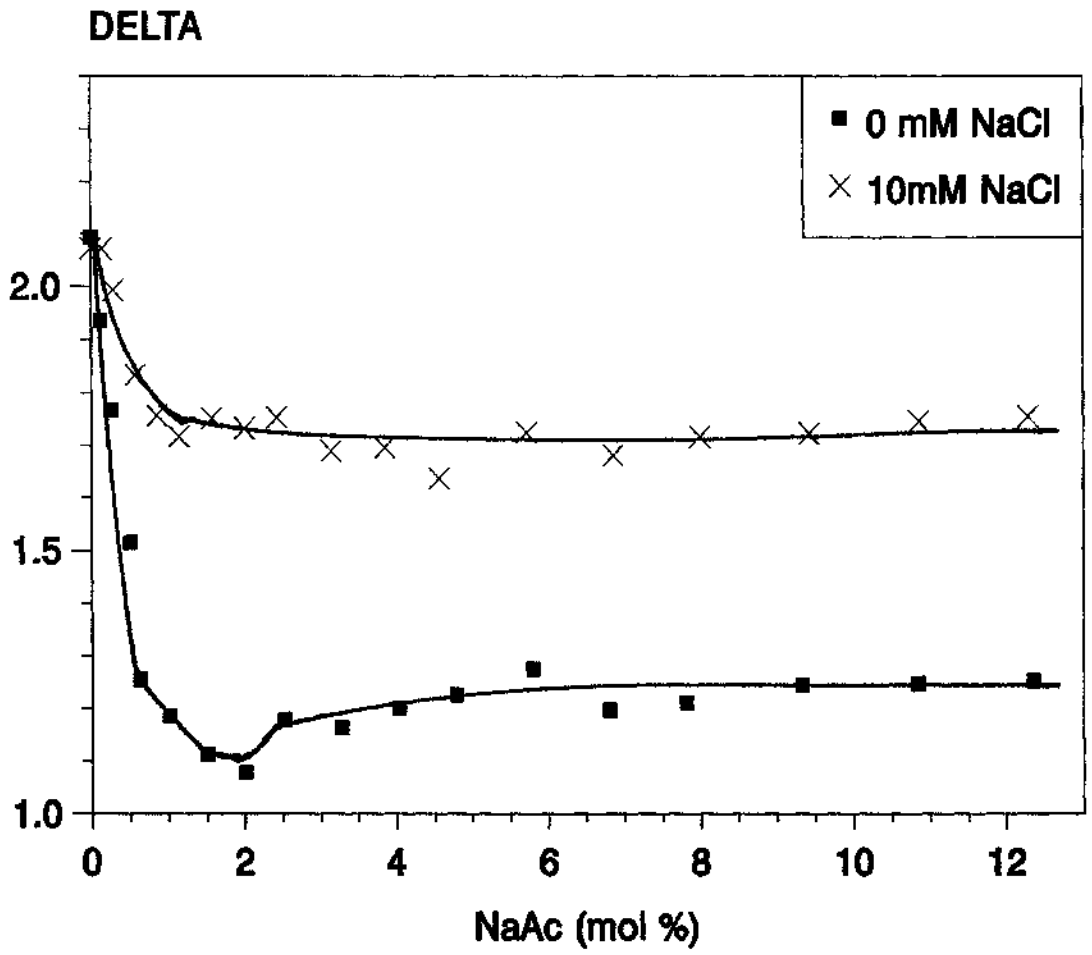

FIG. 4.10 A comparison of the value of δ in water and aqueous salt solution. The δ value recovers to a much higher level.

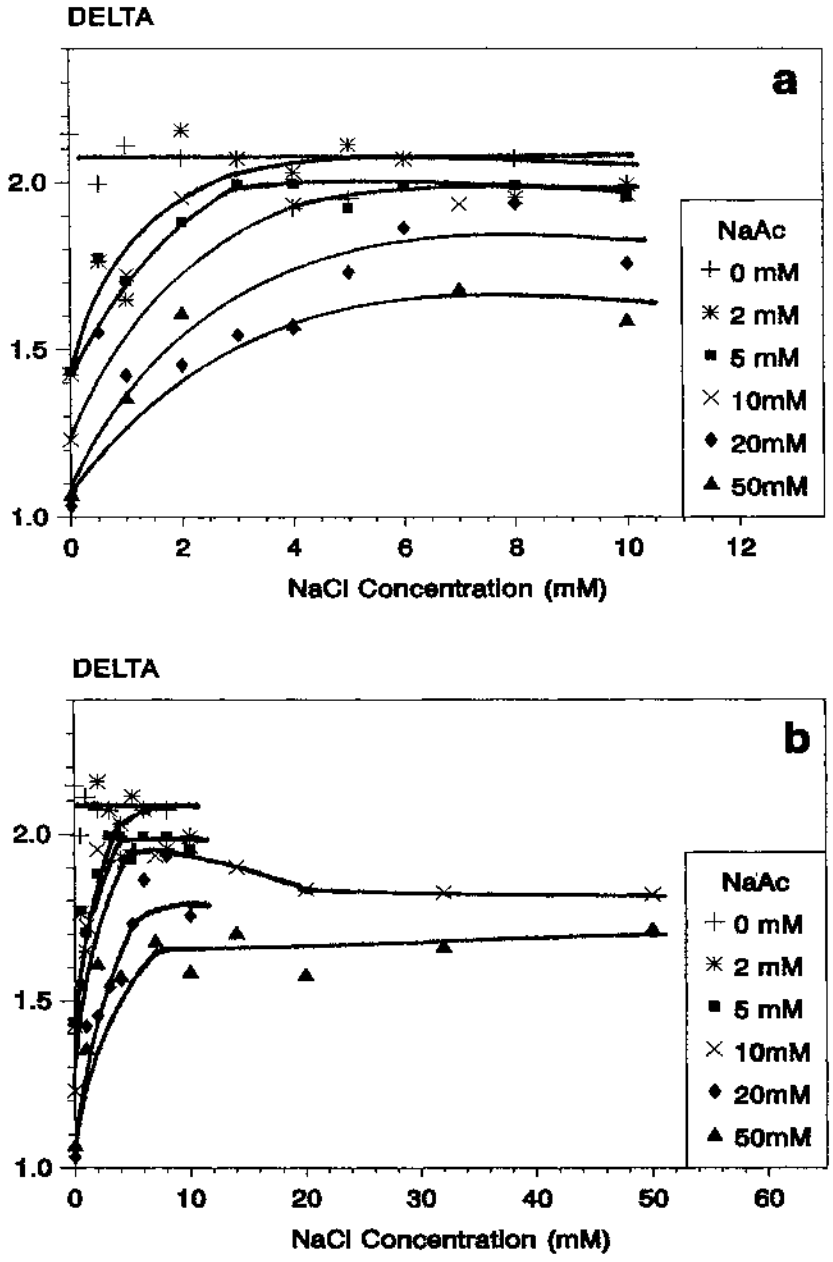

FIG. 4.11 The exponent δ as functions of salt concentration for gels of different degree of ionization. (a) In this salt concentration region, all samples reaches a plateau. (b) As the salt concentration is increased further, the δ values of different ionic gels converge asymptotically to the same value.

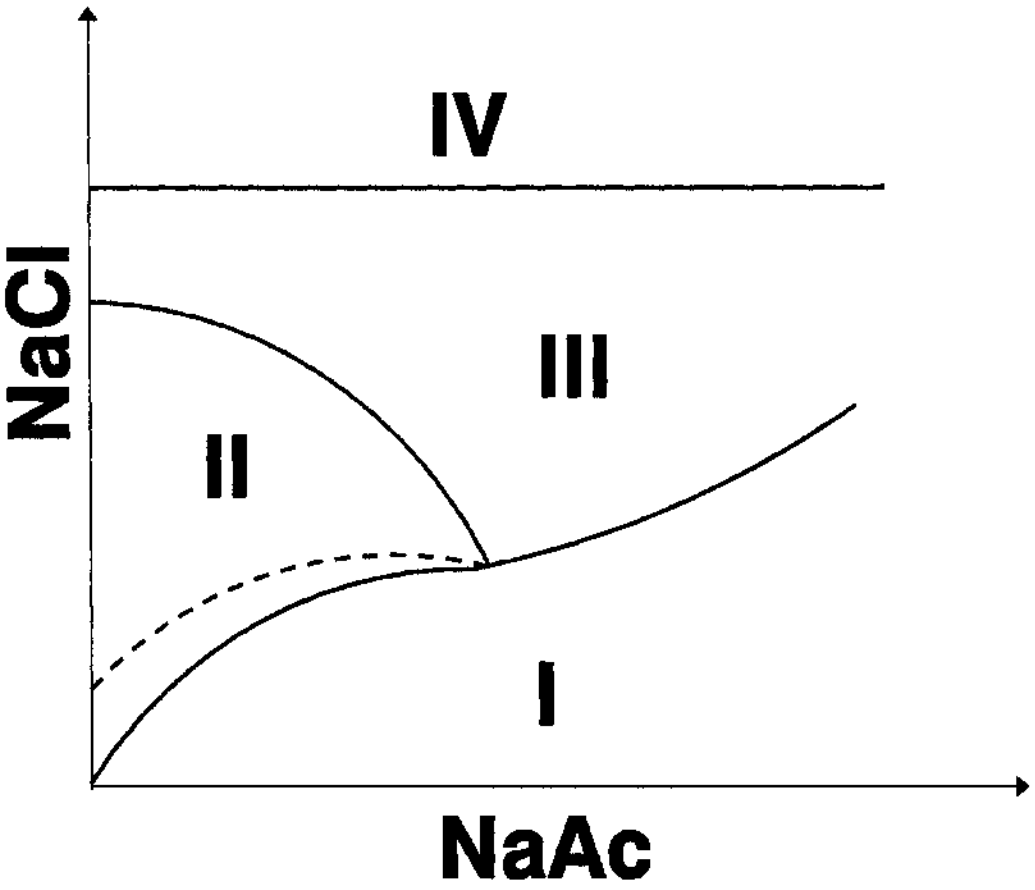

FIG. 4.12 The four regions of ionic polyacrylamide gels in the presence of NaCl.

Fig. 4.11 is the results of gels with different degree of ionization. At low salt concentration (Fig. 4.11(a)), the δ value increases first and then reaches different plateau levels depending on the degree of gel ionization. As the NaAc concentration is further increased (Fig. 4.11(b)), the δ value appears to converge asymptotically to 1.8.

Combining the effects of both ionization and salt concentration, the behavior of δ value can be summarized as shown in Fig. 4.12. Four district regions have been identified for the polyelectrolyte gel system. These regions correspond to different phenomenon and require different theories to explain. The first region is the transition region from no-salt to with-salt. Its boundary line corresponds to the salt and ionization concentrations at which the δ value reaches 80% of its full range. The value of δ changes the most in this region. The second region is the region in which the δ exhibits a peak. In the third region, the δ value is slightly dependent on ionic strength and salt concentration. Once reaching the fourth region, the δ value of the polyelectrolyte system stays at about 1.8. Fig. 4.12 also shows a maximum δ line corresponds to the maxima observed in Fig. 4.11(b). This line terminates at ionization between 20mM and 50mM.

4.5 Conclusions

First, the scaling behavior of elastic properties of polyacrylamide gel in pure water solvent has been systematically studied as a function of chemical composition. We have shown that the ratio of bulk modulus to shear modulus is directly related to the scaling exponent δ. By measuring the thicknesses of constrained and free gels, we have obtained the scaling exponent δ. As BIS and AAm increases, the exponent δ increases and the systems seem to be

approaching the theta condition. As the network charge concentration increases, the exponent δ decreases dramatically. As a result, the concentration dependence of the swelling osmotic pressure is much weaker than non-ionic gels. The value of δ for non-ionic gels is chemical composition sensitive. The valve of δ for highly ionized acrylamide gels is around 1.25.

Second, the behavior of ionized polyacrylamide gels qualitatively agrees with theoretical expections based on polyelectrolyte solution behavior. The ionization-salt concentration space can be divided into four regions. The region-I and III are transitional regions. In region-II, a peak in δ is observed. The last region is the theoretically predicted region in which the observed δ value is a constant and is around 1.8. The measurement on the scaling exponent δ has revealed rich information, which are worth further theoretical studies.

CHAPTER 4 REFERENCES

1. P. G. de Gennes, Scaling Concepts in Polymer Physics, Cornell University Press., 1979.
2. D. W. Schaefer, Polymer **25**, 387(1984).
3. S. Candau, J. Bastide, and M. Delsanti, Adv. Polym. Sci. **44**, 27(1982).
4. F. Horkay and M. Zrinyi, Macromolecules **15**, 1306(1982); **21**, 3260(1988).
5. E. Geissler, F. Horkay, and A-M Hecht, Macromolecules **24**, 6006(1991).
6. J. P. Munch, S. Candau, J. Herz, and G. Hild, J. Phys.(Paris) **38**, 971(1977). S. J. Candau, C. Y. Young, T. Tanaka, P. Lemarechal, and J. Bastide, J. Chem. Phys. **70**, 4694(1979).
7. M. Zrinyi and F. Horkay, Macromolecules **17**, 2805(1984); F. Horkay, E. Geissler, A. Hecht, and M. Zrinyi, Macromolecules **21**, 2589(1988).
8. R. W. Richards and N. S. Davidson, Macromolecules **19**, 1381(1986).
9. E. Geissler, A. Hecht, F. Horkay, and M. Zrinyi, Macromolecules **21**, 2594(1988).
10. Y. Cohen, O. Ramon, I. J. Kopelman, and S. Mizrahi, J. Polym. Sci. (Phys.) **30**, 1055(1992).
11. Y. Li, Z. Hu, and C. Li, J. Appl. Polym. Sci., **50**, 1107(1993).
12. R. S. Rivlin, Phil. Trans. R. Soc. A **241**, 379(1948); Y. Fukahori and W. Seki, Polymer **33**, 502(1992).
13. N. S. Davidson, R. W. Richards, and A. Maconnachie, Macromolecules **19**, 434(1986).
14. T. Odijk, J. Polym. Sci., Polym. Phys. Ed. **15**, 477(1977); T. Odijk and A.C.

Houwaart, J. Polym. Sci., Polym. Phys. Ed.,**16**, 627(1978); T. Odijk, Macromolecules **12**, 688(1979).

15. L. Wang and V. Bloomfield, Macromolecules **23**, 804(1990), and **23**, 194(1990).
16. Z. Hu, C. Li, and Y. Li, J. Chem. Phys. **99**, 7108(1993).

CHAPTER 5

ACOUSTIC ATTENUATION AND VELOCITY OF NIPA GEL NEAR THE VOLUME PHASE TRANSITION

5.1 Introduction

A N-Isopropylacrylamide (NIPA) gel is a cross-linked polymer network in solvent. At room temperature, the gel is in the swelling state. Upon warming up, the volume of the gel shrinks. At the critical temperature, T_c, the gel undergoes the volume phase transition entering into the compact state. This transition is similar to well-known coil-to-globular transition for a single polymer chain in solvent [1]. Not like many other gels that undergo the transition by varying concentration of mixed solvent, the NIPA gel is sensitive to temperature which is easier to control.

The static behavior of phase transition in NIPA gels has been extensively investigated for the past several years. The specific heat capacity of NIPA gels was found to diverge at T_c following critical behavior of the Ising system [2]. The static bulk modulus approaches zero while the shear modulus shows small but finite jump near the critical point [3]. The temperature-dependent swelling curves have been studied as a function of ionic concentration [4] and as a function of uniaxial stress [5]. The transition temperature of NIPA gels can be increased by the positive osmotic pressure, or decreased by negative osmotic pressure [6]. Flory-Huggin's mean field theory has been successfully used to qualitatively describe the static behavior of phase transition in NIPA gels [4,5].

The recent efforts have been directed toward understanding the dynamic behavior of phase transition in gels. It was shown that the kinetics of gel swelling process is related to the relaxation of the gel elasticity and the friction between the network and the solvent [7]. The dynamics of density fluctuations of gels was observed by the dynamic light scattering spectroscopy [8]. It was shown that the collective diffusion coefficient diminishes at the critical point and the kinetics of the transition becomes infinitely slow [9]. The NMR study of polyacrylamide gel in acetone/water mixture found that the proton-lattice relaxation time diverges and the effective diffusion constant approaches zero near the critical acetone concentration [10]. The phase transition having large volume change is accompanied by formation and evolution of transient patterns which appear on the surface of a gel [11]. A recent theoretical model predicts that the apparent collective diffusion constant D_e and the relaxation time τ is gel geometry dependent [12]. Measurements of ultrasonic velocity and the attenuation provide important information about the dynamical aspects of relaxation processes near a critical point. Specifically, critical fluctuations can interact strongly with the acoustic sound waves and result in soft modes and strong wave attenuation. Ultrasonic measurements on liquid helium and binary solution systems have played an important role to establish modern phase transition theory [13]. Previous ultrasonic experiment on PAAM gels showed that attenuation exhibits a maximum as the gel approaches the critical temperature [14]. However, the critical point of PAAM gels is below the freezing point of water. It is difficult to separate the critical fluctuations of gels from ones produced during ice freezing process. In this study, the ultrasonic technique has been used to study the NIPA gels near its phase transition temperature which is far

above the freezing point of water. The result of sound attenuation has been analyzed in term of a dynamic scaling model [15] which was initially developed for the acoustical attenuation of critical binary liquids. The sound velocity has also been discussed.

5.2 Experimental

5.2.1 Sample preparation

The NIPA gel samples were made by standard free radical polymerization [2]. A mixture of 7.8 g of N-isopropyacrylamide (Kodak Co.), 133 mg of methylene-bis-acrylamide (BIS) as crosslinker, and tetra-methyl-ethylene-diamine (240 μl) (TEMED) as accelerator were dissolved in 100 ml of deionized and distilled water. Nitrogen gas was bubbled through the solution to remove oxygen dissolved in the solution. Then ammonium persulfate (40 mg) as initiator was added to the solution. Gels were formed within 30 min.

The sample was taken out from the test tube by a syringe and cut in size (diameter 16 mm and thickness 6 mm). These gels then were put into deionized and distilled water for 3 days to be washed several times with large amount of water to remove possible unreact monomers and short polymers.

5.2.2 Ultrasonic equipment

The longitudinal acoustic velocity and attenuation in the sample have been measured using a computer-controlled ultrasonic system (Model MBA 8400, METAC, Inc.). The block diagram of the ultrasonic system is shown in Fig. 5.1. The principle of this technique is a phase comparison between the ultrasonic echo signal from the sample and the continuous-wave (CW) signal that is used to drive the gated amplifier. This phase sensitive technique

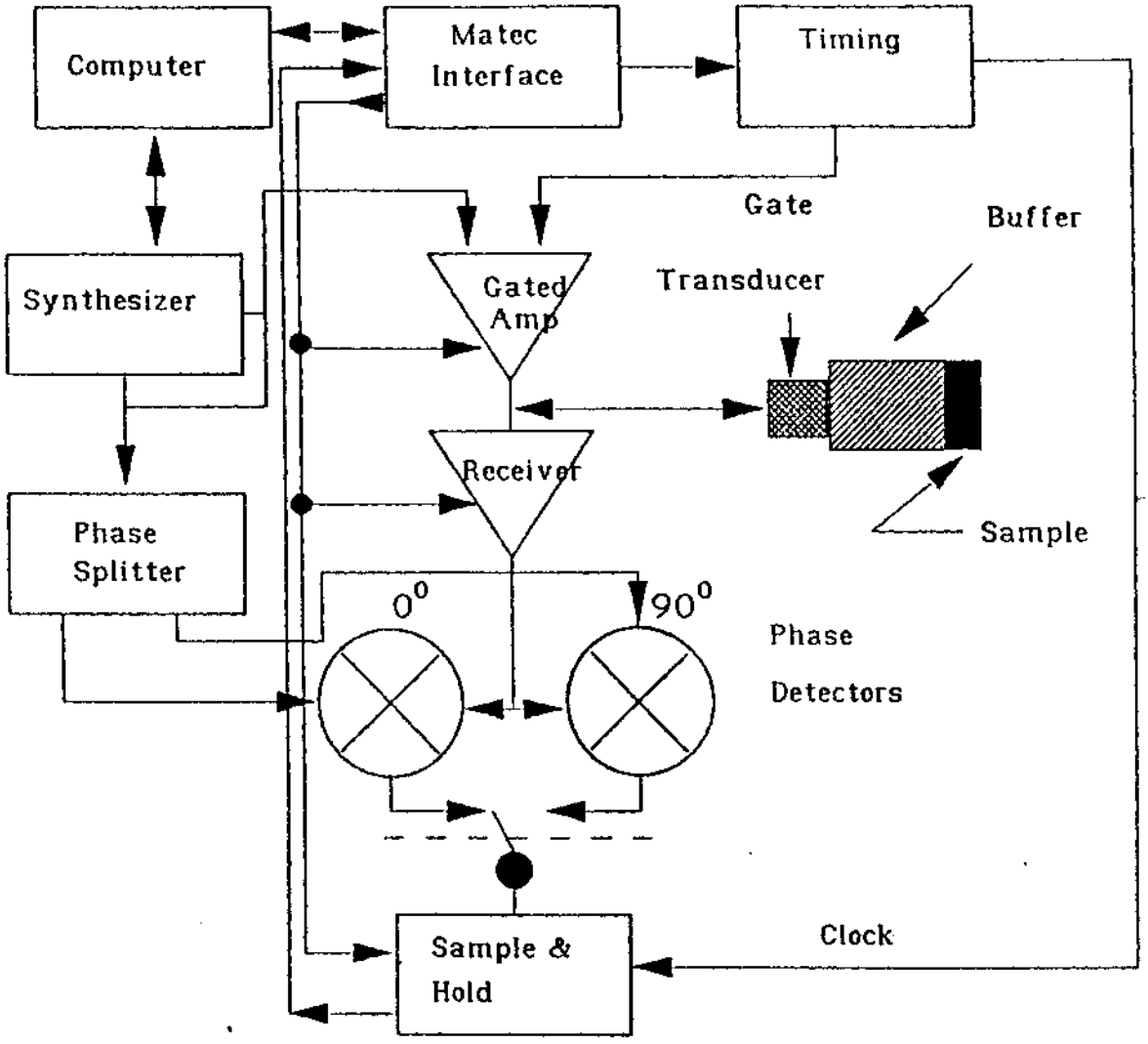

FIG. 5.1 Block diagram of the MBS 8000 Ultrasonic measurement system.

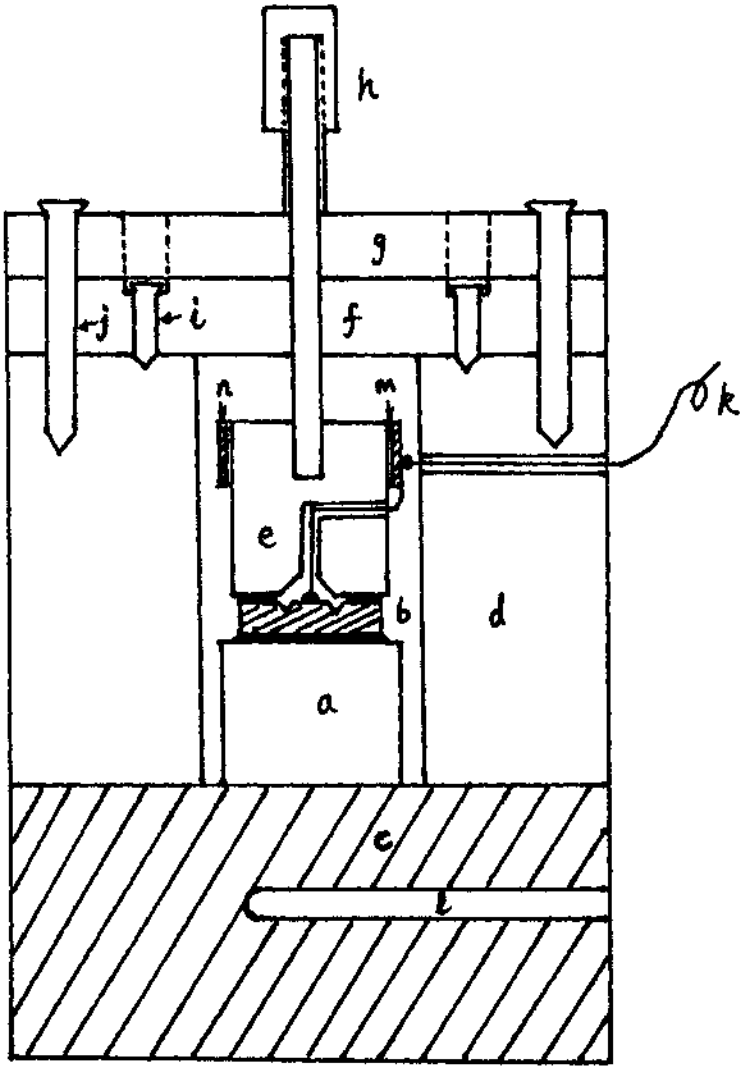

FIG. 5.2 Schematic diagram of cross-section of the sample cell.

(a) gel sample.
(b) transducer.
(c) aluminum base plate.
(d) transparent plastic wall.
(e) piston.
(f) shield cover.
(g) micrometer holder.
(h) micrometer.
(i) parallelism adjust screw.
(j) cell tightening screw.
(k) RF signal wire.
(l) PRT well.
(m) insulator layer
(n) RF signal contactor

significantly improves the signal-to-noise ratio. A overtone-polished longitudinal lithium-niobate piezoelectric transducer was used at fundamental frequency 10 MHz. With amplifications, the 5, 15, 20, and 30 Mhz signals were also visible. The attenuation (α) was calculated from:

$$\alpha = 20\log\left(\frac{A_2}{A_1}\right) \qquad (5.1)$$

where A_1 and A_2 are the amplitudes of the echo number one and two, respectively. The acoustic velocity was determined by measuring the interval traveling time between two echo signals and the thickness of the sample.

5.2.3 Sample cell

An ultrasonic sample cell was made specially for measurement of gels with transparent plastic glass as shown in Fig. 5.2. Basically, it consists of a captured piston riding on a micrometer rod. The piston, to which the transducer is connected, provides smooth vertical motion in changing the cell path length with accuracy of 0.01mm. The shape and the size of the sample can be observed during the experiment. Since the aluminum has much higher acoustic impedance than that of water, it is used as an acoustic wave reflector as mounted in the bottom of the cell. The parallelism between the transducer and the reflector can be adjusted by three adjust screws.

5.2.4 Temperature controller and swelling curve

The temperature was controlled by a thermal/refrigeration bath circulator (Brinkmamm Co., Model Lauda Super RM-6). Additional platinum resistor thermistor was installed to monitor temperature near the sample with the accuracy around 0.05 ^{0}C. The data were taken in warming-up run with rate of 0.05^{0}C/day near the phase transition region.

Two samples with the same size (thickness = 6mm and diameter = 16 mm) were cut from gel in the same test tube then were washed by water for three days. One sample was put into the ultrasonic cell, while another into the glass sample cell for measuring the change of gel size. The swelling ratio $x=(v/v_0)^{1/3} = D/D_0$, where D_0 and D are the initial and final diameters of the sample, is shown in Fig. 5.3 as a function of temperature. As temperature increases, the gel shrinks. Total contraction of the gel volume is about eight times than the volume at the room temperature.

The critical temperature, T_c, can determined by taking the derivative of its swelling ratio curve which is proportional to the thermal expansion coefficient. Since thermal expansion coefficient, γ, is related to the inverse of the bulk modulus K, as expressed by

$$\gamma \sim \frac{1}{K}\left(\frac{\partial \pi}{\partial T}\right)_V \qquad (5.2)$$

the position of the peak in the coefficient thus corresponds to the critical temperature. Using this method, $T_c = 33.83\ ^{0}C$ was obtained for the sample studied.

5.3 Results and discussion

5.3.1 Acoustic attenuation

Fig. 5.4 shows the longitudinal sound attenuation as a function of temperature at 5, 10 and 30 MHz. The attenuation is frequency dependent and increases as temperature approaches T_c. The temperature, T_m, at which the attenuation reaches maximum, shifts to a higher temperature as the ultrasonic frequency decreases. This behavior is similar to the results obtained in critical

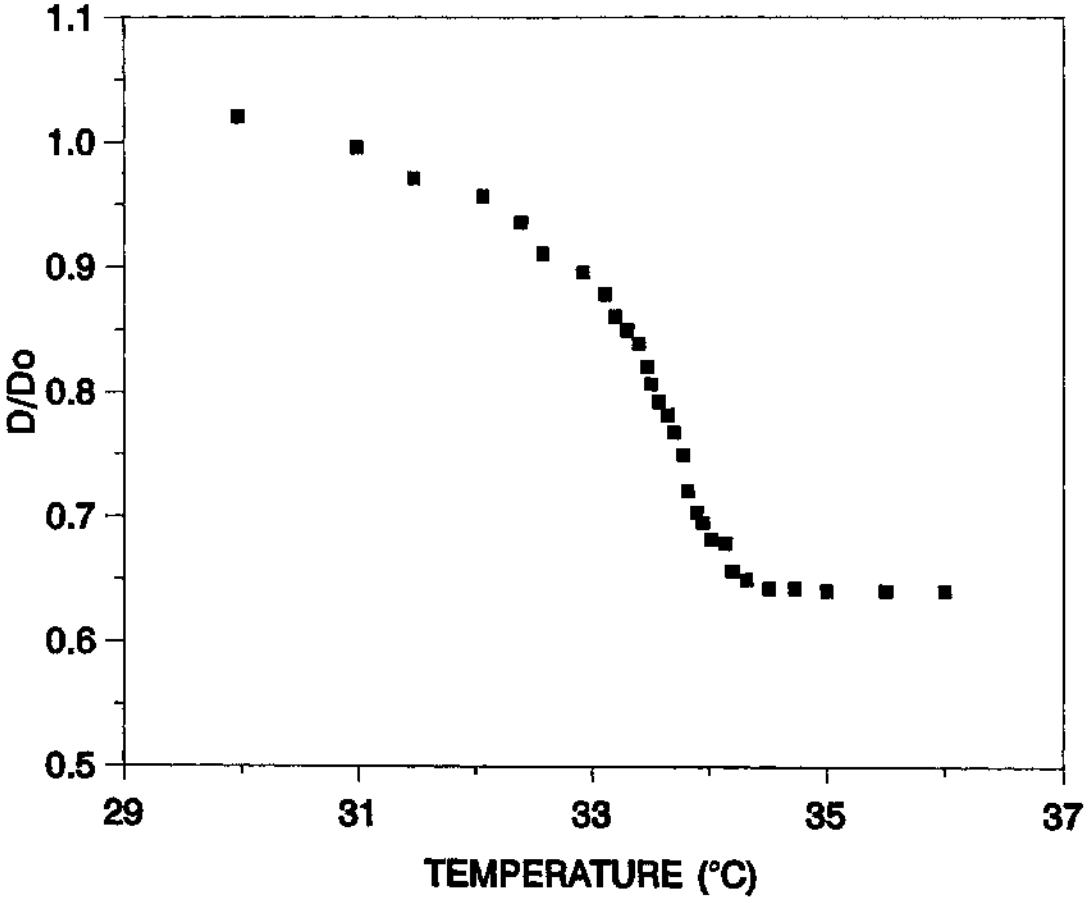

FIG. 5.3 The swelling ratio $x = D/D_0$ of NIPA gel against the temperature, where D_0 and D are the initial and final diameters of the sample.

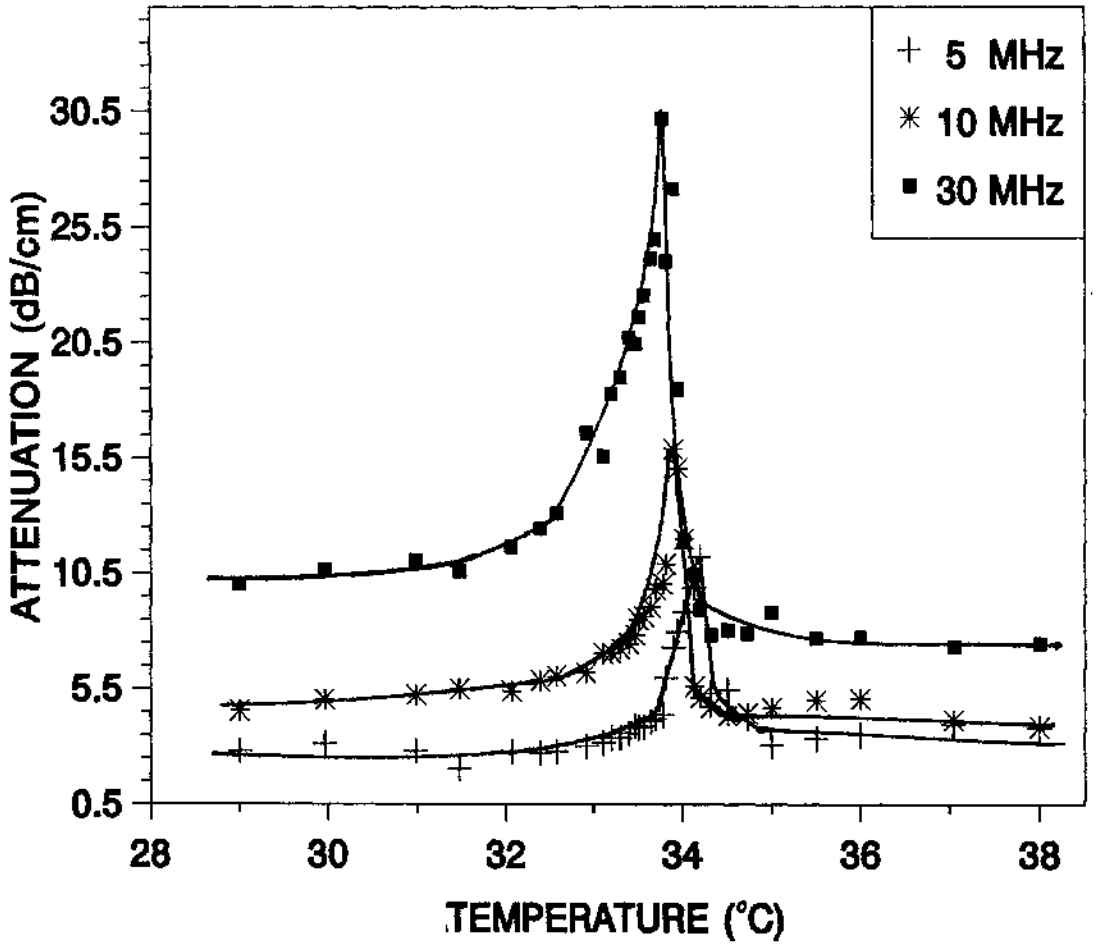

FIG. 5.4 The acoustical attenuation is plotted as a function of temperature at 5, 10, and 30 MHz. The data at 15 MHz are not shown in the figure.

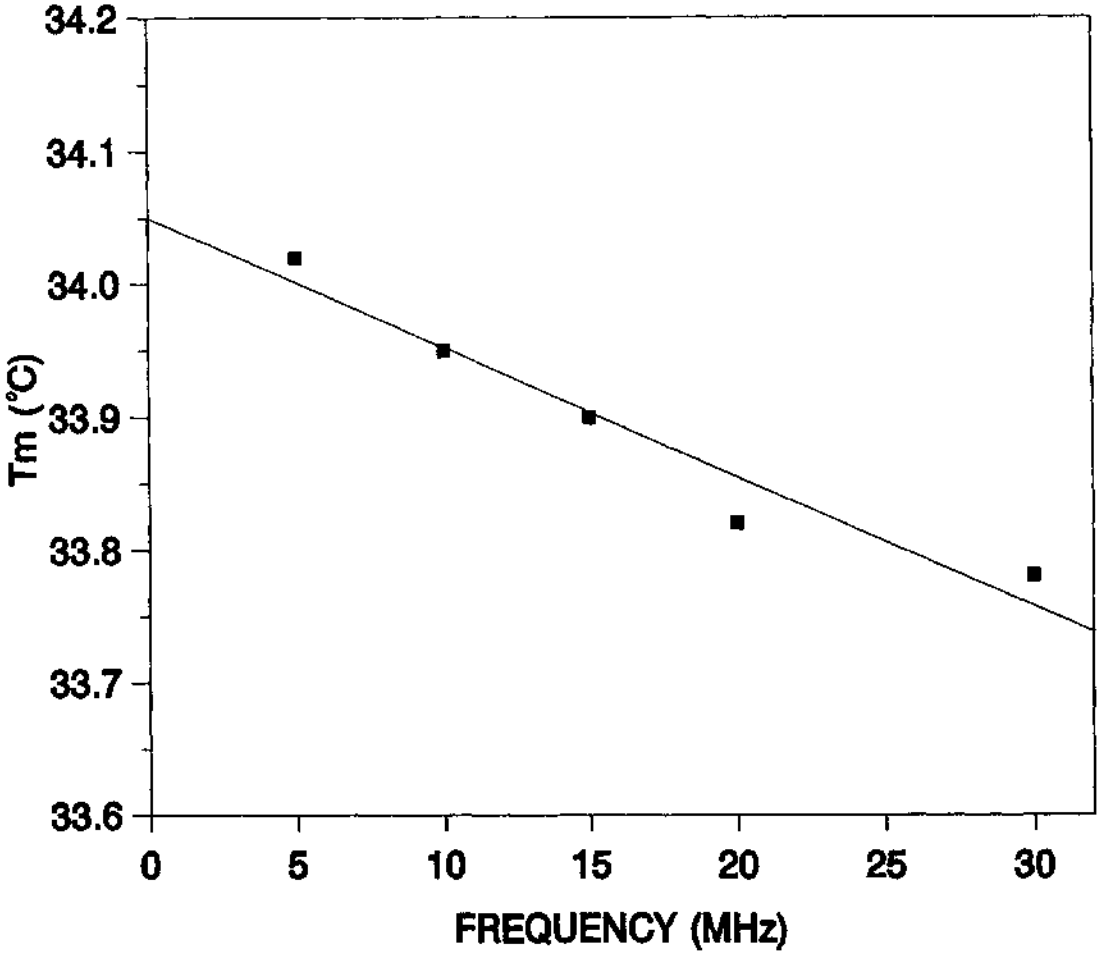

FIG. 5.5 T_m, temperature at which the attenuation reaches maximum, is plotted as a function of ultrasonic frequency. The solid line is the least square fit.

incommensurate phase transition in Rb_2ZnCl_4 [17]. The linear extrapolation of T_m toward zero frequency yields $T_m = 34.04\ ^0C$ as shown in Fig. 5.5.

The observed attenuation, near the critical temperature can be expressed in two terms,

$$\alpha_a = \alpha + \alpha_0 \tag{5.3}$$

where α and α_0 are net attenuation and background attenuation values, respectively. α_0 can be measured far away from the phase-transition temperature.

Ferrell and Bhattachajee [15] have developed a theory for the critical attenuation of sound in a binary mixture that is based on a consideration of temperature fluctuations associated with the adiabatic sound wave. This theory provides a very good description of the magnitude and frequency dependence of the critical attenuation in the binary liquid 3-methylpentane + nitroethane [18] and other binary systems [19].

According to the theory [15], the normalized attenuation α/α_c (α_c is the critical attenuation) should be a function of the reduced frequency ω^*, which in turn should scale as a dynamical scaling function. For the longitudinal mode, the normalized critical attenuation is given by

$$\frac{\alpha}{\alpha_c} = F(\omega^*) \tag{5.4}$$

with

$$\omega^* = \frac{\omega}{\omega_D} \tag{5.5}$$

where ω is ultrasonic angular frequency. ω_D represents a characteristic

temperature dependent relaxation rate and can be further approximated by the Stokes-Einstein expression,

$$\omega_D = \frac{k_B T}{3\pi\eta\xi^3} \tag{5.6}$$

where ξ is coherence length and η is the shear viscosity. In the critical phase transition region, $\xi = \xi_0 t^{-\nu}$ and $\eta = \eta_0 t^{-(z-3)\nu}$ with the reduced temperature $t = (T-T_c)/T_c$. Eq. (5.6) thus can be written as

$$\omega_D = \frac{k_B T_c}{3\pi\eta_0\xi_0^3} t^{z\nu} = \omega_0 t^{z\nu} \tag{5.7}$$

The Ising model value of the critical exponent v for the correlation length is 0.630. With $z = 3.06$ [18], thus $z\nu = 1.93$.

The dynamic scaling function can be expressed in terms of the reduced frequency ω^* as [15]

$$F(\omega^*) = \frac{1}{(1+\omega^{*-0.5})^2} \tag{5.8}$$

The total attenuation at the critical temperature can be written as [15,18]

$$\frac{\alpha_c}{f^2} = Sf^{-[1+(\frac{\alpha}{z\nu})]} + b \tag{5.9}$$

where S, a prefactor, is independent of frequency, f is ultrasonic frequency, α is the critical exponent of the specific heat capacity, and b is contribution of a small Navier-Stokes background attenuation [18]. Considering the hyperscaling relation $\hat{\alpha} = 2-3\nu$, one obtains $1 + (\alpha/z\nu) = 1.06$. Fig. 5.6 shows attenuation data

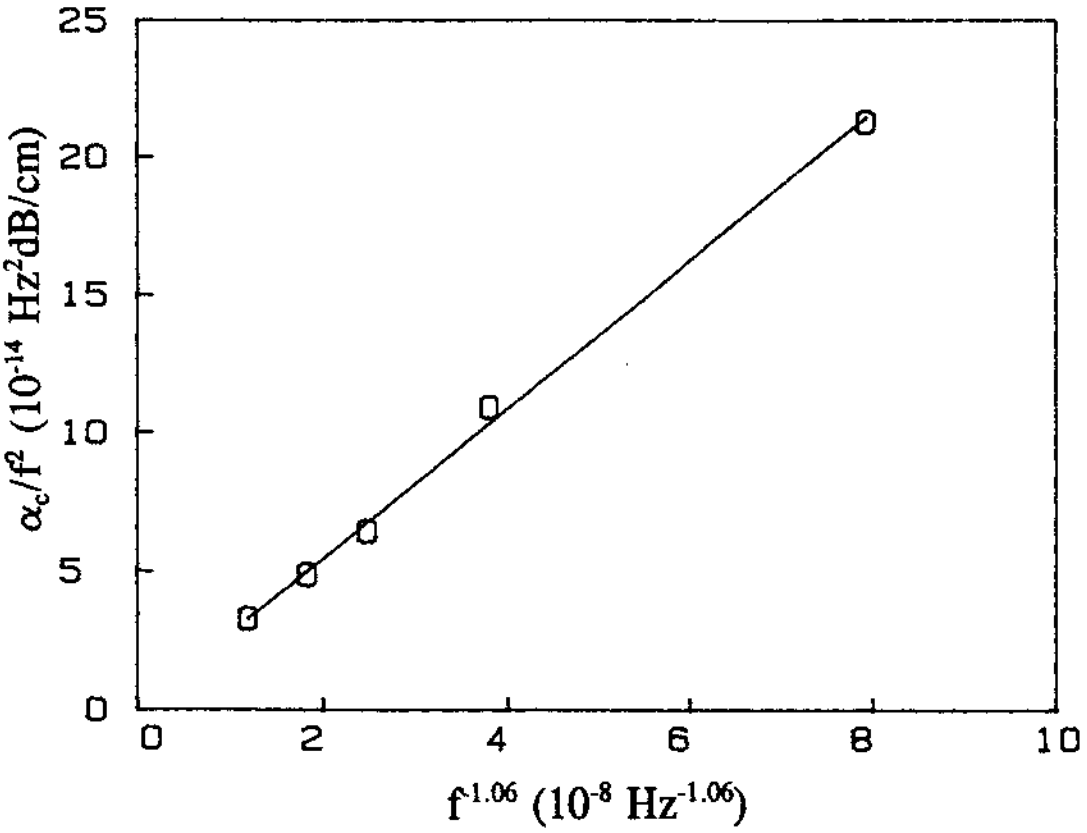

FIG. 5.6 The scaling behavior of the attenuation at T_c. The solid line is the least square fitting to Equation 5.9.

α_c/f^2 versus $f^{-1.06}$. The solid line is the least-square fitting to the Eq. (5.9) with a slope of $2.69 \times 10^{-6} cm^{-1}s^{0.94}$ and an intercept of 9.0×10^{-16} $cm^{-1}s^2$.

Scaling plot of the critical attenuation is shown in Fig. 5.7. Also shown is the scaling function $F(\omega^*)$ defined in Eq. (5.8). The data were fit to the theoretical curve using a value of ω_0 of 3.4×10^{12} Hz and Ising critical exponent $z\nu = 1.93$. The critical attenuation ratio α/α_c reasonably scale with respect to ω^*, i.e., they collapse onto a single curve. The form of the scaling function agrees with the shape of the data curve. This indicates that the NIPA gel undergoes the critical slowing down near T_c, agreeing with previous report [11]. The critical exponents used here are Ising values which agrees with ones obtained in specific heat capacity measurements [2].

Using experimental data on the static correlation length and the shear viscosity, we have calculated ω_0 from Eq. (5.7). The value of viscosity of water at room temperature is 0.899 cP. No value of the coherent length for the NIPA gel is available, but the light scattering experiment yields the coherent length (ξ) of 11 Å for PAAM gels [20]. Using these values, we obtained the value of ω_0 of 3.8×10^8 Hz. This value of ω_0 is apparently smaller than one obtained from ultrasonic data. Furthermore, the critical attenuation ratio does not completely scale with respect to ω^*. The discrepancies between the theory and the experiment may be due to that the theory is specially modeled based on the binary liquids which do not have shear modulus at all. In contrast, the polymer network in gels has the small but finite shear moludus. Even at transition temperature, this small shear modulus does not go to zero [3]. Thus, to understand acoustical phase transition, it is important to incorporate the shear modulus into theory. Furthermore, several different length scales are present in

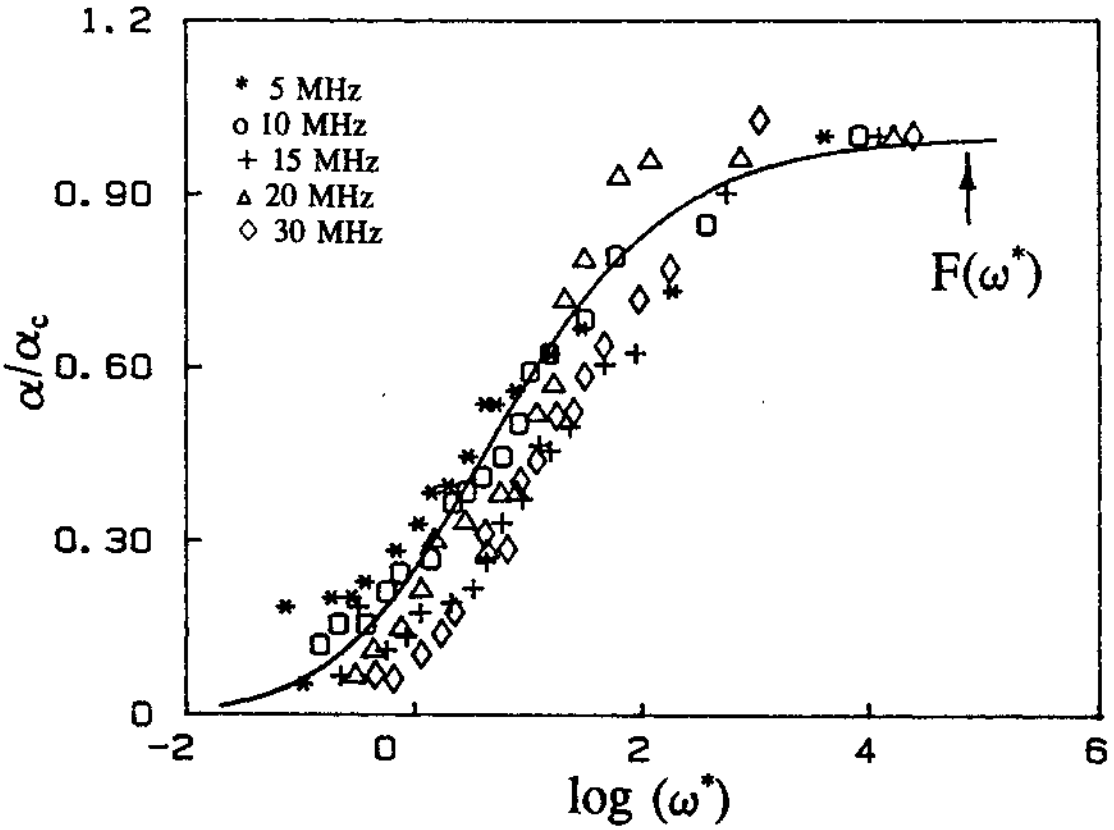

FIG. 5.7 The dynamic scaling behavior of the attenuation at T<Tc. at 5, 10, 15, 20, and 30 MHz. The solid line is the scaling function F(w*) defined in Equation 5.8.

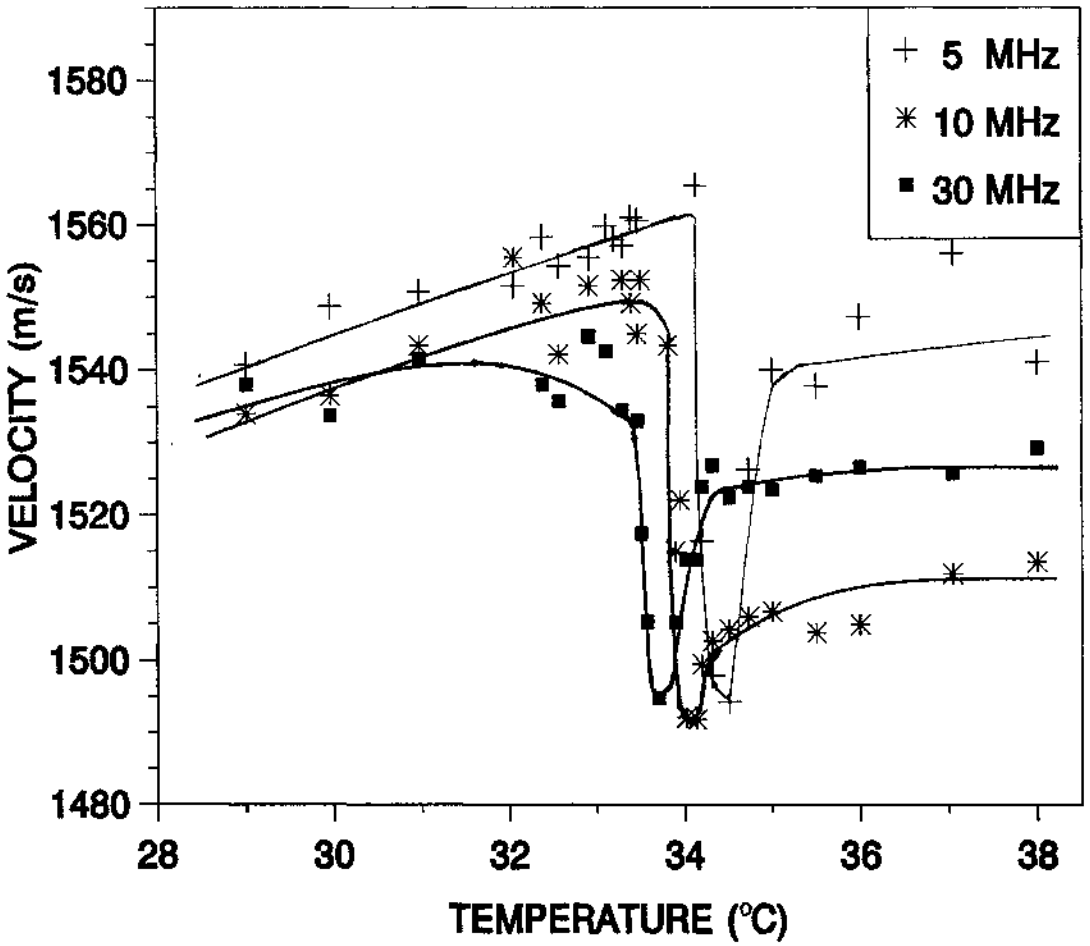

FIG. 5.8 The acoustical velocity is plotted as a function of temperature at 5, 10, and 30 MHz.

gel networks [21]. The competition among these length scales may also play a role in the acoustical attenuation near the phase transition.

5.3.2 Ultrasonic velocity

Comparing to the attenuation measurement, the velocity is more difficult to measure. The measured sound velocities of 5, 10, and 30 MHz frequencies are plotted in Fig. 5.8. Before the volume phase transition temperature, all three velocities increase as the temperature increases. The velocities decrease sharply near the critical transition point and then reached a plateau. This may be explained by the elastic modulus. The relation of longitudinal acoustic velocity and elastic modulus of materials can be written as

$$v=((K+\frac{3}{4}G)/\rho)^{1/2} \qquad (5.10)$$

where K is the bulk modulus, G the shear modulus, and ρ is the density of the material. It was reported that near the critical temperature, shear modulus G remains almost the same but the bulk modulus K drops dramatically toward zero [3,22], also the density of gel increases quickly near the transition point. All these make velocity drop near T_c.

5.4 Conclusion

The ultrasonic technique has been used to investigate the acoustic behavior of NIPA gels near the critical point. The attenuation and velocity depend on both temperature and the ultrasonic frequency. The longitudinal sound velocity decreases near the transition temperature T_c. This observation agrees with previous theoretical and experimental results of bulk modulus and shear modulus obtained by Hirotsu [3]. The acoustic attenuation exhibits the maximum near T_c and can be understood in terms of critical slowing down of

the relaxation process during the phase transition. The dynamic scaling theory of Bhattacharjee and Ferrell [15] provides a qualitatively description of the frequency and temperature dependence of the critical attenuation near T_c. Specifically, the acoustic attenuation versus the characterizing frequency ω^* at different frequencies reasonably scale onto a single curve and the dynamic scaling function is shown to generally agree with the shape of data curve. The analysis suggests that the NIPA gel belongs to the Ising system, agreeing with results of specific heat. It is noted that ω_0 obtained from the scaling fitting is much greater than the value obtained by other independent method. The discrepancy indicates that the modification to the theory is necessary. Since the theory is originally proposed for critical binary liquids, it would be reasonable to take into account of finite shear modulus of gels for the future dynamic scaling model.

CHAPTER 5 REFERENCES

1. Y. Li and T. Tanaka, in Annual Review of Materials Science, **22**, (1992).
2. Y. Li and T. Tanaka, J. Chem. Phys. **90**, 5161(1989); Y. Li, Ph.D Thesis, MIT, unpublished, (1989).
3. S. Hirotsu, J. Chem. Phys. **94**, 3949(1991).
4. S. Hirotsu, Y. Hirokawa and T. Tanaka, J. Chem. Phys. **87**, 1932(1987).
5. S. Hirotsu and A. Onuki, J. Phys. Soc. Jpn. **58**, 1508(1989).
6. S. Hirotsu, J. Phys. Soc. Jpn. **56**, 233(1987); J. Chem. Phys. **88**, 427 (1988).
7. T. Tanaka and D.J. Fillmore, J. Chem. Phys. **70**, 1214(1979).
8. T. Tanaka, S. Ishiwata and C. Ishimoto, Phys. Rev. Lett. **38**, 771(1977).
9. A. Hochberg, T. Tanaka, and D. Nicoli, Phys. Rev. Lett. **43**, 217(1979).
10. F. Tabak, M. Corti, L. Pavesi, A. Rigamonti, J. Phys. C: Condensed Matt. Phys. **20**, 5691(1987).
11. E. Sato Matsuo and T. Tanaka, J. Chem. Phys. **89**, 1695(1988).
12. Y. Li and T. Tanaka, J. Chem. Phys. **92**, 15(1990).
13. C. W. Garland, in Physical Acoustics, Edited by W.P. Mason and R.N. Thurston (Academic Press, New York) 1970, p. 51.
14. J.C. Bacri and R. Rajaonarison, J. Phys.-Letts **40**, L-5(1979).
15. R. A. Ferrell and J. K. Bhattacharjee, Phys. Rev. A **24**, 1643(1981); Phys. Rev. A **31**, 1788(1985).
16. P. J. Flory, Principles of Polymer chemistry (Cornell Univ., Ithaca, New York, 1966), Chap. 12 and 13.

17. Z. Hu, C.W. Garland and S. Hirotsu, Phys. Rev. B **42**, 8503(1990).

18. C. W. Garland and G. Sanchez, J. Chem. Phys. **79**, 3090(1983).

19. S.J. Fast and S.S. Yun, J. Acous. Soc. Am. **81**, 1418(1987).

20. T. Tanaka, Phys. Rev. A **17**, 763(1978).

21. T. A. Witten and P. Pincus, Europhys. Lett. **3**, 315(1987).

22. C. Li, Z. Hu, and Y. Li, Phys. Rev. E **40**, 603(1993).

CHAPTER 6

PATTERN FORMATION OF CONSTRAINED IONIC PAAM GELS

6.1 Introduction

Pattern formation on the surface of polymer gels has recently attracted considerable attention [1-9]. The study of these patterns not only leads to better understanding of gel mechanical properties [2] and gel kinetic process near the volume phase transition [3], but also helps to explain the formation and evolution of patterns found in biological systems.

The acrylamide/sodium acrylate (PAAM/SA) gels are widely used for studying patterns of gels during the swelling process [2, 4-6]. As a gel swells in water, small dots initially appear on the gel surface. These dots then grow into rod shapes and eventually become connected, forming a quasi-hexagonal pattern [2, 4]. The time (t) dependence of the average unit size (λ) of the hexagonal pattern can be described by an empirical relation $\lambda \sim t^{\alpha}$, with $\alpha = 1/2$ [2], or $\alpha = 1/3$ [6]. The collective diffusion of the polymer network is thus believed to play an important role in pattern growth [7]. The hexagonal pattern is apparently composed of numerous cusp-shaped lines [2] which are the result of the folding of the original gel surface [7, 9]. Based on elasticity theory [2, 7-9], the swelling pattern can be understood in terms of frustration of the free gel surface that is constrained by an unswollen bottom surface.

In contrast to the swelling pattern, the patterns produced by the gel shrinking process is much more complex and less understood. In the swelling

process, the surface pattern evolves into a hexagonal pattern following a fairly general path. In the shrinking process, however, many different patterns have been observed. When the lengths of cylindrical acrylamide gels were fixed in an acetone/water mixture, patterns including irregularly arranged bubbles, regularly arranged (necklace-like) bubbles, bamboos, and tubes were observed [1]. When the temperature of N-isopropylacrylamide (NIPA) gel beads was increased, irregularly arranged bubbles were observed as well [3].

Both the swelling and the shrinking patterns are sensitive to the initial and the final states of the transition [1, 3]. These patterns are the result of large equilibrium gel volume change. This change corresponds to the relaxation of a gel osmotic pressure jump. The osmotic pressure jump, either positive (causing swelling) or negative (causing shrinking), can be achieved by changing temperature, solvent, electric field, light, ph of the solvent, or other parameters. For a recent review, see Reference 10.

In this chapter, the effect of the volume phase transition on PAAM/SA gel surface pattern formation is investigated. The samples are gel slabs with one of their surfaces permanently bonded to a rigid substrate. This boundary condition has been used previously to study the swelling pattern [2, 6], but, to the authors' knowledge, not to study the shrinking pattern. By varying the solvent composition, the crossover between different patterns can be studied. The constraint used in this study allows the sample to shrink one-dimensionally. Fixing the length of a cylindrical gel results in two-dimensional shrinking [1]. The shrinking of gel beads can be considered as three-dimensional shrinking. The osmotic pressure jump here is controlled by changing the solvent from water to acetone/water mixtures of various compositions.

6.2 Sample preparation

The PAAM/SA gel samples were made by free radical polymerization. Detail of sample preparation has been described in chapter 2. The standard recipe of acrylamide gel was used. The amount of SA was varied from zero to 600 mg per 100ml solution. A thin film of the solution was cast between a GelBond film (FMC Co.) and a microscope slide with a fixed separation [11]. Since the GelBond film contains polymerization-active chemical groups, the bottom surface of the gel slab was thus covalently cross-linked to the GelBond film during gelation. The samples were kept in water before being used for measurement.

6.3 Results and discussion

The volume of the PAAM/SA gel is known to be acetone concentration dependent [10]. Fig. 6.1 shows the acetone concentration dependence of the equilibrium thicknesses for free and constrained PAAM/SA gel slabs with SA = 600mg/100ml. The critical acetone concentration, X_c, determined by the discontinuous drop of gel thickness, shifts to a higher value for the constrained sample. Near the phase transition point, the constraint corresponds to a positive osmotic pressure, which pushes the transition acetone concentration toward a higher value than that of the free gel. Similar behavior was also observed for NIPA gels whose transition temperatures were increased by an external constraint such as a uniaxial stress [12] or a rigid substrate [13].

In the present study, all samples (gel slabs) were initially immersed in water to reach equilibrium. After about 24 hours, they became fully swollen and exhibited the hexagonal pattern on their surfaces. The solvent of the swollen-in-water gel slabs was then changed from water to different acetone/water

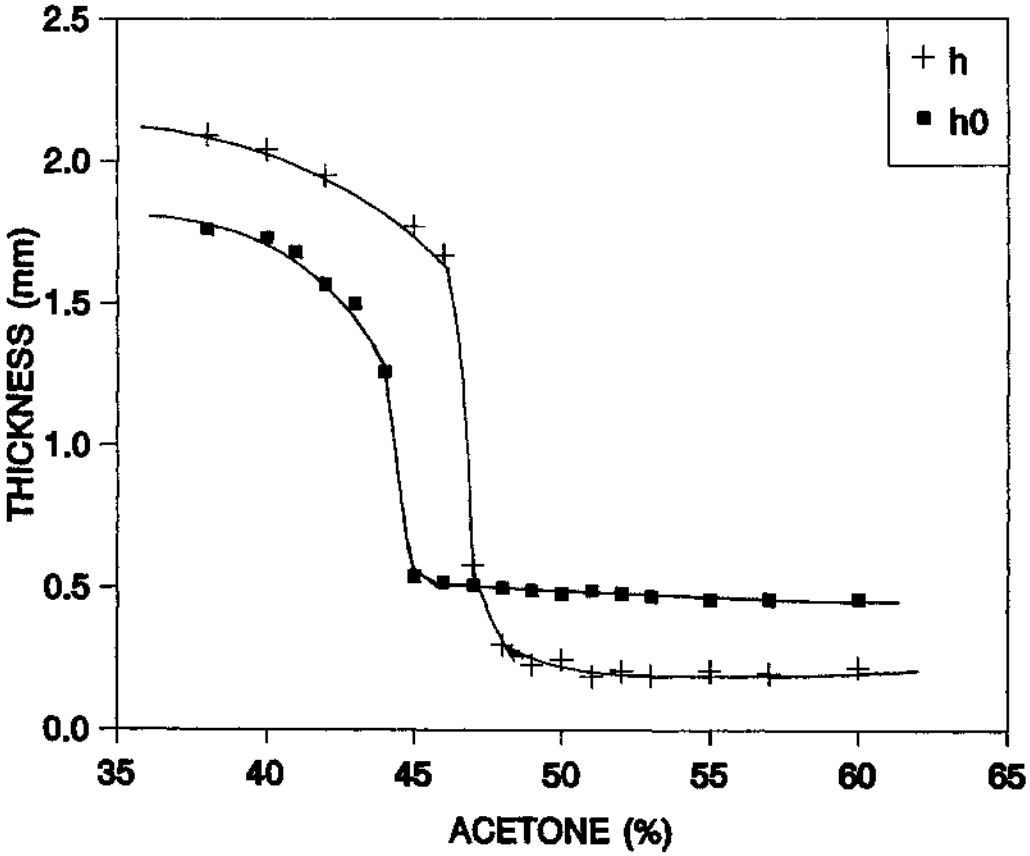

FIG. 6.1. The thicknesses of free (h_0) and constrained (h) PAAM/SA gels with SA = 600mg/100ml as a function of acetone concentration. The initial thicknesses of samples were equal to 1.0 mm. Solid lines are guides to the eye for all figures except the one specified.

mixtures. New patterns emerged on the gel surfaces, different from the initial hexagonal pattern, after about six hours.

6.3.1 "Phase diagram" of patterns

Typical patterns of constrained PAAM/SA gel slabs with SA concentrations of 600mg/100ml are shown in Fig. 6.2 at various acetone concentrations. These patterns can be generally classified into four groups. For acetone concentration less than 46%, the pattern consists of quasi-hexagonal units and is very similar to the gel pattern formed in water. Near the phase transition concentration around 47%, many smaller unit cells grow out from the original larger unit. For convenience of discussion, this kind of pattern is called the grain pattern. Between 55% and 70% acetone concentration, bubbles develop as the gel volume collapses. The bubble pattern remains stable for at least seven days. As acetone concentration is increased to 70%, the gel becomes opaque and its surface pattern disappears.

The pattern evolution as a function of acetone concentration is also studied for samples with ionic strengths equal to 300 mg/100ml and 200mg/100ml. These samples exhibit, again, hexagonal, grain and bubble patterns. Upon decreasing the ionic strength, the onsets of the grain and the bubble patterns shift to lower acetone concentration. Based on these observations, a "phase diagram" of patterns is constructed in Fig. 6.3 for various ionic strengths and acetone concentrations. The different regions are represented by descriptive sketches of the patterns.

6.3.2 The hexagonal pattern

The hexagonal pattern of gels in water has been extensively studied before. Adding acetone in water causes the PAAM/SA gel to shrink. It is noted

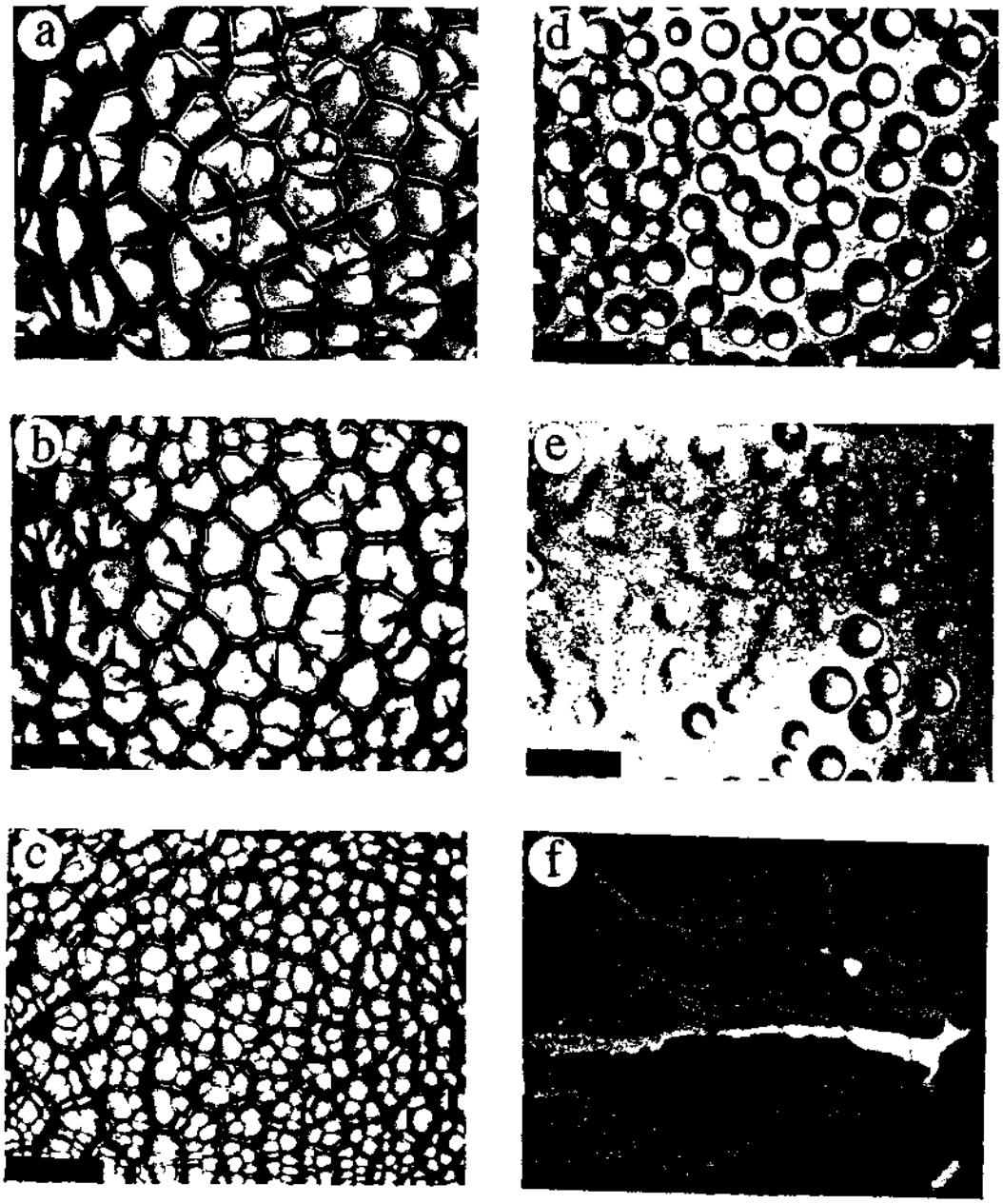

FIG. 6.2 The pattern evolution in ionized polyacrylamide (SA = 600mg/100ml) gel slabs as a function of acetone concentration (wt%). (a) 44%, and (b) 46%, the quasi-hexagonal pattern; (c) 48%, the grain pattern; (d) 60%, and (e) 70%, the bubble pattern, (f) 100%, opaque and no pattern. The difference between patterns in water (not shown) and in 44% acetone/water mixture is small. The black bar indicates a length of 0.5 cm for all figures except the one specified.

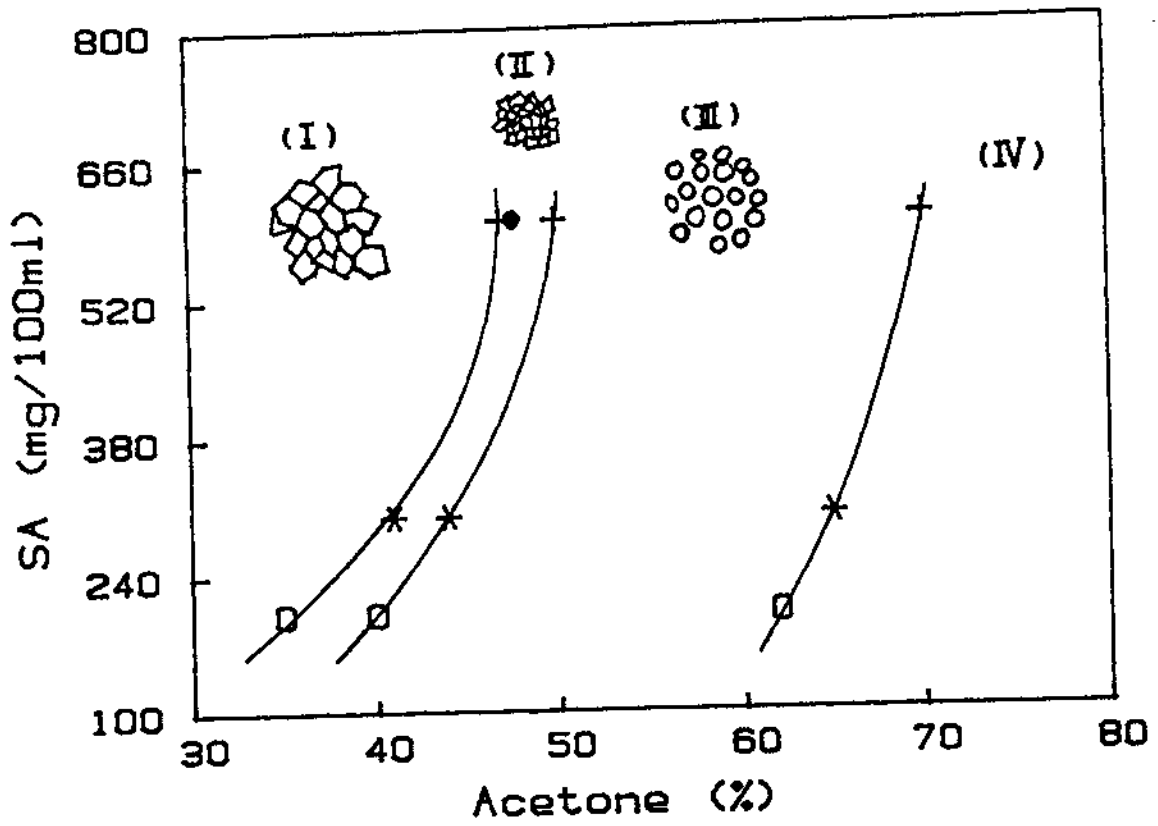

FIG. 6.3 The phase diagram of patterns. There are four regions: (I) the quasi-hexagonal pattern, (II) the grain pattern, (III) the bubble pattern, and (IV) no pattern. Pattern I is time independent, pattern II is stable for about two days, and pattern III is stable for at least seven days. The full circle indicates the volume phase transition concentration for the 600mg/100ml sample.

from this study that if this shrinking is not severe, i.e., if the acetone concentration is not higher than the transition concentration, the hexagonal pattern obtained in water remains basically unchanged. In this regime, the gel pattern can be described by the mechanical instability theory [2, 7-9] which is based on competition between the swollen surface and the unswollen gel core.

It has been shown [2, 7] that the wavelength (λ), i.e., the average distance between adjacent pattern units, is linearly proportional to the distance, h, between the fixed boundary (of either the substrate or the unswollen gel core) and the free gel surface. The linear relation between λ and h is also observed in this study and will be used to compare with results of the bubble pattern in Section 6.3.4. This linear behavior can also be obtained from dimensional analysis. Since the only length scale relevant to the swelling pattern is h, one can write

$$\lambda = F(\frac{K}{G}, \frac{P}{P_c})h. \qquad (6.1)$$

Where F is the scaling function which depends only on K/G, the ratio of bulk modulus to shear modulus, and P/P_c, the ratio of the osmotic pressure from the constraint to the critical constraint pressure [2, 7]. For $P < P_c$, no surface pattern will appear. Some theoretical attempts have been made to determine this function [2, 7-9]. There is, however, no quantitative experimental results that we know which test these theories.

Fig. 6.4 shows the wavelengths for different patterns as a function of acetone concentration. The grain pattern wavelength is about four times smaller than those of hexagonal and bubble patterns. The wavelength of the bubble

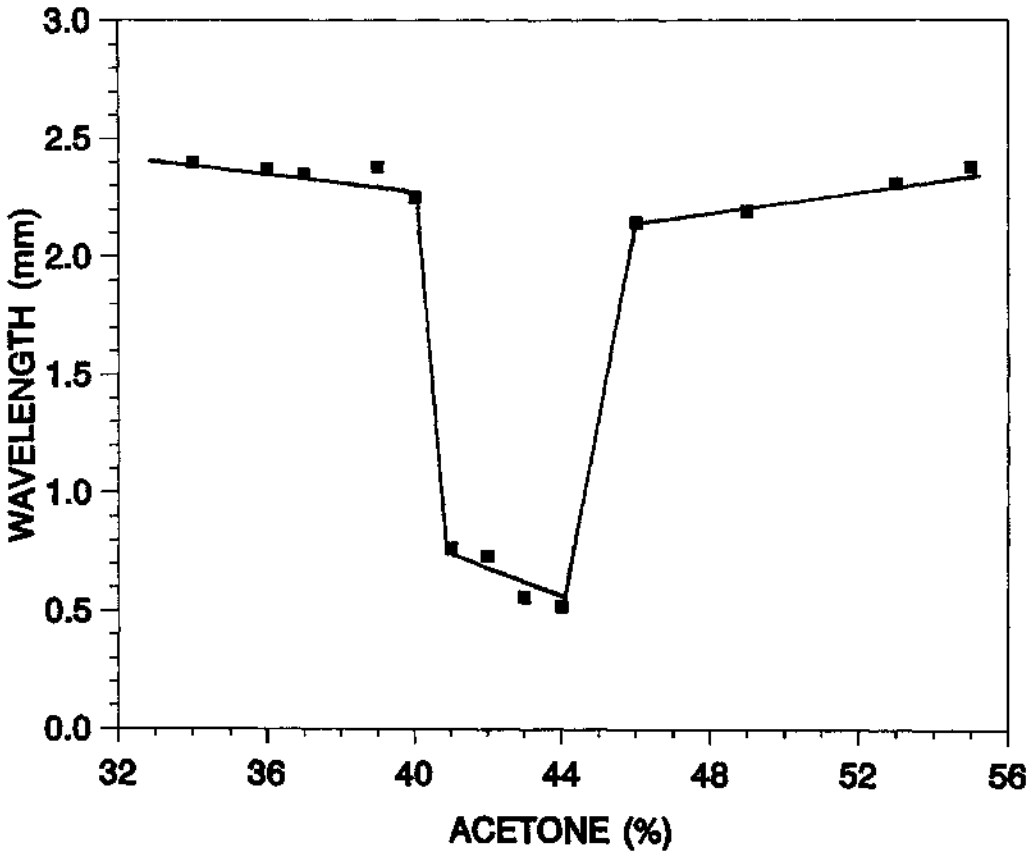

FIG. 6.4 The wavelength of patterns is plotted as a function of acetone concentration for PAAM gels slabs with SA = 300mg/100ml. The grain pattern wavelength is about four times smaller than those of hexagonal and bubble patterns.

pattern is about the same as the hexagonal pattern wavelength and increases slightly as the acetone concentration increases.

6.3.3 The grain pattern

It is noted that the grain pattern observed occurred near the volume phase transition point, as indicated in Fig. 6.3. When the ionic strength is reduced, the transition point moves toward a lower acetone concentration and causes the grain pattern to shift in the same direction. The grain pattern appears to be a transit pattern between more stabled hexagonal and bubble patterns.

The swelling profile of a constrained slab gel is schematically shown in Fig. 6.5. For $X < X_c$, where X is acetone concentration, the sample has a monotonic swelling profile (Fig. 6.5a). As the acetone concentration is suddenly changed from $X<X_c$ to $X\sim X_c$, the surface of the gel slab starts to shrink, yielding a more complex swelling profile with a dense surface. The dense surface has high tension and prefers to minimize its total area. This surface tension reduces the depth of the cusps of the original hexagonal patterns and thereby changes the local network density (the swelling profile) near the cusp lines. Since the total amount of water trapped under the dense surface is roughly constant, it is conceivable that these changes in the swelling profile create the grain pattern (Fig. 6.5b). Base on this argument, the depth of the grain patterns should be shallower than that of the hexagonal pattern in the swollen state. It is reasonable to expect the grain patterns to have relatively short life times. This agrees with the experimental observations.

FIG. 6.5 A schematic description of the grain pattern formation. (a) Profile of the average degree of swelling (inverse of network concentration), along the axis perpendicular to the gel surface. Upon changing the acetone concentration from zero percent to $X_c + \Delta X$, a relatively dense surface will appear due to the collapse of the portion of the sample on the surface. (b) The dense surface stretches the cusp lines and rearranges the solvent under it causing the formation of the grain pattern.

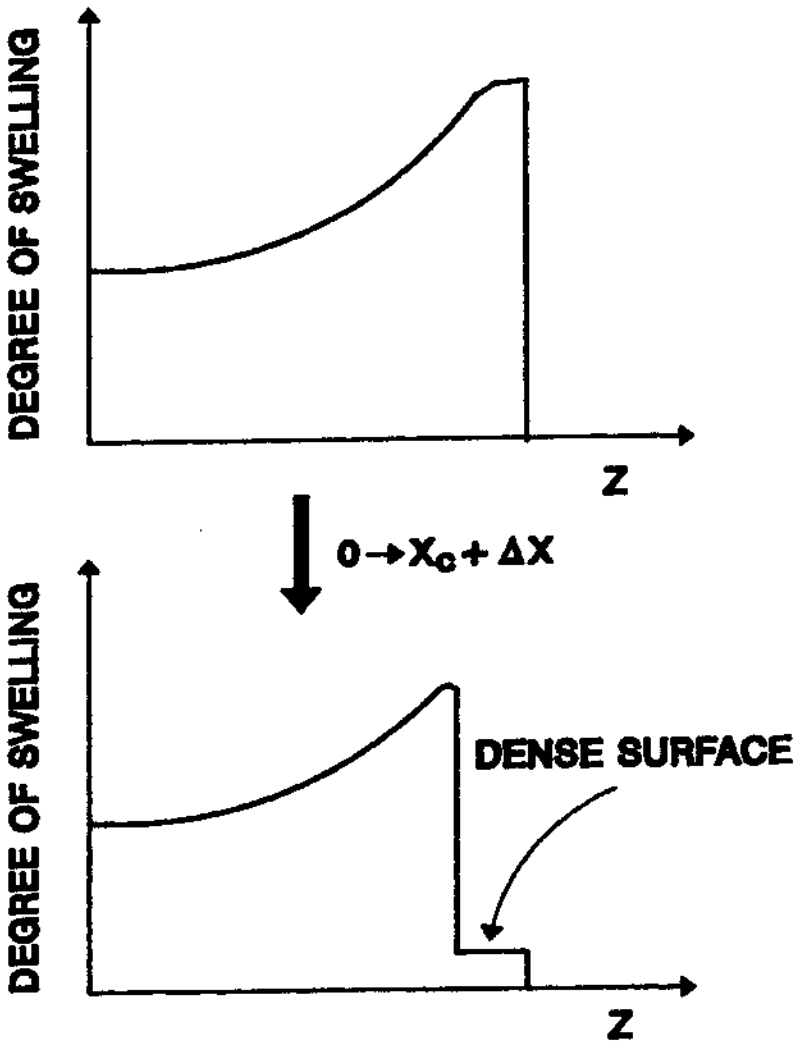
DEGREE OF SWELLING
Z
0→Xc+ΔX
DEGREE OF SWELLING
DENSE SURFACE
Z

[a]

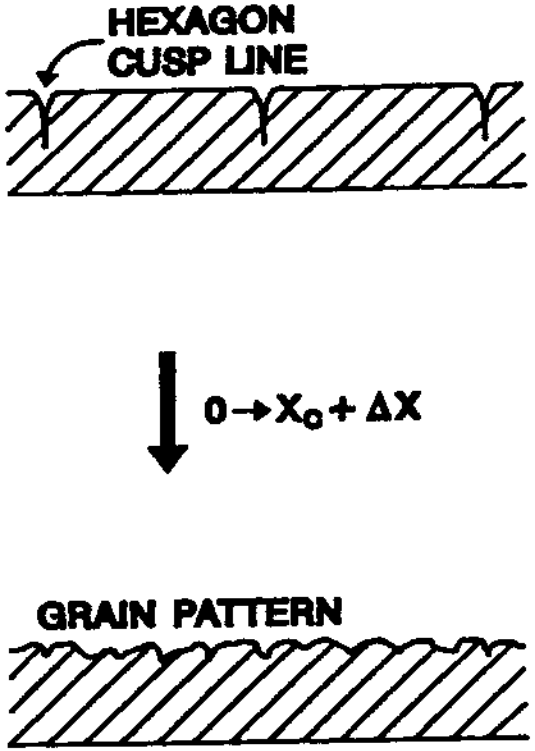
HEXAGON
CUSP LINE
0→Xc+ΔX
GRAIN PATTERN

[b]

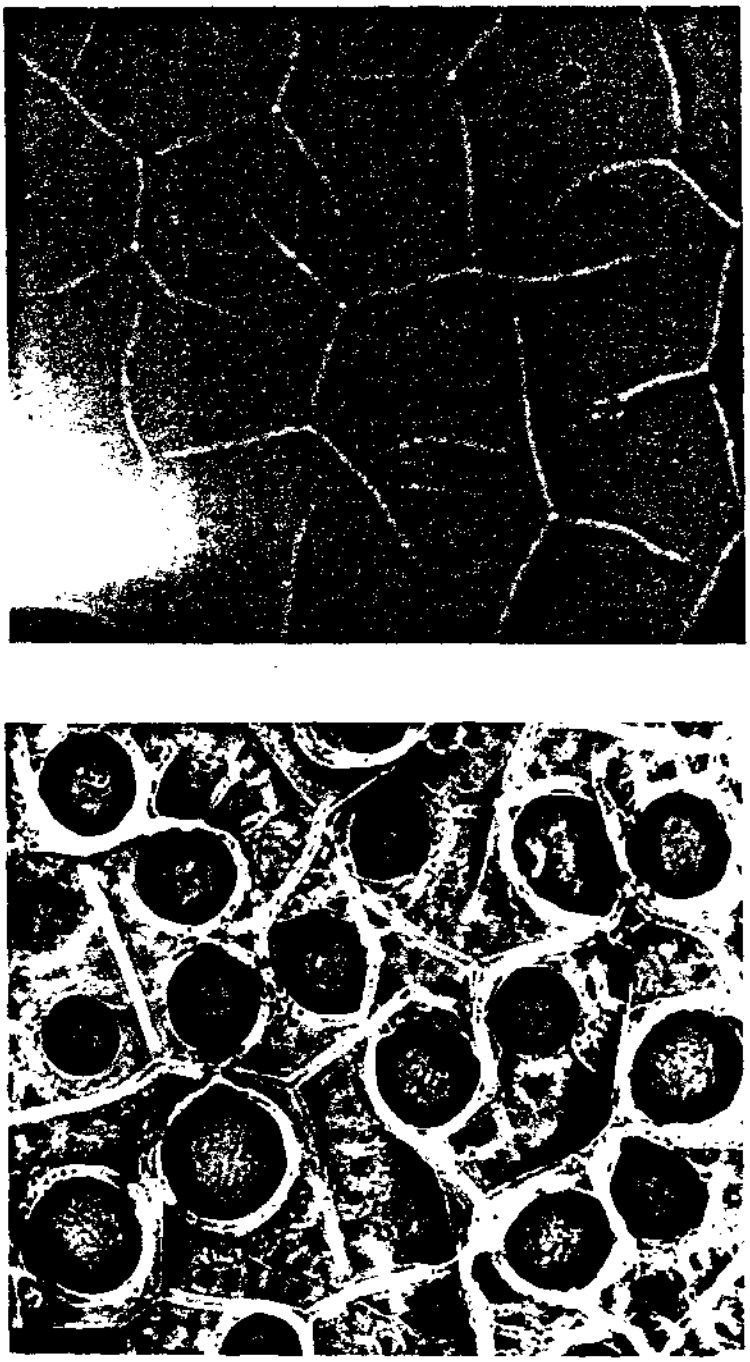

FIG. 6.6 The hexagonal pattern (top) in the gel slab with SA = 600mg/100ml evolves to the bubble pattern (bottom) after the gel is immersed to 55% acetone concentration. The initial thickness of the gel slab is 0.193 mm. The bubbles apparently grow from the middle of the hexagonal cells. The black bar indicates a length of 0.5 mm.

6.3.4 The bubble pattern

As we have just discussed, when the acetone concentration is slightly higher than the critical value, the grain pattern appears. For even higher concentration, the surface shrinking is more severe. Thus an "impermeable" dense surface is formed and the bubble pattern occurs. The process of formation for the bubble patterns is revealed by Fig. 6.6. For an acetone concentration higher than X_c, the cusp lines of the original hexagonal pattern serve as nuclei for shrinking. The shrinking process widens the upper portion of the cusp structure first and drive solvent toward the center of the hexagon. This causes the formation of a bubble in the middle of the hexagon (Fig. 6.7a & 6.7b). As the rest of the cusp structure eventually widens, the bubble grows larger and the hexagon disappears (Fig. 6.7c).

The effect of the dense surface layer can be further demonstrated in Figure 6.8 which shows the bubble pattern of the SA300mg/100ml PAAM gels as a function of acetone concentration in details. At the bubble onset concentration, X=45%, the bubbles are small and the number of bubbles in unit surface area is large (a). The slightly increasing acetone concentration to X=46% results in larger bubbles which fairly cover whole surface (b). As the acetone concentration increases, the number of bubbles in the surface decreases (c, d and e). For X=65%, bubbles almost disappear (f). This suggests that the impermeable dense surface become thicker with increase of the acetone concentration. When the dense layer is too thick, the bubbles are suppressed.

Fig. 6.9 (a, b and c) shows the hexagonal pattern of gels of different initial thicknesses in water. When these gels are put in an acetone/water mixture with 55% acetone concentration, the bubble patterns form on the gel

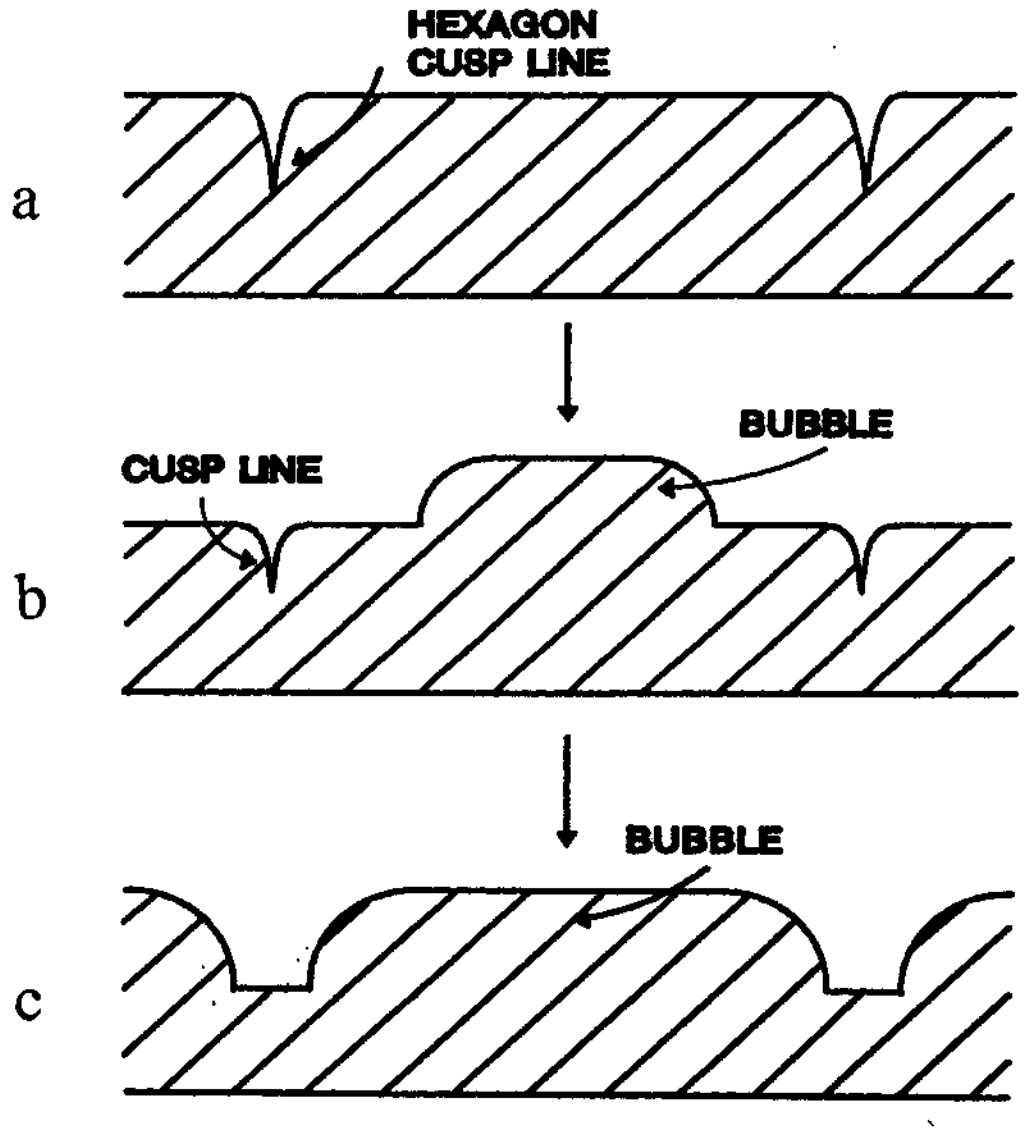

FIG. 6.7 Mechanism of the bubble formation. (a) Cross section area of the hexagonal pattern. (b) As the acetone concentration is changed from $X < X_c$ to $X > X_c$, the cusp lines behave as nuclei for shrinking resulting in bubble formation in the middle of the original hexagonal cells. (c) Further widening of the cusp lines causes the bubble to grow larger and the hexagonal (cusp lines) to disappear.

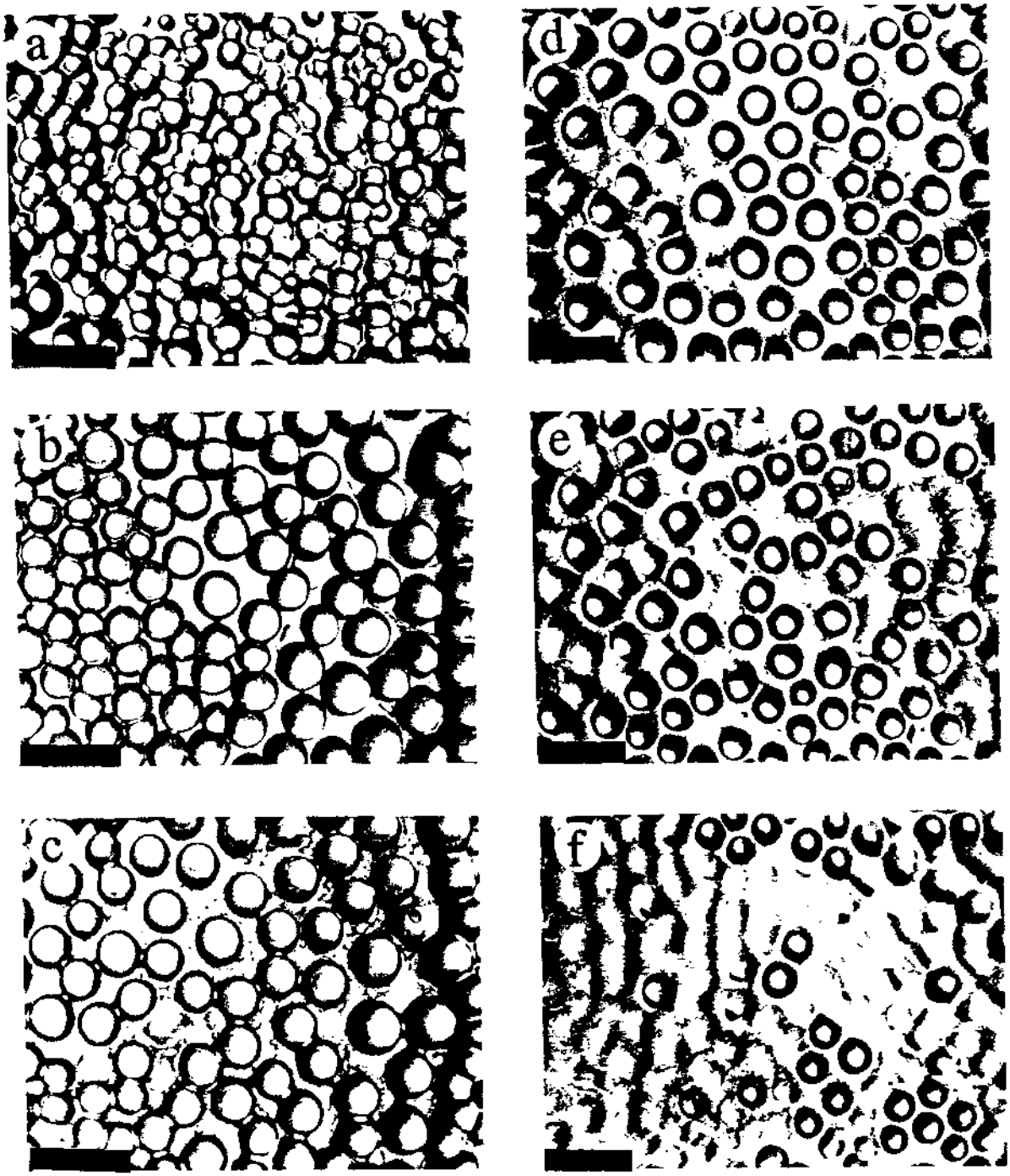

FIG. 6.8 The bubble pattern evolution in ionized polyacrylamide gel slabs (SA = 300mg/100ml) as a function of acetone concentration (wt%). (a) 45%, (b) 46%, (c) 55%, (d) 58%, (e) 61%, and (f) 65%. As the acetone concentration increases, the number of bubbles in the gel surface decreases.

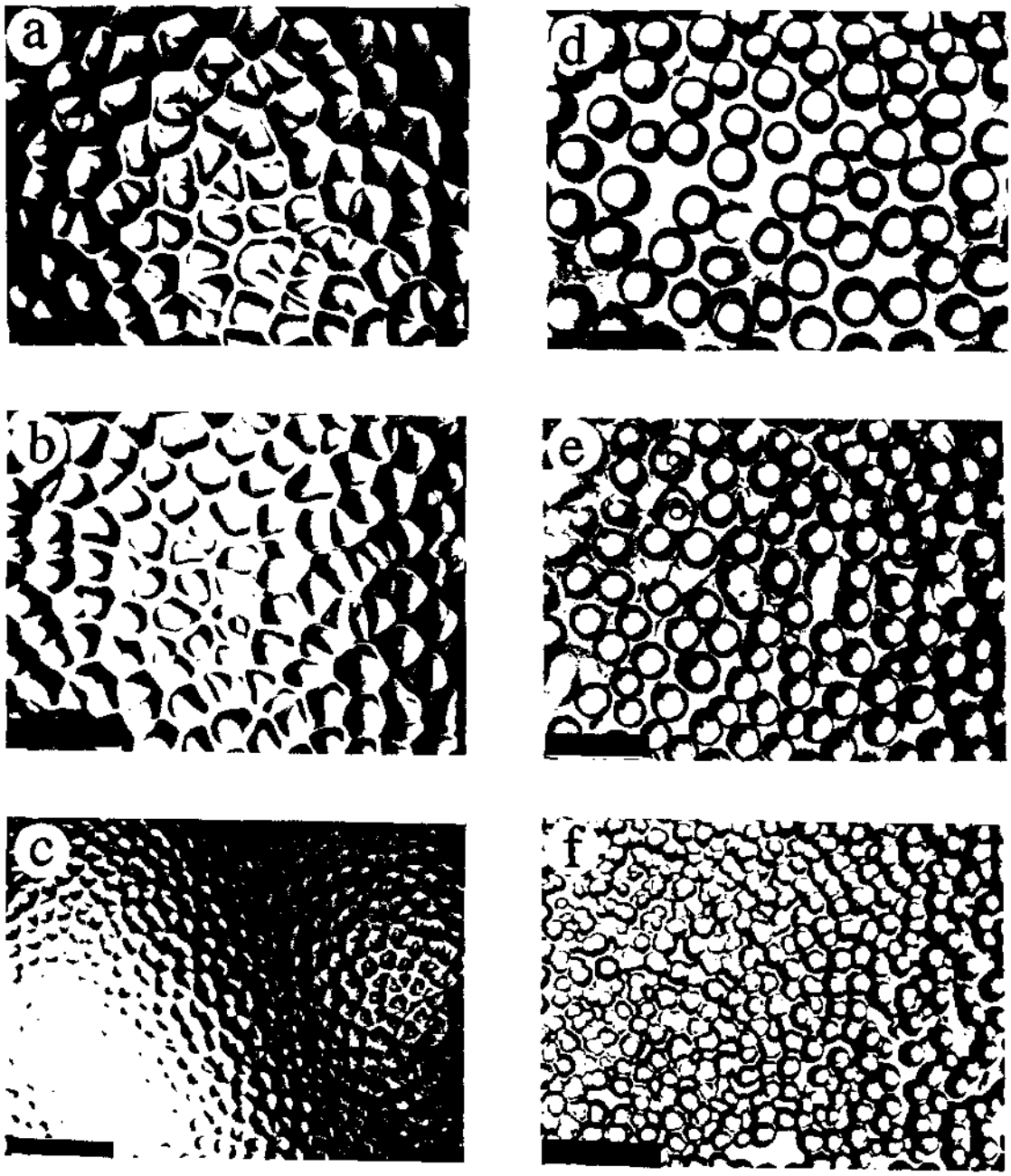

FIG. 6.9 (a) Swelling patterns of gel slabs with SA = 600mg/100ml in water. The initial thickness from top to bottom is: 0.813 mm, 0.559 mm, 0.315 mm, respectively. (b) Corresponding shrinking patterns in 55% acetone concentration.

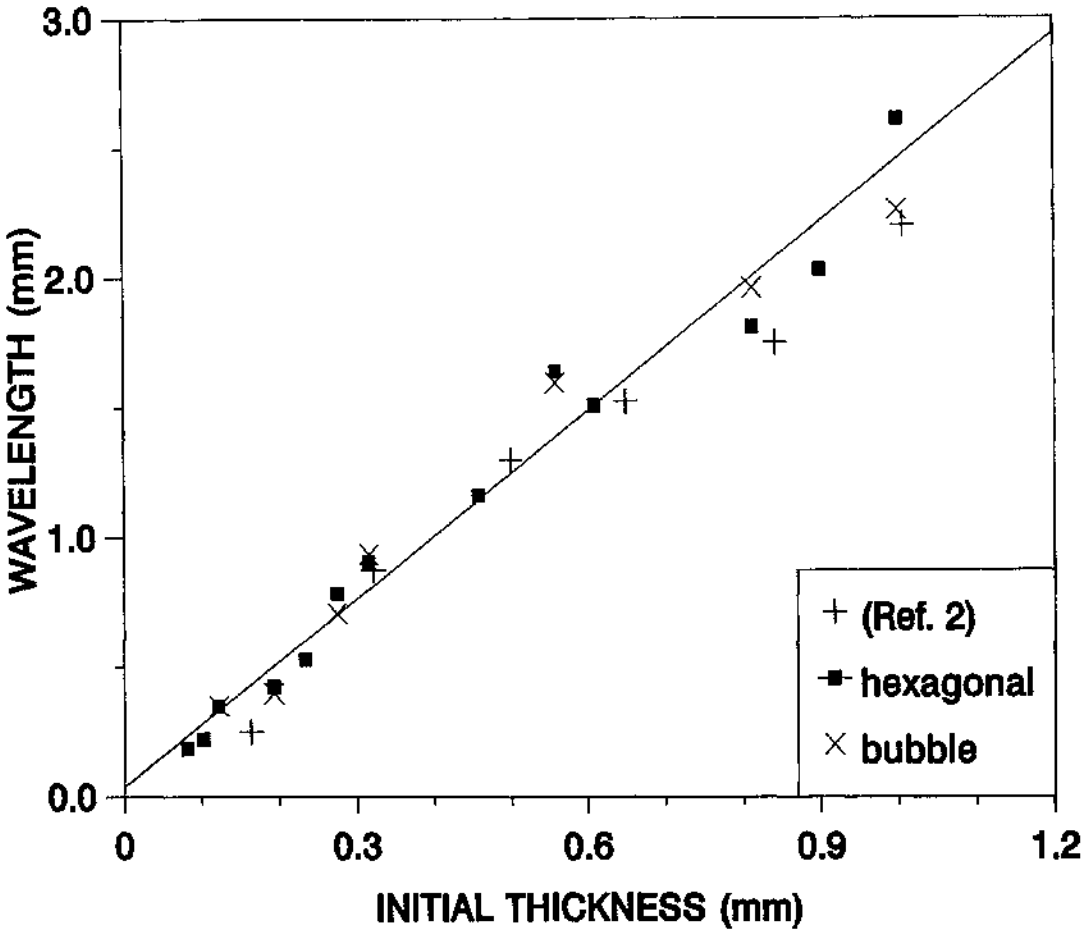

FIG. 6.10 Initial-thickness dependence of the wavelength for patterns of gel slabs. Cross symbols represent the bubble pattern and solid squares represent the hexagonal patterns. The solid line is the least square fit to the data. Plus symbols are results from previous measurements [2] on the hexagonal pattern.

surfaces in about six hours, as shown in Fig. 6.9 (d, e and f). The wavelength of the bubble pattern also increases as the gel thickness increases, similar to the wavelength behavior for the hexagonal pattern. Fig. 6.10 shows the wavelengths for the hexagonal pattern (■ symbol) and the bubble pattern (× symbol) as a function of initial sample thickness. The solid line with the slope of 2.42 can describe both sets of data very well. This is expected based on Figure 6.7. The results obtained from previous measurements (+ symbol) [2] on the swelling hexagonal pattern are also included in Fig. 6.7 for comparison. The agreement among these data is obvious.

6.3.5 Comparing the hexagonal cells with langmuir monolayer cells

By examining the cell-side distribution of hexagonal patterns, it is found that there are only about one-half of the cells in six sides. Fig. 6.11 is a plot of

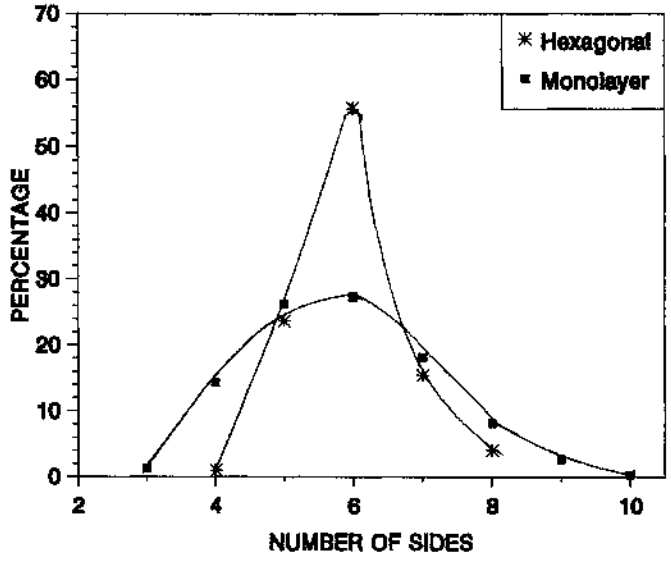

FIG. 6.11 Cell-side distributions for hexagonal pattern. The results of monolayer are from ref. 14.

cell-side distribution. The average side $<n>$ is equal to 6.04. The monolayer cell distribution data [14] are also plotted in Fig. 6.11 for a comparison. As one can see from Fig. 6.11, the peak width of gel cell-side distribution is much narrower than that for the monolayer pattern.

Fig. 6.12(a) and Fig. 6.12(b) show, respectively, the average area and perimeter plotted against number of side, n. From the study of biological systems, Lewis [15] proposed that the average area of a cell, $<A_n>$, should be a linear function of the number of sides, a relation now called Lewis's Law. But for soap foams [16], grain boundaries [17,18] and langmuir monolayers [14], it is the average perimeter of cells, $<P_n>$, not the area, that is linear in n. Both theories seems describing our data well. From physical point of view, the Lewis law should be better for describing our data because the gels are similar to the biological systems, to some extend.

6.3.6 Discussion

The mechanism of the pattern evolution as a function of acetone concentration for constrained gel slabs may be summarized as following. First, the hexagonal pattern consisting of cusp lines forms on the gel surface in pure water. When the sample is immersed in an acetone/water mixture near the phase transition point, new lines are generated to form many smaller cells, resulting in a grain pattern. The depths of the cusp lines become shallow. On the other hand, if the gel is directly immersed in a higher acetone concentration, the gel severely shrinks and develops the bubbles from the middle of the original hexagonal cells. The initial state of the swelling hexagonal pattern appears very important for the latter development of the grain and bubble patterns.

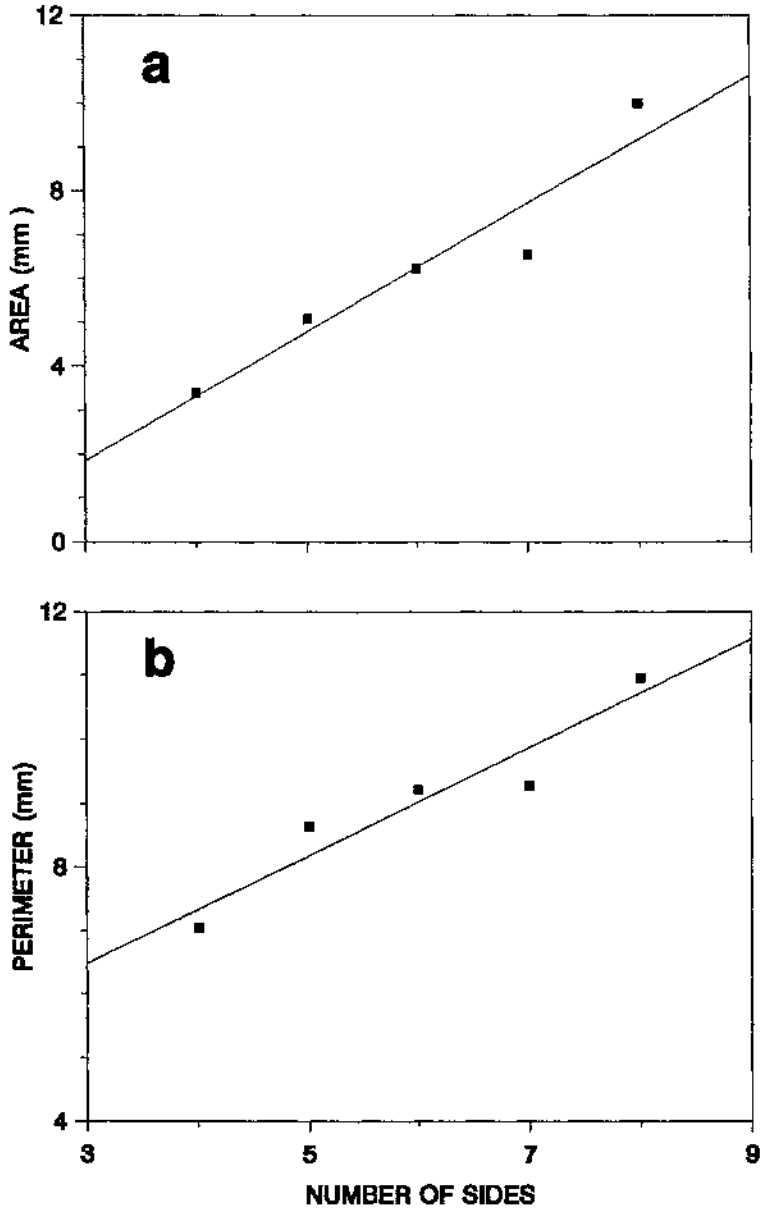

FIG. 6.12 (a) Average cell area as a function of the number of sides (n); (b) average cell perimeter as a function of n. The lines represent linear least-squares fit to the data.

Pattern formation in shrinking gels is a kinetic process. It is noted that all shrinking patterns are in a meta-stable state. If the time is long enough, the shrinking pattern will disappear since the gel will eventually reach a homogeneous collapsed state. This occurs by diffusion through the thin bubble layers and results in the disappearance of the pattern.

It is interesting to compare the non-constrained (gel beads) [3], one-dimensionally constrained (cylindrical gel with fixed depth) [1], and the two dimensionally constrained (gel slabs fixed on a substrate) gel shrinking patterns. As the number of constrained dimensions, d_c, increases (0 to 2), the number of patterns reaches maximum at $d_c = 1$.

6.4 Conclusion

Pattern formation in constrained PAAM/SA gel slabs has been investigated in acetone/water mixtures. The shrinking patterns have been classified into three groups and are presented as a "phase diagram" for various acetone concentrations and ionic strengths. New features of patterns provided by this study suggest that the patterns not only depend on external parameters such as temperature and acetone concentration, but also depend on the boundary conditions (i.e., constraints). The wavelength of the bubble pattern is found to be linearly proportional to the initial thickness of the sample and is the same as the hexagonal pattern wavelength. This indicates that there is a memory effect during a crossover between the patterns. Both the grain and the bubble patterns can be qualitatively explained in terms of formation of a dense ("impermeable" to solvent) surface.

CHAPTER 6 REFERENCES

1. E. Sato-Matsuo and T. Tanaka, Nature **358**, 482(1992).
2. T. Tanaka, S.T. Sun, Y. Hirokawa, S. Katayama, J. Kucera, Y. Hirose and T. Amiya, Nature, **325**, 796(1987); in Molecular conformation and dynamics of macromoleculues in condensed systems, (Elsevier Sci. Publishers, 1988).
3. E. Sato-Matsuo and T. Tanaka, J. Chem. Phys. **89**, 1695(1988).
4. T. Komori, H. Takahashi and N. Okamoto, Colloid and Polym. Sci. **266**, 1181(1988).
5. W. R. Drummond, M. L. Knight, M. L. Branmnon and N. A. Peppas, J. Controlled Release **7**, 181(1988).
6. T. Hayashi, H. Tanaka, T. Nishi, Y. Hirose, T. Amiya and T. Tanaka, J. Appl. Polym. Sci.: Appl. Polym. Symposium **44**, 195(1989).
7. T. Hwa and M. Kardar, Phys. Rev. Lett. **61**, 106(1988).
8. K. Sekimoto and K. Kawasaki, Phys. A **154**, 384(1989); J. Phys. Soc. Jpn. **57**, 2597(1988).
9. A. Onuki, J. Phys. Soc. Jpn. **57**, 703(1988).
10. Y. Li and T. Tanaka, Annual Review of Materials Science, **22**, 243(1992).
11. Y. Li, Z. Hu and C. Li, J. Appl. Polym. Sci. **50**, 1107(1993).
12. S. Hirotsu, J. Chem. Phys. **94**, 3949(1991).
13. C. Li, Z. Hu and Y. Li, Phys. Rev. E **48**, 603(1993).
14. K.J. Stine, S.A. Rauseo, B.G. Moore, J.A. Wise, and C.M. Knobler, Phys. Rev. A **41**, 6886(1990).
15. F.T. Lewis, Anat. Rec. **38**, 341(1928).

16. J.A. Glazier, S.P. Gross, and J. Stavans, Phys. Rev. A **36**, 306(1987).

17. D.J. Srolovitz, M.P. Anderson, P.S. Sahni, and G.S. Grest, Acta Metall. **32**, 793(1984); Phys. Rev. Lett. **50**, 263(1983).

18. D.A. Aboav, and T.G. Langdon, Metallogr. **2**, 171(1969).

CHAPTER 7

TEMPERATURE AND TIME DEPENDENCE OF SURFACE PATTERNS IN CONSTRAINED IONIC NIPA GELS

7.1 Introduction

When the osmotic pressure of a gel is suddenly and drastically changed, a large degree of swelling or shrinking can occur. Accompanied with these volume change processes, surface patterns usually develop [1-5]. In the swelling process, the patterns are typically honeycomb-like, or, hexagonal [1, 2]. Stable swelling patterns can be obtained by constraining part of the gel [2, 3]. The formation of the swelling patterns can be understood based on elasticity theory [2, 6-8]. The swelling patterns reported so far are mostly observed in polyacrylamide-derivative (PAAM) gels [1-4] or hydroxyethyl methacrylate and methacrylic acid co-polymer gels [5].

Bubble patterns are often associated with a large degree of volume shrinking in unconstrained hydrogels [9-10]. Sato-Matsuo and Tanaka observed a variety of patterns on the surface of acrylamide gel cylinders with fixed length in acetone/water mixtures. These patterns include surface bubbles, necklace-like bubbles, bamboos, tubes, and many combinations of different patterns [10]. We recently observed grain, and bubble patterns in the shrinking process of acrylamide gel slabs with one of their surfaces fixed onto a rigid substrate [11]. The shrinking patterns depend not only on the gel initial and final states, but also on the mechanical constraint (boundary conditions) and gel geometry [9-11]. Unlike swelling patterns, which can be "frozen" (stable in time) by

permanent constraint, the shrinking patterns are, in principle, metastable or unstable. Depending upon the details, the presence of shrinking patterns can be as short as one minute [9] on free shrinking gel beads, up to several days on constrained gel slabs [11], and up to several months for some patterns on the surface of gel cylinders with fixed length [10].

The observation of shrinking patterns in thermal sensitive N-isopropyl-acrylamide (NIPA) gels was first reported by Sato-Matsuo and Tanaka [9]. In response to a sudden temperature jump, the gel beads in water undergo a shrinking process and exhibited bubbles on their surfaces. Here we report the observations of patterns in constrained ionic NIPA gel slabs as a function of temperature and time. The constraint from the substrate introduces different patterns with much longer temporal stability compared to that of freely shrinking gels. The results will be compared to the patterns obtained in constrained PAAM gels in acetone/water mixtures.

7.2 Experimental

The NIPA gel samples were made by free radical polymerization. The sample preparation was detailed in chapter 3. A mixture of 7.8 g of N-isopropyacrylamide (Kodak Co.), 133 mg of methylene-bis-acrylamide as crosslinker, tetra-methyl-ethylene-diamine (240 μl) as accelerator, and sodium acrylate (600mg, ionic group), were dissolved in 100 ml of deionized and distilled water. Nitrogen gas was bubbled through the solution to remove dissolved oxygen. Then ammonium persulfate (40 mg) as an initiator was added to the solution. A thin film of the solution was cast between a GelBond film (FMC Co) and a microscope slide with a fixed separation. Since the GelBond

film contains polymerization-active chemical groups, the bottom surface of the gel slab was thus covalently cross-linked to the GelBond film. The samples were left untouched in a water bath both to swell and to wash away the unreacted chemicals before being used for measurement. The temperature of samples was controlled by a circulation water bath (Brinkmann Lauda Super RM-6) and was stable to 0.1°C over 24 hours.

7.3 Results and discussion

All samples were initially kept in water at room temperature (fully swollen) for three days and the hexagonal pattern developed on their surfaces. The gel patterns were then studied in warm-up runs with two different thermal paths detailed as following.

In the first approach (series A), a number of samples were heated from room temperature to a different temperature and each was maintained at its temperature for at least 24 hours. During this period, the gel surface pattern was examined using a camera. In the second approach (series B), the temperature of a single gel was raised stepwise to higher temperatures. The gel was kept in each temperature for 24 hours.

The thicknesses of free and constrained gels as a function of temperature in series B is shown in Fig. 7.1. Taking the point at which the thickness decreases discontinuously as the transition temperature T_c, the value of T_c for the constrained gel is higher (by about 3°C) than the value for the unconstrained gel. This is caused by the fact that once the temperature is beyond 38°C, the constraint corresponds to a positive osmotic (expanding) pressure. This osmotic pressure pushes the phase transition temperature higher.

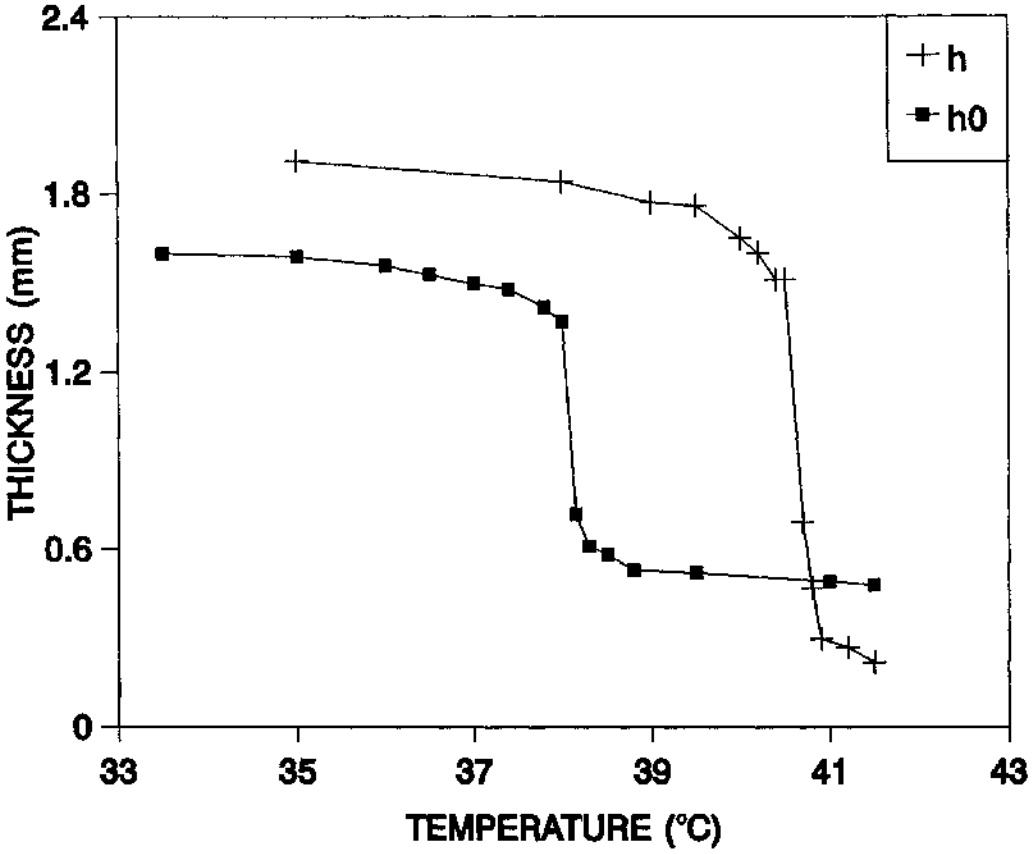

FIG. 7.1 The thickness of free (■) and constrained (+) NIPA/SA gels with SA = 600mg/100ml as a function of temperature. The arrow indicates the onset of the bubble pattern. The initial thicknesses of samples are equal 1.0 mm. The measurements of the constrained gels were done the same samples used to obtain the pattern. Solid lines are guides to the eye for all figures.

Similar behavior has been observed in neutral and lower ionic concentration constrained NIPA gel [12-13].

7.3.1 Temperature dependence of patterns

Fig. 7.2 shows the typical patterns of constrained NIPA/SA gel slabs with SA = 600mg/100ml for various temperatures in series A. These pictures were taken after the samples reached designated temperatures for certain periods of time as indicated in the figure caption. The sequence of patterns in series A can be classified in four groups. For $T < 40.0\ C^0$, gels have the hexagonal pattern. From 40.0 C^0 to 40.2 C^0, many smaller unit cells grow out from the original larger unit cells and the grain pattern forms. Bubbles develop on the gel surface between 40.3 C^0 to 40.8 C^0. Above 40.9 C^0, the gel slabs become opaque and their patterns disappear. The hexagonal, grain, and bubble patterns are stable for weeks, about 5 hours, and about two days, respectively.

Fig. 7.3 shows the temperature dependence of patterns of gels in series B. These pictures were taken about 24 hours after the gel reached each temperature. In this series, we have observed the hexagonal pattern for $T <$ 40.7 °C and the bubble pattern for $T \geq$ 40.7°, but not the grain pattern. The bubbles disappear at 41.5°C. A striking feature in series B is that the average distance between the neighboring pattern cells, that is, the wavelength, increases as the temperature is raised toward T_c as shown in Figure 4. This seems to indicate there is a kinetic effect involved in the observed hexagonal patterns. From Figures 7.1 and 7.3, it is clear that the bubble pattern is associated with the collapsed gel state.

In summary, there are two major differences between the patterns of series A and B: first, the wavelength of the hexagonal pattern stays about the

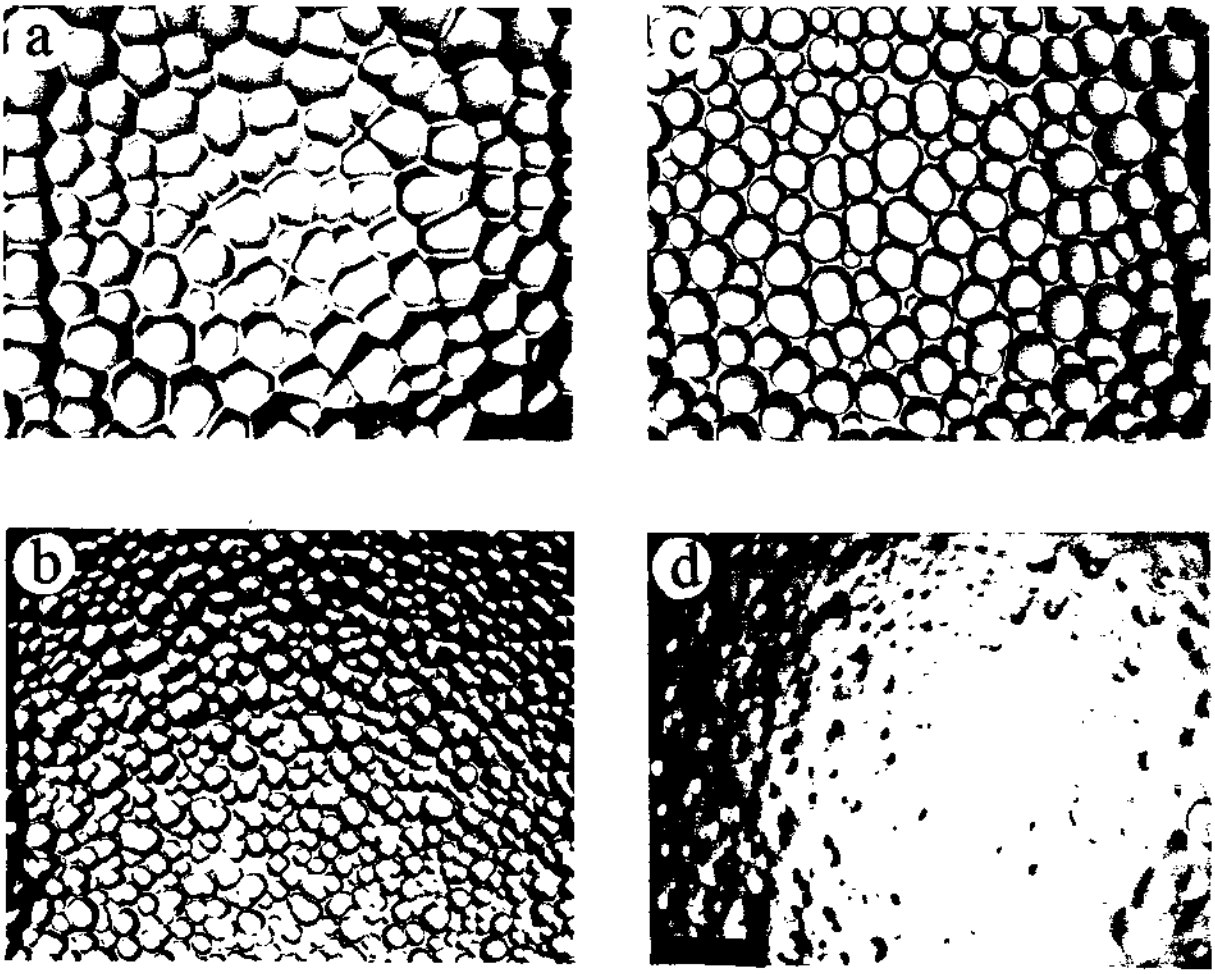

FIG. 7.2 The pattern evolution for ionized N-isopropyacrylamide gel slabs (SA = 600mg/100ml) as a function of temperature in series A. The time at which each photograph was taken after the sample reaches the temperature is shown in parenthesis. (a) 38°C, the quasi-hexagonal pattern (24 h); (b) 40.2°C, the grain pattern (3 h); (c) 40.5°C, the bubble pattern (20 h), (d) 42°C, no pattern (6 h). The black bar indicates a length of 0.5 cm for all figures except the one specified.

FIG. 7.3 The pattern evolution for ionized N-isopropyacrylamide gel slabs (SA = 600mg/100ml) as a function of temperature in series B. (a) 22 ^{0}C, (b) 39.0 ^{0}C, (c) 39.5 ^{0}C, (d) 40.2 ^{0}C, (e) 40.5^{0}C, (f) 40.7 ^{0}C, (g) 40.9 ^{0}C, (h) 41.5 ^{0}C. No grain pattern was observed in this series.

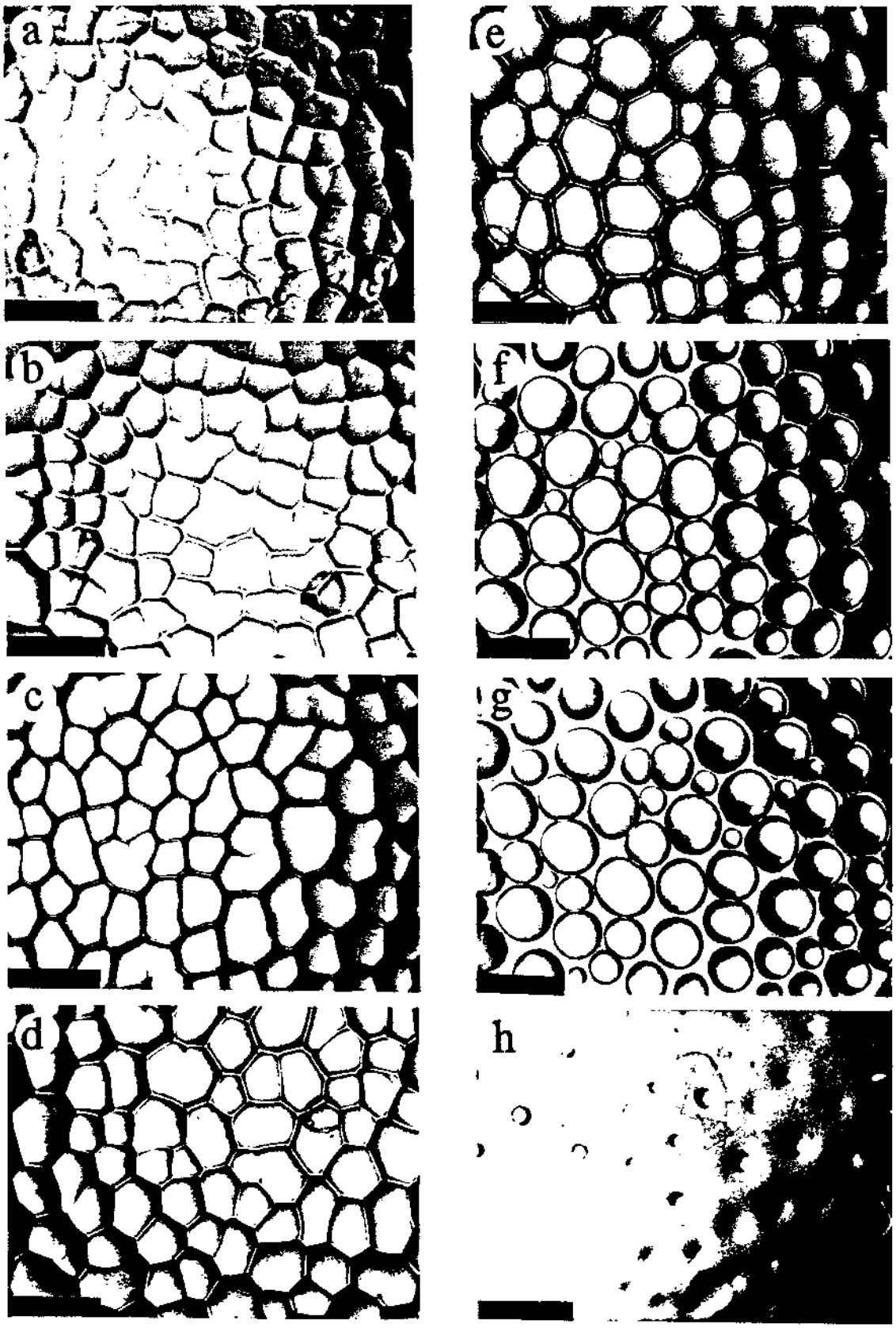
a
b
c
d
e
f
g
h

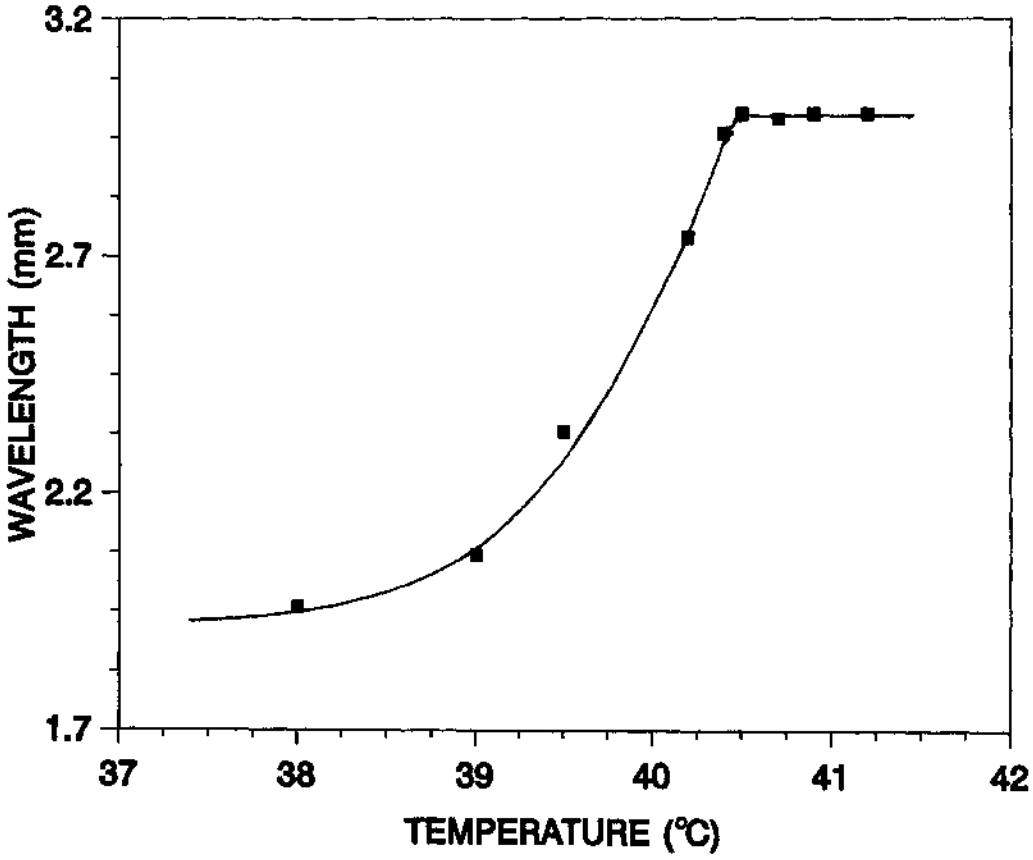

FIG. 6.4 The wavelength of patterns in Figure 7.3 is plotted as a function of temperature. The hexagonal pattern wavelength appears to increase as T approaches T_c.

same in A, while the pattern wavelength for $T < T_c$ increases with temperature in B; and second, the wavelength in A is smaller than the wavelength in B. This can be clearly seen by comparing patterns for series A and B side by side as shown in Fig. 7.5. The hexagonal and bubble patterns (Figure 7.5a & 7.5b) were obtained at 10 h and 15 h, respectively after the sample reached 40.5 ^{0}C from room temperature in series A. The corresponding patterns in series B (Figure 7.5c & 7.5d) were obtained at 40.5 ^{0}C for the hexagonal pattern and 40.7 ^{0}C for the bubble pattern. The pattern wavelength in series B is about 1.7 times larger than one in the left near 40.7 ^{0}C.

These differences may be due to different shrinking behavior for the two series. The thicknesses of gels in series B (plus signs) and A (circles) are shown in Fig. 7.6 as a function of temperature. In series B, the gel monotonically reduces its size, while in series A, as the final value of the temperature jump increases, the gel volume first decreases and reaches a minimum near T_c. For higher temperatures, the final gel volume settles at a higher value. This indicates that when temperature is suddenly raised above T_c, the morphology of the gel network is partially frozen, i.e., the gel is relatively large comparing with the gel which is slowly heated through T_c. The transition temperature in series B is higher than one in A by 0.3 ^{0}C. The onset temperature of the bubble pattern in B also shifts to corresponding higher temperature.

7.3.2 Pattern evolution with time

Fig. 7.7 shows the time dependence of patterns as a gel slab at room temperature is suddenly immersed into the 40.5 ^{0}C thermal bath. Initially, small dots start to appear and the cusp-lines of the original hexagonal cells (a) begin to disappear (b). At a certain point, the original hexagonal lines totally disappear

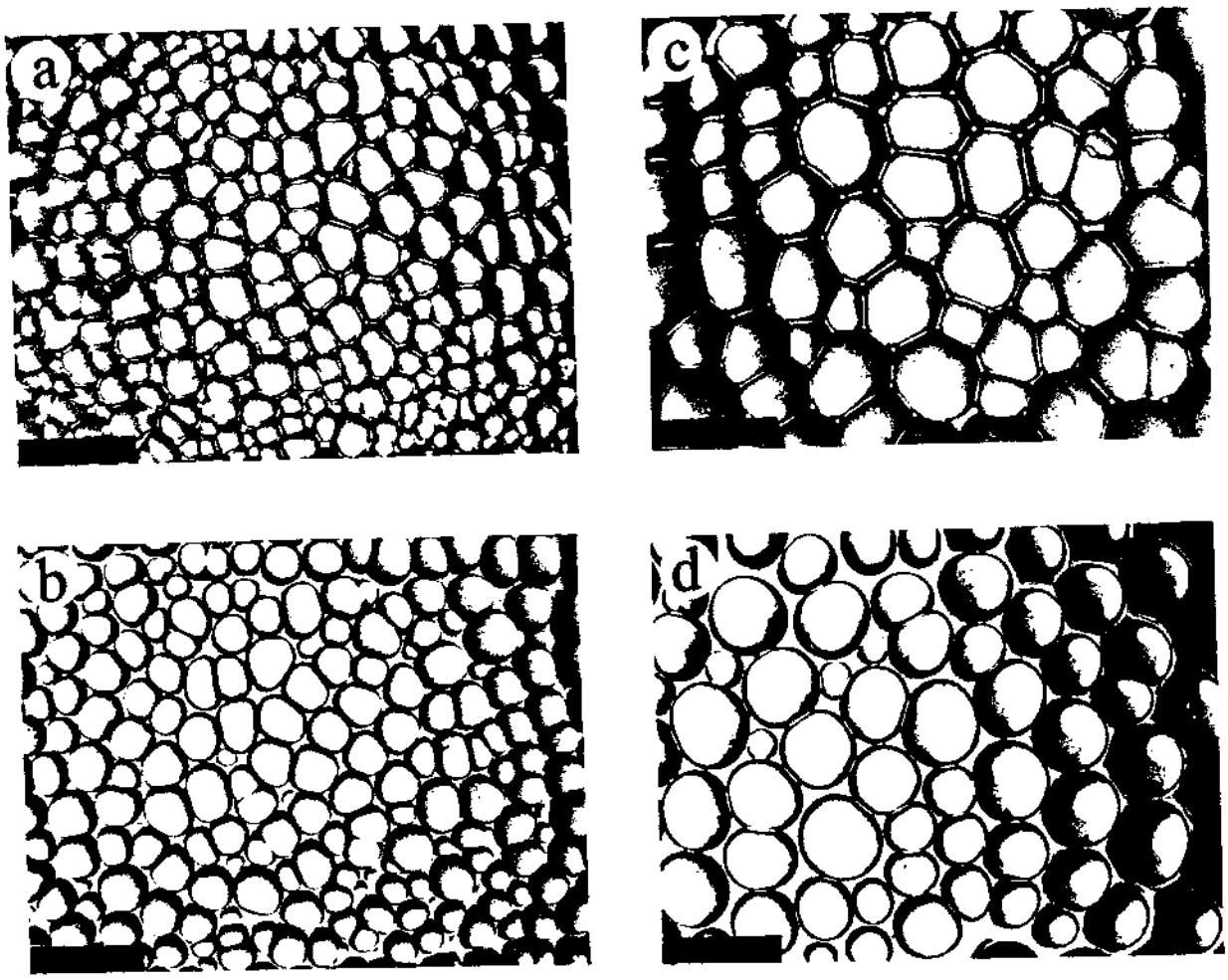

FIG. 7.5 Comparison the pattern wavelength between series A and B. (a) and (b) The hexagonal and bubble pattern were obtained at 10 hr and 15 hr, respectively, after the sample reached 40.5 ^{o}C from room temperature in series A. (c) and (d) The hexagonal pattern and the bubble pattern were obtained at 40.5 ^{o}C and at 40.7 ^{o}C in series B, respectively.

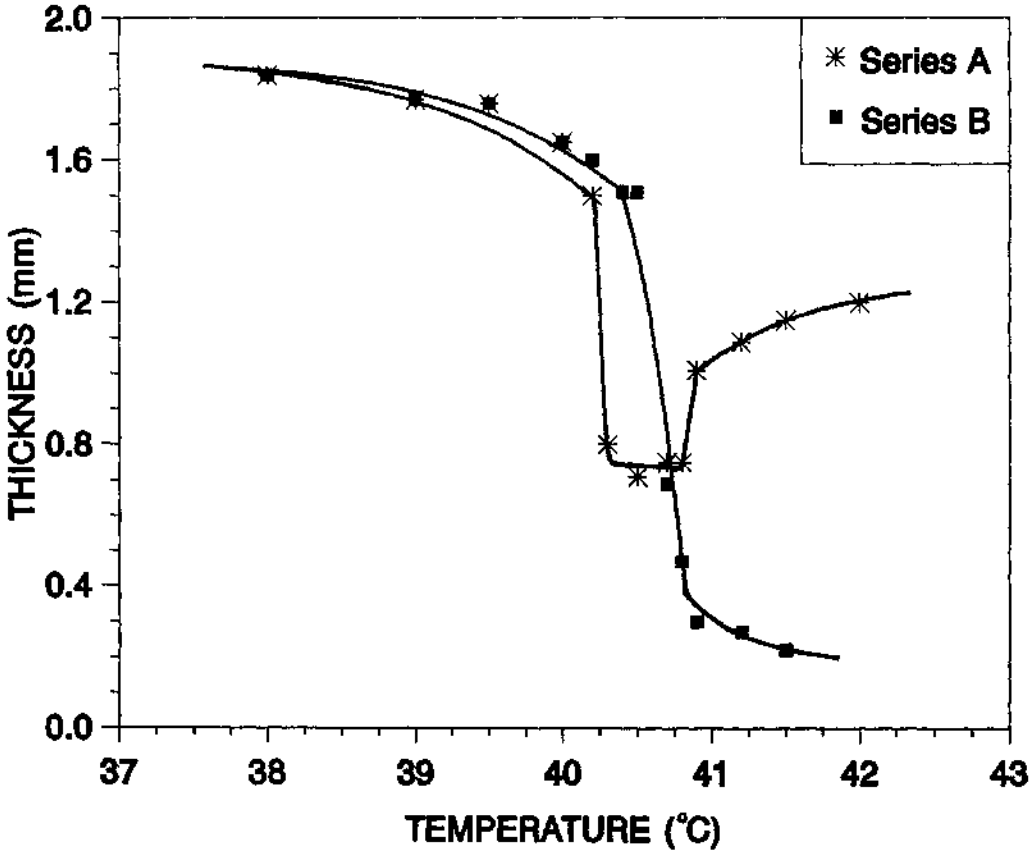

FIG. 7.6 The thickness of NIPA/SA gels with SA = 600mg/100ml as a function of temperature for different thermal paths (series A and series B). The initial thicknesses of samples were equal 1.0 mm.

FIG. 7.7 Pattern evolution as a function of time when a room-temperature NIPA gel was immersed in a 40.5 ^{0}C thermal bath. (a) 0, (b) 30 min, (c) 2 h (d) 7 h, (e) 10 h, (f) 15 h, (g) 30 h, (h) 48 h.

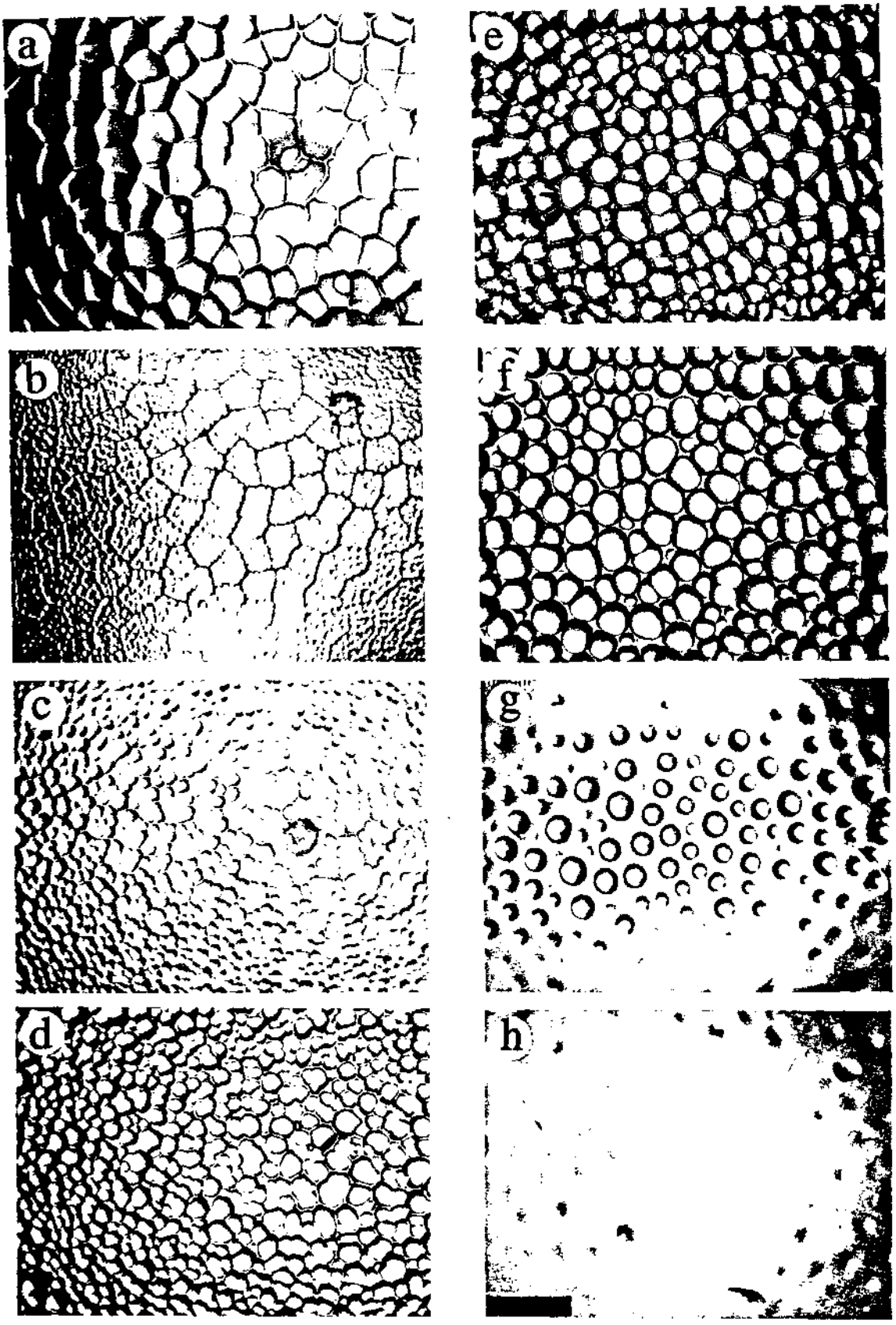
a
b
c
d
e
f
g
h

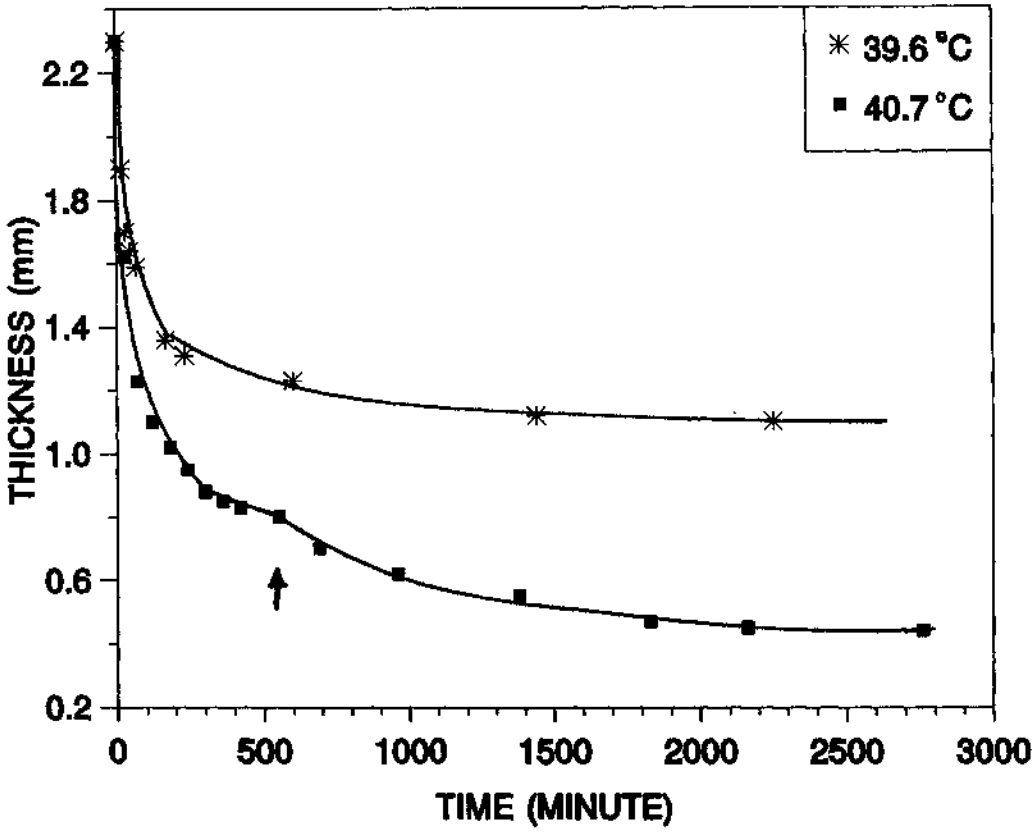

FIG. 7.8 The time dependent thickness of NIPA/SA gels with SA = 600mg/100ml. Two identical room temperature gels were heated to 39.6 °C, curve 1 (×), and 40.7 ° C, curve 2 (■), respectively. The arrow indicates the onset of the bubble pattern.

and the dots grow into small lines, forming the grain pattern (c). After about five hours, the grain pattern develops into hexagonal patterns (d, e) with a wavelength smaller than the original one. The new wavelength of the new hexagonal pattern appears to increase with time. For about another five hours, the hexagonal pattern turns into the bubble pattern (f). As time progresses, the bubbles reduce their size and gradually disappear (g). After about 48 hours, the bubbles completely disappear (h). This observation shows that both the grains and bubbles are metastable patterns.

Time dependent shrinking profiles of NIPA/SA gels with SA = 600mg/100ml have also been investigated. Two identical gels were heated from room temperature to below T_c, and above T_c, respectively. Their thicknesses were then measured as a function of time as shown in Figure 7.8. Curve 1 (×) represents the gel at 39.6 °C, which shrinks smoothly. At 40.7 °C, curve 2 (■), the gel enters the collapsed state and yields a more complex shrinking profile. Initially, the gel shrinks rapidly, then it temporarily stops shrinking, and finally it starts to shrink again after the plateau period. Comparing the patterns and the curve 2, we have identified that the end of the plateau period is the onset of the bubble pattern. This observation agrees with previous measurement on free spherical NIPA gels [9]. This plateau period is believed to be related to the formation of a dense shell of the shrunken gel surface which ultimately causes the formation of the bubble pattern.

7.3.3 Comparing patterns in PAAM and in NIPA gels

We have previously reported pattern formation in constrained polyacrylamide (PAAM) gels [11]. Comparing the NIPA/water (series A) gel system and the PAAM/acetone/water system with similar parameters, that is,

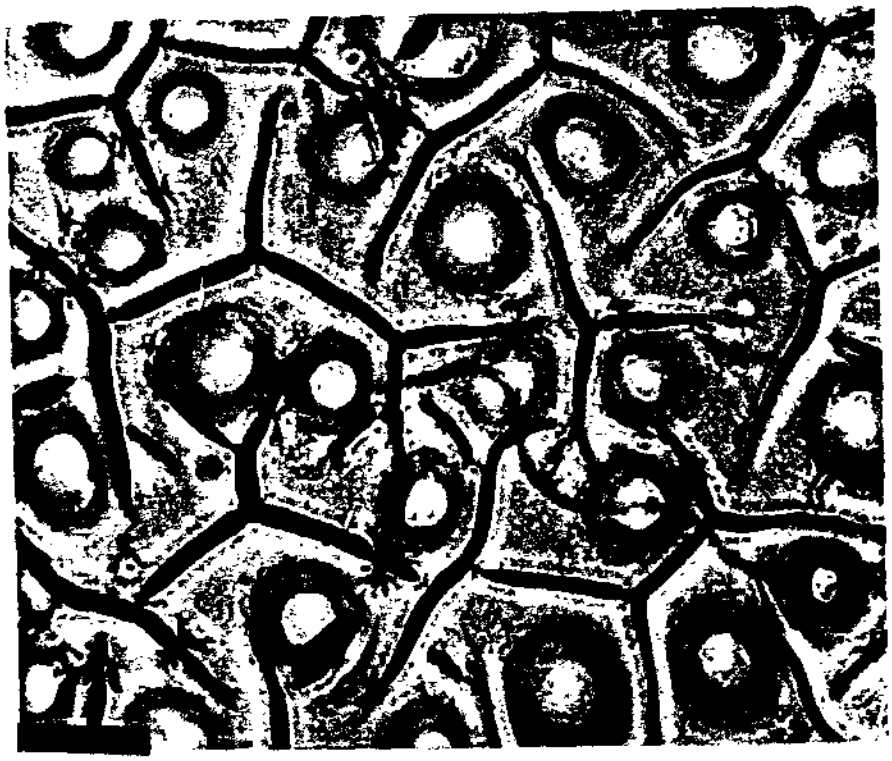

FIG. 7.9 The development of the bubble pattern of the acrylamide/sodium acrylate gel slab with SA = 600mg/100ml. The initial thickness of the gel slab is 0.122 mm. The bubbles apparently are present in the middle of hexagonal cells. The black bar indicates a length of 0.5 mm.

having the same size, boundary condition, and ionic strength (SA = 600mg/100ml), shows three major differences. (1) The shrinking patterns (i.e., grains and bubbles) last much longer in PAAM than in NIPA gels. (2) For NIPA gels near T_c, after the grain pattern, the new hexagonal pattern forms with time. This second hexagonal pattern is different from the one formed at room temperature, i.e., they cannot overlap each other. In contrast, the PAAM gel does not have the second hexagonal pattern. (3) For NIPA gels, each hexagonal cell evolves into a bubble, while for PAAM gels, a bubble can be present in the middle of a hexagonal cell. This is shown in Fig. 7.9, which is a typical picture of a constrained ionic PAAM gel (SA = 600/100ml) three hours after being put in acetone/water mixture with acetone concentration 55%. The thickness of the PAAM gel at preparation was 0.122 mm. The gel was initially fully swollen in pure water and had honeycomblike patterns on its surface.

7.3.4 Comparison with langmuir monolayer cells

The cell-side distribution of the hexagonal pattern of NIPA gels in the series B at the temperature of 40 ^{o}C is plotted in Fig. 7.10. The average side $<n>$ is equal to 5.88. The monolayer cell distribution data [14] are also plotted in Fig. 7.10 for a comparison. As one can see from Fig. 7.10, the peak width of gel cell-side distribution is much narrower than that for the monolayer pattern, agreeing with the results for the PAAM gel.

Fig. 8 (a) and Fig. 8 (b) show, respectively, that the average area and average perimeter are linearly proportional to the number of side, n. This indicates that both Lewis Law and the perimeter Law are suitable to describe the hexagonal surface pattern of the NIPA gel.

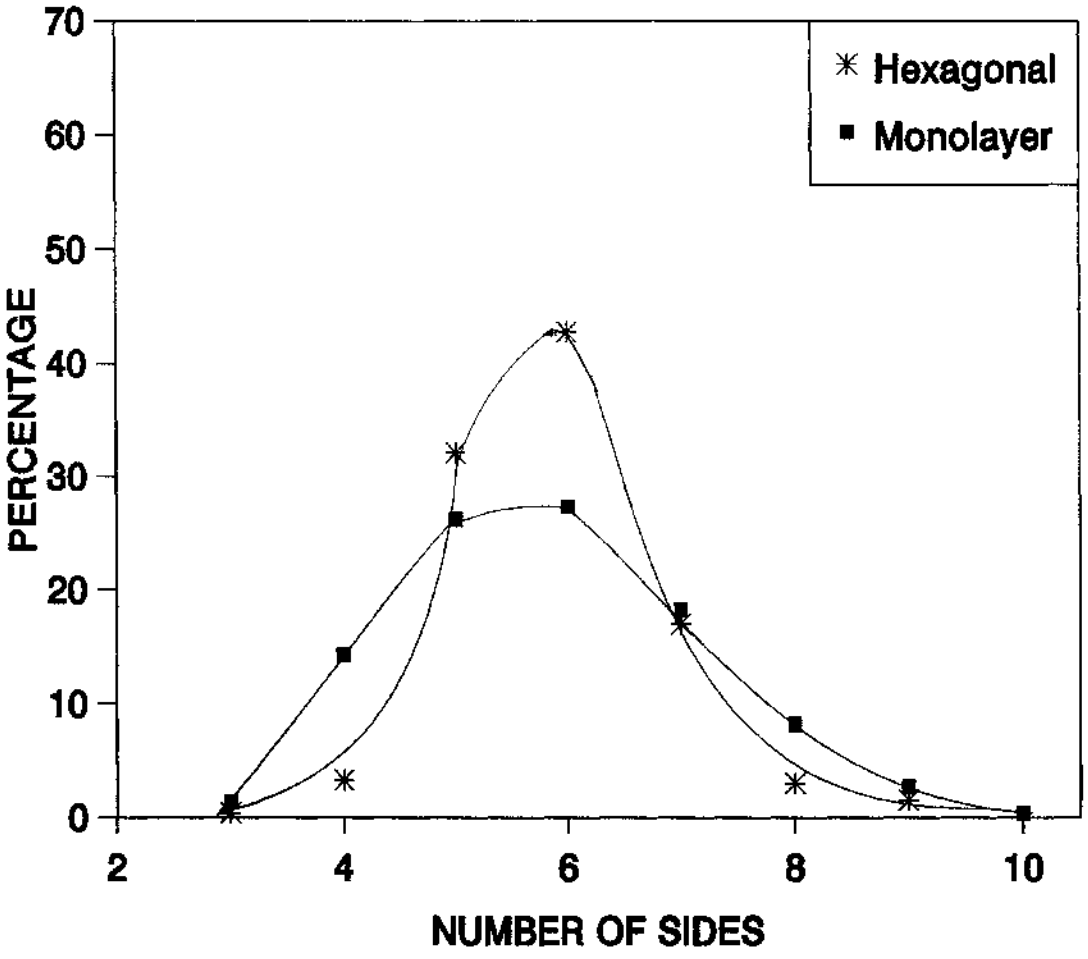

FIG. 7.10 Cell-side distributions of NIPA hexagonal pattern. The * one are the monolayer results obtained by reference 14.

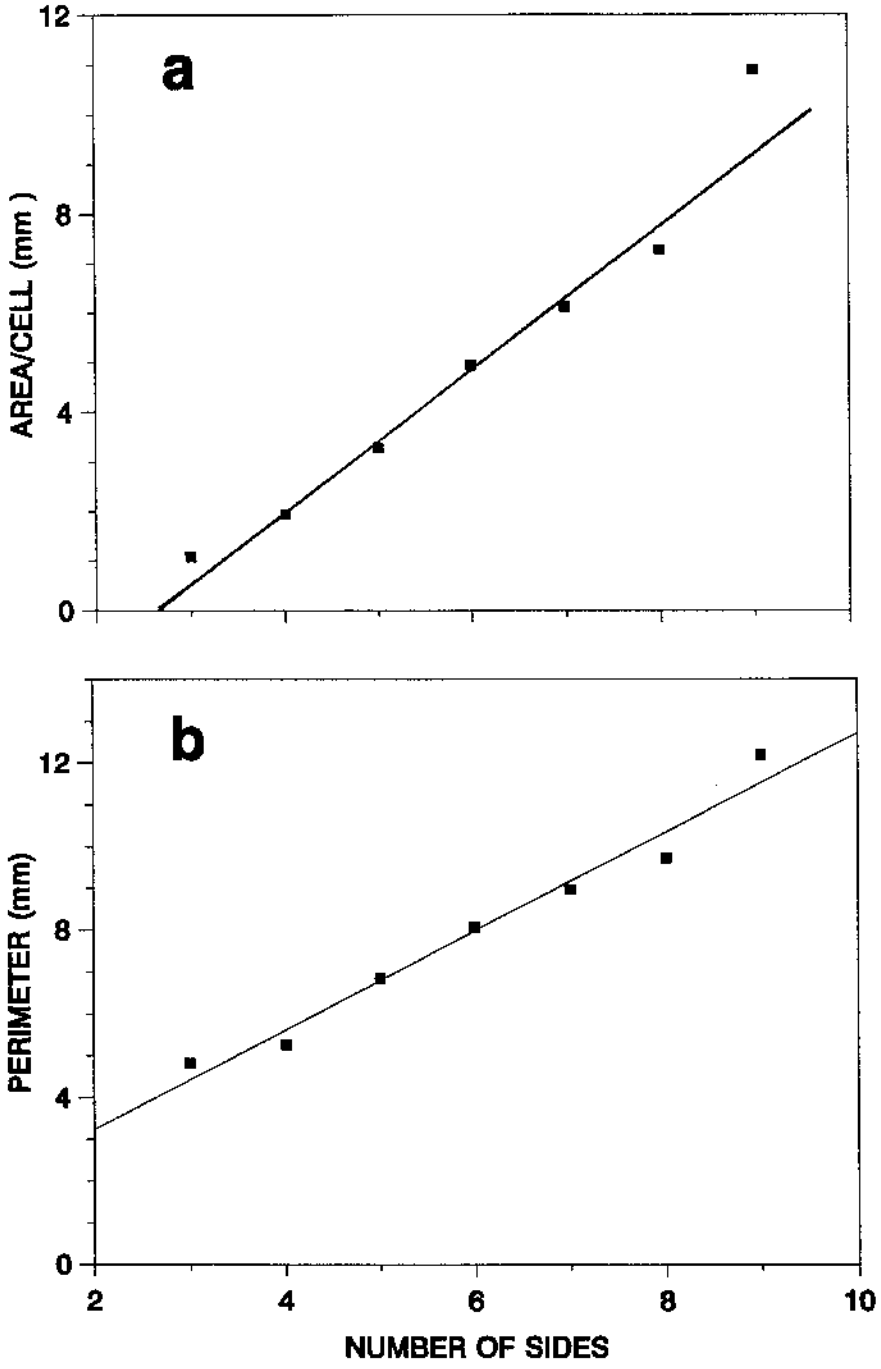

FIG. 7.11 (a) Average cell area as a function of cell sides n; (b) average cell perimeter as a function of n. The lines represent linear least-squares fits to the data.

7.3.5 Discussion

The mechanism of the pattern evolution as a function of temperature for constrained NIPA gel slabs may be described by the following steps. First, the hexagonal pattern consisting of cusp lines forms on the surface of the gel in pure water at room temperature. When the temperature of the sample is raised slightly above T_c, the surface of the gel slab starts to shrink to form a dense layer. The dense surface has a high tension and prefers to minimize its total area. This surface tension reduces the depth of the cusps of the original hexagonal patterns and thereby changing the local network density (the swelling profile) near the cusp lines. Since the total amount of water trapped under the dense surface is roughly constant, it is conceivable that these changes in the swelling profile create the grain patterns. Based on this argument, the depth of the grain patterns should be shallower than that of the hexagonal patterns in the swollen state. It is reasonable to expect the grain patterns to have relatively short life times. This agrees with the experimental observation. This is also very similar to the observation in PAAM gels [11].

On the other hand, if the temperature of the gel is suddenly changed from $T < T_c$ to $T > T_c$, the gel shrinks severely and the bubbles evolve from the original hexagonal cells as sketched in Fig. 7.12. At such higher temperatures, the cusp lines behave as nuclei for shrinking. The shrinking process widens the cusp lines and drives water toward the center of the hexagons, eventually forming a visible water bubble there, as shown in Fig. 7.12(a). In the case of PAAM gels as shown in Fig. 7.10(b), a similar process occurs except that initially only the upper part of the cusp lines widens, which creates a bubble in each cell. The lower part of the cusp lines keeps the original hexagonal pattern

FIG. 7.12 Descriptive sketches for bubble pattern formation in NIPA (a) and PAAM gels (b). NIPA gels do not have the intermediate bubble-in-hexagon pattern.

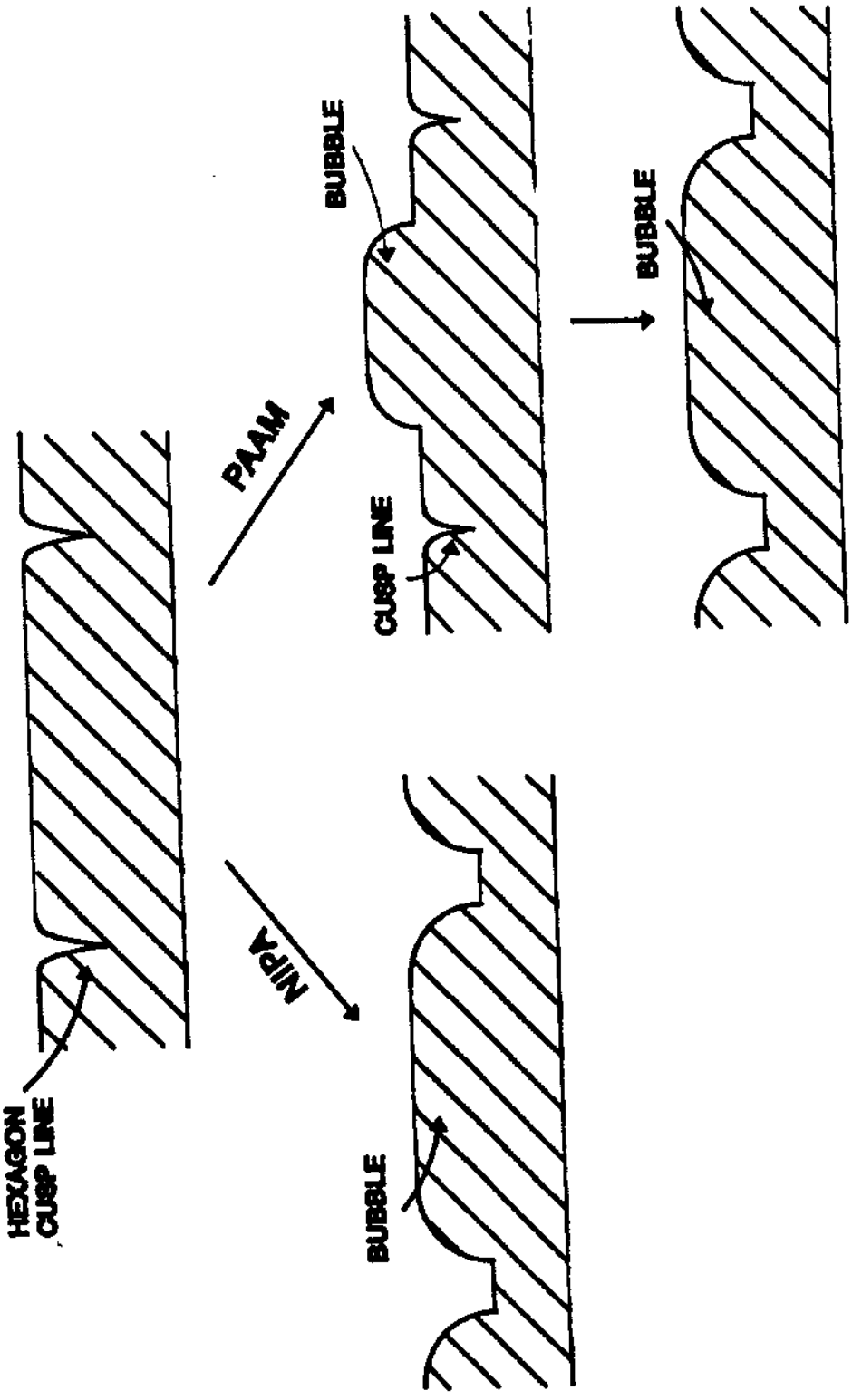

[a]

[b]

visually intact. Eventually, the cusp lines completely widen and the hexagonal pattern disappears.

7.4 Conclusion

Pattern formation in constrained ionic NIPA gels have been investigated for various temperature, time and thermal paths. The sequence of patterns, hexagonal, grain and bubble, has been classified for various temperatures. Two different thermal paths, called series A and B, have been employed. The wavelength of the hexagonal pattern stays about the same in A, but increased in B when the temperature is increased. Near T_c, the wavelength of both hexagonal and bubble patterns of series A are smaller than their counter parts of series B. These differences are attributed to the differences of their shrinking profiles. The time dependence of gel thickness has revealed that there is a plateau period, in agreement with previous observations of free spherical NIPA beads. The experiments show that each hexagonal cell evolves into a bubble for NIPA gels, while a bubble can be present in the middle of a hexagonal cell for PAAM gels. The mechanism of shrinking patterns can be qualitatively explained in terms of the dense surface produced during the shrinking process. Like that in monolayers, the average cell side $<n>$ of the hexagonal pattern is 5.88.

CHAPTER 7 REFERENCES

1. T. Tanaka, S.T. Sun, Y. Hirokawa, S. Katayama, J. Kucera, Y. Hirose and T. Amiya, Nature, **325**, 796(1987).
2. T. Tanaka, S.T. Sun, Y. Hirokawa, S. Katayama, J. Kucera, Y. Hirose and T. Amiya, in Molecular conformation and dynamics of macromolecules in condensed systems, (Elsevier Sci. Publishers, 1988).
3. T. Hayashi H. Tanaka, T. Nishi, Y. Hirose, T. Amiya, and T. Tanaka, J. Appl. Polym. Sci.: Appl. Polym. Symposium **44**, 195(1989).
4. T. Komori, H. Takahashi and N. Okamoto, Colloid and Polym. Sci. **266**, 1181(1988).
5. W. R. Drummond, M. L. Knight, M. L. Branmnon and N. A. Peppas, J. Controlled release **7**, 181(1988).
6. T. Hwa and M. Kardar, Phys. Rev. Lett. **61**, 106(1988).
7. K. Sekimoto and K. Kawasaki, Phys. A **154**, 384(1989); J. Phys. Soc. Jpn. **57**, 2597(1988).
8. A. Onuki, J. Phys. Soc. Jpn. **57**, 703(1988).
9. E. Sato-Matsuo and T. Tanaka, J. Chem. Phys. **89**, 1695(1988).
10. E. Sato-Matsuo and T. Tanaka, Nature **358**, 482(1992).
11. Y. Li, C. Li and Z. Hu, "Pattern formation of constrained PAAM gels in acetone/water mixture", (submitted to J. Chem. Phys.)
12. S. Hirotsu, J. Chem. Phys. **94**, 3949(1991).
13. C. Li, Z. Hu and Y. Li, Phys. Rev. E **48**, 603(1993).
14. K.J. Stine, et. al., Phys. Rev. A **41**, 6884(1990).

CHAPTER 8

CONCLUSIONS

This dissertation includes the study of the elastic properties, scaling behavior of polymer gels, ultrasonic attenuation and velocity of gels near the transition point, and the surface patterns of polymer gels. The major conclusions can be summarized into seven points:

1. Poisson's ratio is one of the most important quantities of a gel system. The measurement of Poisson's ratio is complicate because of the gel's inter-mediate state between the solid and liquid. A simple measurement technique makes it possible to systematically investigate the elastic properties of polymer gel systems. Using Landau's Elastic Theory, a new method for Poisson's ratio measurement based on the different swelling behaviors of constrained and free gel slabs is proposed. This method was tested in polyacrylamide gels and was proven to be precise and easy to use.

2. Poisson's ratio of NIPA gels exhibits a negative dip near the phase transition and the position of the dip shifts to a higher temperature as ionic concentration increases. The theoretical simulations of Poisson's ratio in NIPA gels is in a good agreement with the experimental results. In contrast to NIPA gels, Poisson's ratio of neutral PAAM gel shows no negative values throughout the measured transition region.

3. The scaling behavior of elastic properties of polyacrylamide gel in pure water solvent has been systematically studied as a function of chemical composition. It has been shown that the ratio of bulk modulus to shear modulus is directly

related to the scaling exponent δ. As the BIS (crosslinker) and AAm (monomer) increase, the exponent δ increases and the systems seem to be approaching the theta condition. As the network charge concentration (ionic group) increases, the exponent δ decreases dramatically. As a result, the concentration dependence of the swelling osmotic pressure is much weaker than non-ionic gels. The value of δ for non-ionic gels is chemical composition sensitive. The valve of δ for highly ionized acrylamide gels is around 1.25.

4. The behavior of ionized polyacrylamide gels qualitatively agrees with theoretical expectations based on polyelectrolyte solution behavior. The ionization salt concentration space can be divided into four regions. The region-I and III are transitional regions. In region-II, a peak in δ is observed. The last region is the theoretically predicted region in which the observed δ value is a constant and is around 1.8. The measurement on the scaling exponent δ has revealed rich information, which are worth further theoretical studies.

5. The ultrasonics is a non-destructive technique for monitoring the phase transformation of solid materials. The ultrasonic investigation of NIPA gels reveals that ultrasonic attenuation and velocity of NIPA gel depend on both temperature and the ultrasonic frequency. The acoustic attenuation exhibits the maximum near T_c and can be understood in terms of critical slowing down of the relaxation process during the phase transition. The dynamic scaling theory of Bhattacharjee and Ferrell provides a qualitatively description of the frequency and temperature dependence of the critical attenuation near T_c. Specifically, the acoustic attenuation versus the characterizing frequency ω^* at different frequencies reasonably scale onto a single curve and the dynamic scaling function is shown to generally agree with the shape of data curve. The analysis

shows that the NIPA gel belongs to the Ising system, agreeing with results of specific heat measurement. It is noted that ω_0 obtained from the scaling fitting is much greater than the value obtained by other independent methods. This discrepancy indicates that the modification to the theory is necessary. Since the theory is originally proposed for critical binary liquids, it would be natural step to take into account of finite shear modulus of gels for the future dynamic scaling model.

6. The shrinking patterns on the constrained PAAM/SA gel slabs in acetone/ water mixtures have been classified into three groups and are presented as a "phase diagram" for various acetone concentrations and ionic strengths. New features of patterns provided by this study suggest that the patterns not only depend on external parameters such as temperature and acetone concentration, but also depend on the boundary conditions (i.e., constraints). The wavelength of the bubble pattern is found to be linearly proportional to the initial thickness of the sample and is the same as the hexagonal pattern wavelength. This indicates that there is a memory effect during a crossover between the patterns. Both the grain and the bubble patterns can be qualitatively explained in terms of formation of a dense ("impermeable" to solvent) surface.

7. Pattern formation in constrained ionic NIPA gels have been investigated for various temperature, time and thermal paths. The sequence of patterns, hexagonal, grain and bubble, has been classified for various temperatures. Two different thermal paths, called series A (the samples were heated from room temperature to a different temperature and were kept for about 24 hours) and B (the temperature of a single gel was raised stepwise to higher one and kept for about 24 hours), have been employed. The wavelength of the hexagonal

pattern stays about the same in A, but increased in B when the temperature is increased. Near T_c, the wavelength of both hexagonal and bubble patterns of series A are smaller than their counter parts of series B. These differences are attributed to the differences of their shrinking profiles. The time dependence of gel thickness has revealed that there is a plateau period, in agreement with previous observations of free spherical NIPA beads. The experiments show that each hexagonal cell evolves into a bubble for NIPA gels, while the bubble is developed from the middle of a hexagonal cell for PAAM gels. The mechanism of shrinking patterns can be qualitatively explained in terms of the dense surface produced during the shrinking process.

The above study has increased our overall understanding of the polymer gels and opened the door for further improving gel mechanical properties. This dissertation also shows that polymer gel research is an exciting area and many unsolved problems are worth further investigation.

BIBLIOGRAPHY

1. D.A. Aboav, and T.G. Langdon, Metallogr. **2**, 171(1969).
2. J.C. Bacri and R. Rajaonarison, J. Phys.-Letts **40**, L-5(1979).
3. L. Brannon-Peppas and N. A. Peppas, Int. J. Pharm. **70**, 53(1991).
4. S. J. Candau, C. Y. Young, T. Tanaka, P. Lemarechal, and J. Bastide, J. Chem. Phys. **70**, 4694(1979).
5. S. Candau, J. Bastide, and M. Delsanti, Adv. Polym. Sci., **44**, 27(1982).
6. S.J. Candau, F. Ilman, F. Schosseler, and J. Bastide, Mat. Res. Soc. Symp. Proc. **173**, 3(1990).
8. Y. Cohen, O. Ramon, I. J. Kopelman, and S. Mizrahi, J. Polym. Sci. (Phys.) **30**, 1055(1992).
9. M. Daoud and P. G. de Gennes, J. Phys. (Paris), **38**, 85(1977).
10. N. S. Davidson, R. W. Richards, and A. Maconnachie, Macromolecules **19**, 434(1986).
11. P. G. de Gennes, Scaling Concepts in Polymer Physics, Cornell University Press, 1979.
12. W. R. Drummond, M. L. Knight, M. L. Branmnon and N. A. Peppas, J. Controlled Release **7**, 181(1988).
13. S.J. Fast and S.S. Yun, J. Acous. Soc. Am. **81**, 1418(1987).
14. R. A. Ferrell and J. K. Bhattacharjee, Phys. Rev. A **24**, 1643(1981).
15. R. A. Ferrell and J. K. Bhattacharjee, Phys. Rev. A **31**, 1788(1985).
16. P.J. Flory, Principles of Polymer Chemistry, Cornell University, Ithaca, New York, 1953.

17. Y. Fukahori and W. Seki, Polymer **33**, 502(1992).

18. C. W. Garland, in Physical Acoustics, Edited by W.P. Mason and R.N. Thurston (Academic Press, New York) 1970, p. 51.

19. C. W. Garland and G. Sanchez, J. Chem. Phys. **79**, 3090(1983).

20. E. Geissler and A. M. Hecht, Macromolecules, **13**, 1276(1980).

21. E. Geissler and A. M. Hecht, Macromolecules, **14**, 185(1981).

22. E. Geissler, A. M. Hecht, F. Horkay, and M. Zrinyi, Macromolecules, **21**, 2594(1988).

23. E. Geissler, F. Horkay, and A-M Hecht, Macromolecules **24**, 6006(1991).

24. J.A. Glazier, S.P. Gross, and J. Stavans, Phys. Rev. A **36**, 306(1987).

25. T. Hayashi, H. Tanaka, T. Nishi, Y. Hirose, T. Amiya and T. Tanaka, J. Appl. Polym. Sci.: Appl. Polym. Symposium **44**, 195(1989).

26. S. Hirotsu, J. Phys. Soc. Jpn. **56**, 233(1987).

27. S. Hirotsu, Y. Hirokawa and T. Tanaka, J. Chem. Phys. **87**, 1932(1987).

28. S. Hirotsu, J. Chem. Phys. **88**, 427(1988).

29. S. Hirotsu and A. Onuki, J. Phys. Soc. Jpn. **58**, 1508(1989).

30. S. Hirotsu, Macromolecule **23**, 905(1990).

31. S. Hirotsu, J. Chem. Phys. **94**, 3949(1991).

32. A. Hochberg, T. Tanaka, and D. Nicoli, Phys. Rev. Lett. **43**, 217(1979).

33. F. Horkay and M. Zrinyi, Macromolecules, **15**, 1306(1982).

34. F. Horkay, E. Geissler, A. M. Hecht, and M. Zrinyi, Macromolecules, **21**, 2589(1988).

35. F. Horkay and M. Zrinyi, Macromolecules **21**, 3260(1988).

36. Z. Hu, C.W. Garland and S. Hirotsu, Phys. Rev. B **42**, 8503(1990).

37. Z. Hu, C. Li, and Y. Li, J. Chem. Phys. **99**, 7108(1993).

38. T. Hwa and M. Kardar, Phys. Rev. Lett. **61**, 106(1988).

39. T. Komori, H. Takahashi and N. Okamoto, Colloid and Polym. Sci. **266**, 1181(1988).

40. L.D. Landau and E.M. Liftschitz, Theory of Elasticity (Pergamon Press, New York, 1986).

41. R. Lakes, Science **235**, 1038 (1987).

42. F.T. Lewis, Anat. Rec. **38**, 341(1928).

43. C. Li, Z. Hu, and Y. Li, Phys. Rev. E **40**, 603(1993).

44. C. Li, Z. Hu, and Y. Li, submitted to Phys. Rev.

45. Y. Li, Phys. Status Solidi **38**, 171 (1976).

46. Y. Li, Ph.D thesis, Structure and Critical Behavior of Polymer Gels, Massachusetts Institute of Technology, 1989.

47. Y. Li and T. Tanaka, J. Chem. Phys., **90**, 5161(1989).

48. Y. Li and T. Tanaka, J. Chem. Phys. **92**, 15 (1990).

49. Y. Li and T. Tanaka, Ann. Rev. Mat. Sci. **22**, 243(1992).

50. Y. Li, Z. Hu and C. Li, J. Appl. Polym. Sci. **50**, 1107(1993).

51. Y. Li, C. Li and Z. Hu, in ACS Symposium Series xx, Edited by N.A. Peppas and F.L. Buchholz, May 1994.

52. Y. Li, C. Li and Z. Hu, submitted to J. Chem. Phys.

53. J. P. Munch, S. Candau, J. Herz, and G. Hild, J. Phys.(Paris) **38**, 971(1977).

54. T. Odijk, J. Polym. Sci., Polym. Phys. Ed. **15**, 477(1977).

55. T. Odijk and A.C. Houwaart, J. Polym. Sci., Polym. Phys. Ed.,**16**, 627(1978).

56. T. Odijk, Macromolecules **12**, 688(1979).

57. A. Onuki, Phys. Rev. A **38**, 2192(1988).

58. A. Onuki, J. Phys. Soc. Jpn. **57**, 703(1988).

59. Y. Osada and S. B. Ross-Murphy, Scientific American, May, 82(1993).

60. A. Peters and S. J. Candau, Macromolecules, **19**, 1952(1986).

61. R. K. Prud'homme and Y. Yin, ACS Polym. Mat. Sci. Eng. **69**, 527(1993).

62. R. W. Richards and N. S. Davidson, Macromolecules **19**, 1381(1986).

63. R. S. Rivlin, Phil. Trans. R. Soc. A **241**, 379(1948);

64. E. Sato-Matsuo and T. Tanaka, J. Chem. Phys. **89**, 1695(1988).

65. E. Sato-Matsuo and T. Tanaka, Nature **358**, 482 (1992).

66. D. W. Schaefer, Polymer **25**, 387(1984).

67. H. G. Schild, Prog. Polym. Sci. **17**, 163(1992).

68. K. Sekimoto and K. Kawasaki, Phys. A **154**, 384(1989); J. Phys. Soc. Jpn. **57**, 2597(1988).

69. T. Shiga, Y. Hirose, A. Okada, and T. Kurauchi, J. Appli. Polym. Sci. **44**, 249(1992).

70. D.J. Srolovitz, M.P. Anderson, P.S. Sahni, and G.S. Grest, Acta Metall. **32**, 793(1984); Phys. Rev. Lett. **50**, 263(1983).

71. K.J. Stine, S.A. Rauseo, B.G. Moore, J.A. Wise, and C.M. Knobler, Phys. Rev. A **41**, 6886(1990).

72. F. Tabak, M. Corti, L. Pavesi, A. Rigamonti, J. Phys. C: Condensed Matt. Phys.**20**, 5691(1987).

73. T. Tanaka, S. Ishiwata and C. Ishimoto, Phys. Rev. Lett. **38**, 771(1977).

74. T. Tanaka, Phys. Rev. A **17**, 763(1978).

75. T. Tanaka and D.J. Fillmore, J. Chem. Phys. **70**, 1214(1979).

76. T. Tanaka, Scientific American **244**, 124(1981).

77. T. Tanaka, S-T. Sun, Y. Hirokawa, S. Katayama, J. Kucera, Y. Hirose, and T. Amiya, Nature, **325**, 796(1987).

78. T. Tanaka, S-T. Sun, Y. Hirokawa, S. Katayama, J. Kucera, Y. Hirose, and T. Amiya, Molecular Conformation and Dynamics of Macromolecules in Condensed Systems, Ed. M. Nagasawa, Elsevier, Amsterdam 1988.

79. K. Urayama, T. Takigawa, and T. Masuda, Macromolecules **26**, 3092 (1992).

80. L. Wang and V. Bloomfield, Macromolecules **23**, 194(1990).

81. L. Wang and V. Bloomfield, Macromolecules **23**, 804(1990).

82. T. A. Witten and P. Pincus, Europhys. Lett. **3**, 315(1987).

83. K.W. Wojciechowski and A.C. Branka, Phys. Rev. A **40**, 7222(1989).

84. M. Zrinyi and F. Horkay, Macromolecules **17**, 2805(1984).